The Metallogeny of Gold-Bearing Banded Iron Formation on the Margins of the Crazy Bear Metamorphic Complex, Bathurst Inlet, Nunavut

R.G. Therriault

Submitted in partial fulfillment of the requirements of an Honors Bachelor of Science Degree in Earth Sciences, The University of Western Ontario.

March, 2003

Abstract

The Bathurst Inlet Terrane, forming the northeast portion of the Slave Province, contains numerous banded iron formation (BIF) hosted lode gold prospects. The BIF units occur within cordierite facies metagreywackes on the margins of the Crazy Bear Metamorphic Complex (CBMC). This complex is characterized by core migmatites bordered by sillimanite schists/gneisses with cordierite-bearing metagreywackes occurring on the periphery. The front of aluminosilicate growth is marked by a belt of high strain wherein prograde andalusite is overprinted by retrograde sericite-chlorite.

Study of gold-bearing BIF on the Hen and Bear Creek claims provides insight into gold mineralization in the region. Silicate facies BIF is characterized by coarse grunerite splays, calcic amphiboles, hedenbergite, coarse almandine garnet and chlorite-retrograded biotite. Oxide facies is distinguished by thin bands of net-textured magnetite surrounding coarsely annealed amphibole + quartz. Sulphide facies bands host greater than 5% pyrrhotite and pyrite with trace disseminations of chalcopyrite, arsenopyrite and gold.

Textural evidence indicates the gold concentration occurred near peak thermal metamorphic conditions. Gold is attributed to the progradation of a dehydration front outward from the CBMC. Ca, S, As, Cu and Au were leached from the metasediments and transported to the prograde-retrograde mylonitic front. Precipitation of these elements occurred where fluid ponded in structural traps within the chemically reactive BIF units causing weak skarnification and local sulphidization.

Acknowledgments

There are several people who have aided me extensively during the course of this project. Without their help and support this project would never have been possible. I would like to thank Robin Wyllie and the NTI squadron for friendship and funding, Robert Barnett and Shear Minerals Inc. for technical help and financial support and Jeff Cormier, Whitney Walters, Peter MacDonald and the Graduate Club staff for keeping me moderately sane and spirited throughout the last year. Most importantly I would like to thank my thesis advisor, Dr. Norman Duke. His time and patience during the 2002 field season and throughout the academic year did not go unnoticed. Numerous conversations from thermal fronts to the antioxidant powers of tea have made this past year both educational and enjoyable.

TABLE OF CONTENTS

CHAPTER FOUR: GEOCHEMISTRY

CHAPTER FIVE: DISCUSSION AND CONCLUSIONS

LIST OF FIGURES

FIGURE PAGE

LIST OF PLATES

LIST OF TABLES

TABLE PAGE

Chapter 1.0

Introduction

1.1 General Statement on Iron Formation-Hosted Lode Gold Deposits in Canada

Iron formation has proven to be an important source of gold in Archean terranes within Canada. Such deposits occur within volcanic-sedimentary sequences throughout both the Superior and Slave Provinces. The vast majority of gold-enriched iron formations are Algoma-type, occurring dominantly within turbiditic metasedimentary sequences capping mafic to felsic volcanic flows (Ford, 1988). Examples of Algoma-type iron formation from the Superior Province include the Beardmore-Geraldton area (Mason *et al.*, 1983; Macdonald, 1983), the Curshaw and Mulga iron formations near Timmins (Fyon *et al.*, 1983) and the Central Patricia and Pickle Crow mines of the Kenora district (Macdonald, 1983).

In the Slave Province gold-bearing iron formation occurs within granite-metasedimentary terranes, occurring as relatively thin and semicontinuous units interbedded within thick sequences of variably metamorphosed turbiditic greywackes intruded by Neoarchean granitoids. The type example of this association is the presently active Lupin Mine located on the southwest shore of Contwoyto Lake. The discovery of the Lupin deposit in the early 1960's helped to spur vigorous exploration for auriferous iron formation particularly in the Bathurst Inlet region of the Slave Province.

Debate continues concerning the genesis of many iron formation hosted lode gold deposits and is polarized between syngenetic exhalative and epigenetic granite-related interpretations. Adherents to the syngenetic model suggest that sulphides and gold are precipitated contemporaneously with the deposition of the iron formation. The often-continuous nature of sulphide banding and the close association of gold with heavily sulphidized zones is used as evidence to support such a model (Macdonald, 1983).

Alternatively, the epigenetic model proposes that most if not all of the gold is concentrated by post-diagenesis hydrothermal activity. Highly sulphidized and gold enriched alteration haloes on late quartz veins are typical of many auriferous iron formation deposits, including Lupin (Lhotka and Nesbitt, 1989; Bullis *et al.*, 1994) and the Beardmore-Geraldton region of northwestern Ontario (Mason *et al.*, 1983; Macdonald, 1983). This has lead to the suggestion that migrating hydrothermal fluids transported the gold as sulphur complexes and precipitated it in sulphidized selvages around quartz veins. Such alteration haloes are best developed within iron rich sediments and generally show a decrease in gold, arsenic, pyrrhotite and pyrite away from quartz veins. The continuous and conformable nature of the sulphide-rich layers is explained by preferential sulphide replacement of primary iron silicate/oxide bands.

1.2 Thesis Objective

The portion of the Slave Province east of Bathurst Inlet is characterized by numerous occurrences of banded iron formation (BIF) that is significantly enriched in gold. The gold-bearing iron formation is preserved in cordierite schists and metagreywacke sequences exterior

to sillimanite and migmatite gneisses coring the Crazy Bear Metamorphic Complex (CBMC). Regionally, the iron formation is dominated by silicate facies, while oxide and sulphide facies occur more locally. Proximity of gold-bearing iron formation to the margins of the Crazy Bear Metamorphic Complex on the Hen and Bear Creek claims suggests that gold enrichment may relate to prograde and retrograde metamorphic events attending crustal thickening, migmitization, granite emplacement and thermal doming attending Neoarchean extensional unroofing.

The primary aim of this thesis is to characterize the host rock setting of the Hen claims. The Bear Creek claims are considered for comparison only. The broad objective is to determine how the metamorphic history of the Bathurst Inlet region relates to gold mineralization. This will be accomplished through detailed microscopic examination of metamorphic mineral assemblages and textures both within auriferous iron formation and the enveloping metasediments. The petrographic results will be supplemented with bulk rock major and trace element geochemistry and mineral chemistry. The conclusions reached will contribute to the general understanding of the genesis of iron formation hosted gold deposits.

1.3 Location and Physiography

The Hen and Bear Creek claims are located in the northeastern part of the Slave Province, east of Bathurst Inlet (Figure 1; Figure 2). The Hen claims are situated south of Crescent Lake, approximately 575 km northeast of Yellowknife, while the Bear Creek claims

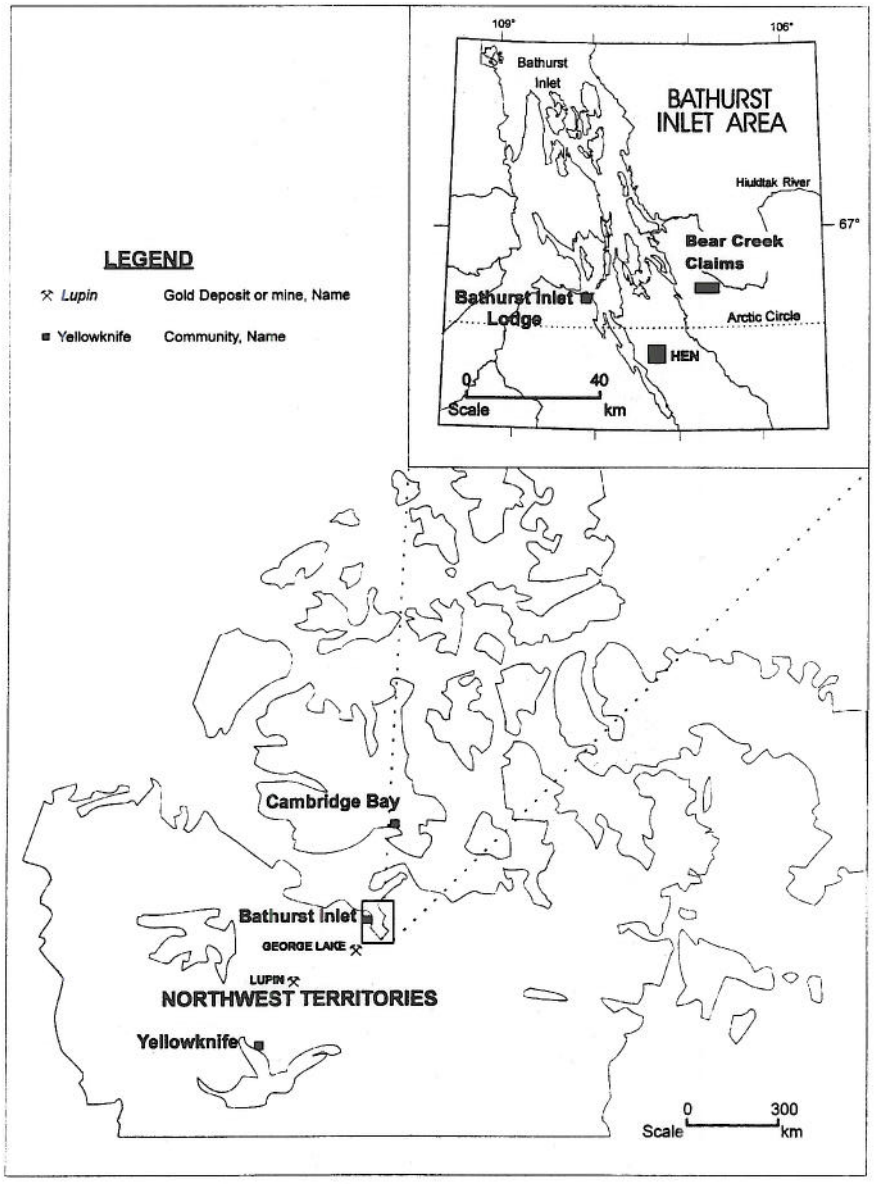

Figure 1: Location of study area within the Slave Province (modified from Freeman, 1994).

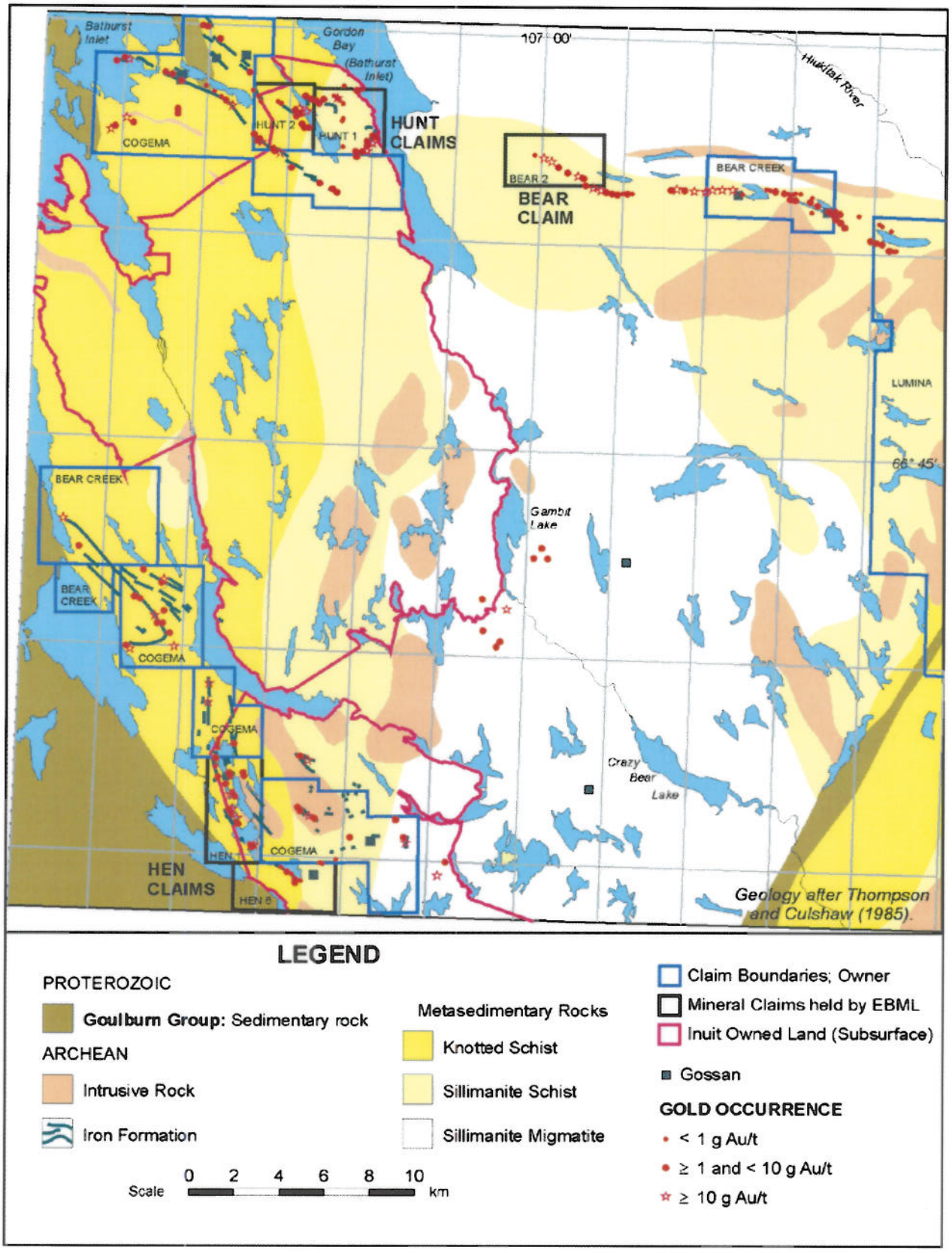

Figure 2: General geology and claim groups of the Bathurst Inlet region (modified from Freeman, 1994).

are positioned further to the north, just south of the Hiukitak River. The area is accessible only by aircraft.

Rugged ridges and narrow valleys of 300-400 meters relief characterize the topography of the Bathurst Inlet region. Glaciation has removed much of the sediment cover leaving relatively well-exposed bedrock. There is typically between 20-50% outcrop, although extensive lichen cover inhibits field observations.

As the area is well above the tree line, vegetation is limited to sparse brush concentrated in protected areas along drainage systems. Herds of caribou and muskox are common. Grizzly bears, wolves, wolverines, and foxes were sighted over the course of the 2002 field season.

1.4 Previous Work

The Geological Survey of Canada (GSC) sponsored reconnaissance mapping at a scale of 1:506880 in the Bathurst Inlet region during the mid 1960's (Fraser, 1964; 1968; 1972). Goulburn Group sediments of Proterozoic age infilling the Kilohigok basin (Figure 2) were also mapped by the GSC (Fraser, 1964; Campbell and Cecile, 1975; 1976; 1981; Campbell, 1978; Tirrul, 1985). Extensive work has been carried out on metamorphic and structural relationships of rocks in the eastern Slave, especially along the Thelon Tectonic Zone (Wright, 1957; Thompson, 1978; Henderson and Thompson, 1981; Henderson *et al.*, 1982; Thompson and Ashton, 1984; Henderson and Macfie, 1985; James, 1985; Thompson *et al.*,

1985; Thompson *et al.,* 1986; Henderson *et al.,* 1987). The work of Thompson *et al* (1978; 1984; 1985; 1986) in the Tinney Hills area is especially applicable to the present study.

Following the success of the Lupin deposit, several companies carried out base metal, uranium and gold exploration in the Bathurst Inlet region (Freeman, 1994). The International Nickel Company of Canada staked the Ox claims northwest of the Hen claims. In 1964 these claims were allowed to lapse and were restaked in 1968 as the Cot claims by Trans Canada Oils Ltd and Moresby Mines (Cathro, 1980; Freeman, 1994). Trenching and chip sampling on the property yielded assays up to 29.5 grams of gold per ton (g Au/t) across 3.84 m (Freeman, 1994). In 1982 and 1983 the old Cot claims were restaked as the G&T claims by Mr. G. Warner of Bear Creek Hills Estates Ltd. (Buhlmann, 1984; Smith, 1986; Freeman, 1994). In early 1984 Silver Hart Mines Ltd. made an option agreement with Mr. G. Warner and staked the Char and Fox claims. Results from rock grab and chip sampling assayed as high as 17.1g Au/t (Smith, 1986).

In the mid 1980's Echo Bay Mines Ltd. carried out a regional exploration program in the Bathurst Inlet region, conducting detailed sampling of the Hunt, Hen, Bear and Egg claims. The Hen claims were staked during Echo Bay's initial 1984 reconnaissance. Additional prospecting, mapping, grab and chip sampling and ground geophysical surveys were undertaken throughout the 1984 and 1985 field seasons. Assay results as high as 187.7 g Au/t and 3.8 g Au/t across 1.0m were obtained (Fraser *et al.*, 1985). In 1990 and 1991 Cogema Canada Ltd. staked the Ross claim groups over portions of expired Hen claims (Figure 2). In 1993 Echo Bay Mines Ltd. revisited several showings on the Hen properties to assess the

potential for future exploration (Freeman, 1994). Several targets were identified with assay results as high as 31.03 g Au/t and more follow-up prospecting was recommended (Freeman, 1994).

The Bear Creek claims on the northern boundary of the CBMC were staked by Echo Bay Mines Ltd. in 1985 covering a thick continuous gossanous unit and additional smaller iron formations (Muller, 1985; Fraser and Erdmer, 1986). Sampling in the 1985 and 1986 field seasons yielded sporadic gold values typically less than 2g Au/t. Because of poor results no future exploration was recommended (Muller, 1985; Fraser and Erdmer, 1986). Based on the mapping of Thompson (1978; 1984; 1985), Mr. G. Warner staked 2 claims internal to what are now the Bear claims. Helicopter reconnaissance by Echo Bay Mines in 1985 led to staking of the Bear 1-10 claims (Fraser and Erdmer, 1986). Several gold targets were identified in the 1985 and 1986 field seasons with assays as high as 18g Au/t on grab samples and diamond drill core. Future exploration was recommended for specific gold zones (Fraser and Erdmer, 1987). Recently, Shear Minerals Inc. acquired data and land holdings from Echo Bay's Hen, Hunt and Bear claim groups.

Echo Bay's exploration reports for the Hen and Bear Creek claims were obtained with the courtesy of Shear Minerals Inc. This information proved to be invaluable during the 2002 field season for pinpointing anomalous gold targets. Detailed mapping of the claim groups by Echo Bay and regional geology by Thompson (1978; 1984, 1985, 1986) proved to be instrumental in deciphering the complex structural and metamorphic history of the area.

1.5 Methods

Approximately 150 representative hand-samples and 70 assay samples were collected from the Hen and Bear Creek claims during the 2002 summer field season. From these, a representative sample suite was selected for detailed investigation of the relationship of gold to the metamorphic history of the CBMC. Thirty samples were cut and polished for thin section examination of metamorphic textures and mineral assemblages. Seven samples of oxide, silicate and sulphide facies iron formation and two samples of the metasedimentary host rock were crushed, powdered, and submitted to Charlie Wu of the University of Western Ontario for bulk rock XRF analysis. The XRF analyses were determined on a Philips PW-1400 wavelength dispersive spectrometer equipped with an Rh-target X-ray tube. The mineral chemical analysis were determined on a JEOL 733 5-wavelength electron microprobe at R.L. Barnett Geological Consulting Inc. in Lambeth, Ontario courtesy of Shear Minerals Inc. Seventy assay samples of iron formation were sent to Activation Laboratories Ltd. in Ancaster, Ontario to be analyzed for 49 trace elements courtesy of Nunavut Tunngavik Inc. Activation Laboratories Ltd. Code 1D (enhanced INNA) and Code 1F (4-acid digestion and ICP) were applied to determine trace element compositions. The results of bulk rock, mineral and trace element analyses are presented in table format in Appendix A, B and C respectively. The overall objective of the geochemical work was to: 1) compare and contrast major oxide values within the iron formation and metasediments, particularly total iron, aluminum, silica, sodium, potassium and calcium; 2) obtain mineral chemistry information for amphibole, garnet, micas and chlorite in order to document prograde-retrograde overprints at sites of gold mineralization,

and; 3) report representative gold and trace element values for the iron formation and attempt to amalgamate these results within a coherent metallogenic scheme to account for the gold concentrations.

1.6 Format of Text

This study begins with a brief overview of Slave Province geology. This is followed by a more detailed examination of geology and metamorphism of the Bathurst Inlet region. Chapter three is devoted to petrographic description of BIF and host rocks on the Hen and Bear Creek claims on the margins of the CBMC. Thin section observations focus on characterizing prograde-retrograde mineral assemblages. Chapter four will present the mineral chemistry data as well as major and trace element trends. Chapter five will focus on developing a metallogenic model linking the metamorphic evolution of the CBMC to gold mineralization.

Chapter 2.0

Regional Geology of the Bathurst Terrane

2.1 Geology of the Slave Province

The Slave Province, forming the northeast part of the Canadian Archean Shield, is composed of old basement gneisses, greenstone belts, metasediments and metamorphic complexes (Figure 3). The province is bound on the south, west and north by the Proterozoic Bear Province and on the east by the Proterozoic Churchill Province (Thompson, 1978). It is made up of approximately 35% Archean supracrustal rocks of the Yellowknife Supergroup and 65% granite-gneiss-migmatite terranes (Thompson, 1978). The supracrustals are dominated by thick successions of turbiditic greywackes and pelites with minor conglomerate, quartzite and silicate facies iron formation (Ford, 1988). Mafic volcanics form linear north-south trending belts concentrated in the central part of the province. Volcanic belts in the west typically lack a felsic component distinguishing them from the more calc-alkaline Hackett River-type belts occurring in the east (Ford, 1988). The volcanic sequences typically underlie the sedimentary assemblages but stratigraphic interlayering signifies overlapping depositional environments. The granite-gneiss-migmatite terranes are thought to be in part derived from Yellowknife Supergroup sediments. However, 3.96-2.85 Ga gneisses in the western Slave likely acted as basement to younger volcanic and sedimentary successions of the Yellowknife Supergroup (James and Mortensen, 1992; Thompson, 1978).

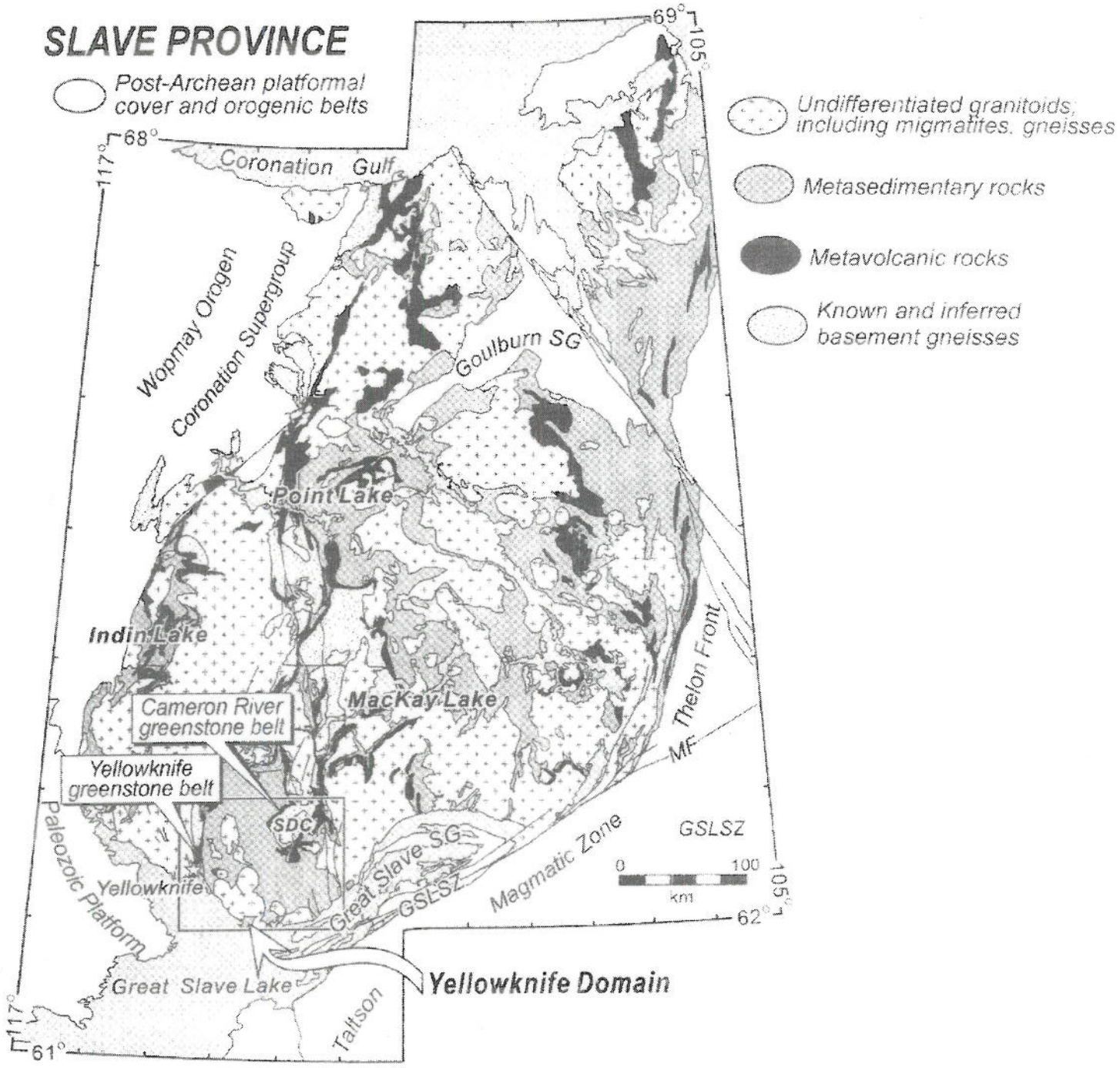

Figure 3: Geology of the Slave Province. GSLSZ, Great Slave Lake Shear Zone; MF, MacDonald Fault; SDC, Sleepy Dragon Complex; SG, supergroup. (Modified after Bethune *et al.,* 1998).

Neoarchean granitoid suites dating between 2.63-2.58 Ga occur throughout the province (van Breeman *et al.*, 1987; Bethune *et al.*, 1999). Examination of these suites has shown that in most cases they syndate the main regional metamorphic overprint (Davis and Bleeker, 1999).

Deformation in the Slave Province has been subdivided into three events (Thompson, 1978). D_1 is characterized by isoclinal folds with steeply dipping axial surfaces and a poorly preserved bedding-parallel S_1 cleavage. D_2 deformation refolded D_1 structures and imparted a steep axial planar north-trending S_2 cleavage, which is overgrown by cordierite and andalusite porphyroblasts. D_3 is attributed to the emplacement of granitoid plutons and resulted in crenulation of the S_2 schistosity and pinitization of cordierite. Peak thermal conditions are represented by medium grade, low pressure Pyreneean type metamorphism (Thompson, 1978). The transection of D_2 by isograds indicates that peak thermal metamorphism was reached post-peak kinematic. Retrogression of cordierites during D_3 indicates that thermal conditions had begun to wane during D_3.

2.2 Geology of the Crazy Bear Metamorphic Complex (CBMC)

2.2.1 Lithologies

The Bathurst Inlet Terrane is bound on the west by the northwest-trending Bathurst Fault, which separates Archean metasediments from Proterozoic sediments (Figure 4). The Bathurst fault is thought to be a Neoarchean structure rejuvenated during the Proterozoic with

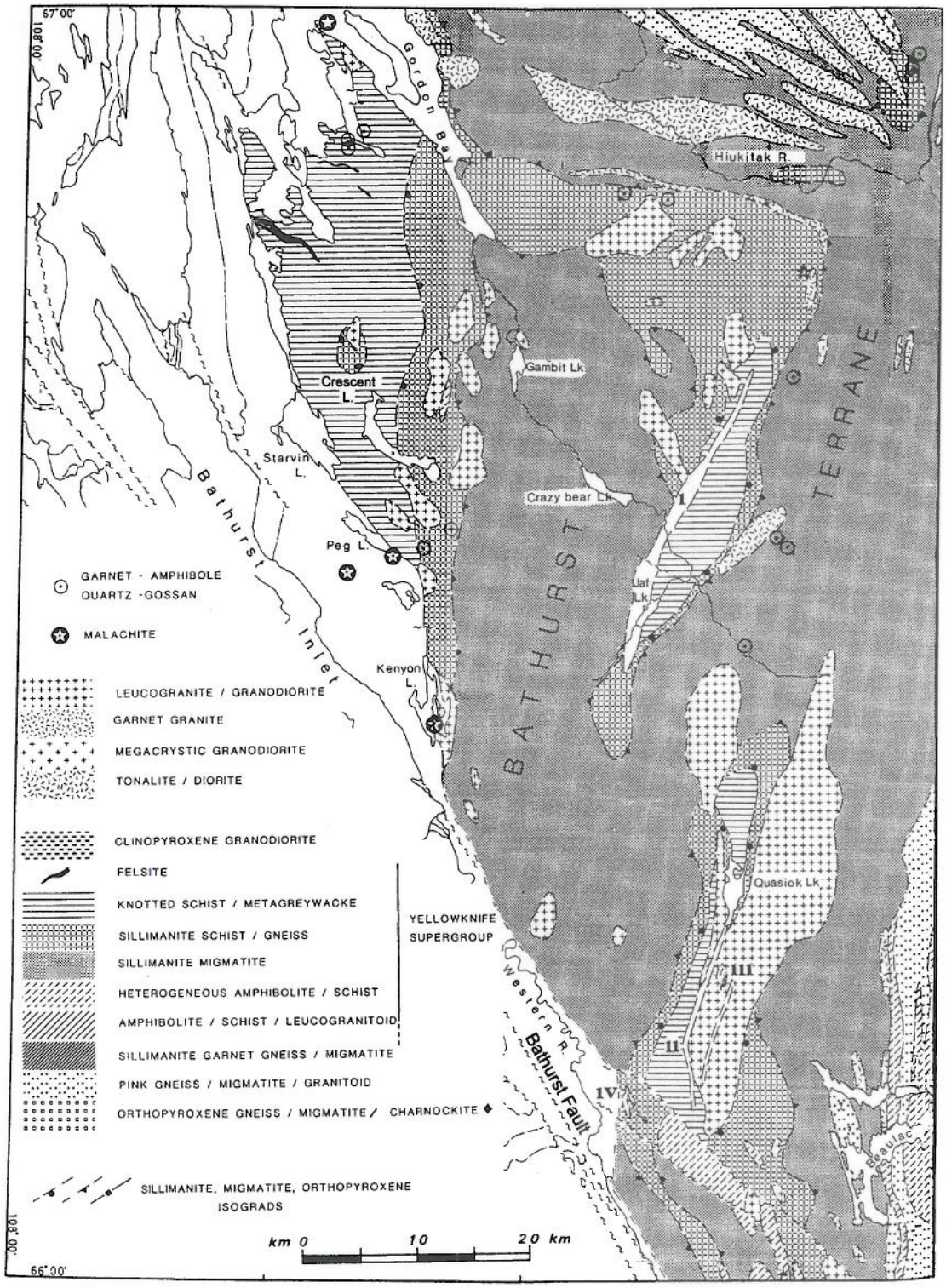

Figure 4 : Geology of the Bathurst Inlet region. The unhatched area is Goulburn Group (Modified from Thompson, 1985).

approximately 130 km of left-lateral movement (Freeman, 1994). Metamorphic grade increases across the Bathurst Inlet Terrane towards the Thelon Tectonic Zone separating the Slave Province from the Churchill Province.

The Bathurst Inlet area is underlain by high-grade aluminosilicate-bearing schists, gneisses and migmatites derived from turbiditic pelities and psammites of the Archean Yellowknife Supergroup (Freeman, 1994). Neorchean granitic to tonalitic intrusives and basic dyke swarms also occur throughout the Bathurst Inlet region. Aphebian-aged Goulburn Group sediments occupy the Kilohigok rift and onlap the Slave west of Bathurst Inlet (Figure 4; Thompson, 1978). The Goulburn Group sediments are characterized by unmetamorphosed shallow-marine quartzites and dolomites.

The Bathurst Inlet Terrane is characterized by three lithotypes, which together form the Crazy Bear Metamorphic Complex (Figure 5). Migmatite constitutes the core and is defined by greater than 5-10% leucosome (Thompson, 1985). Restite is characterized by sillimanite and biotite with scattered occurrences of cordierite, andalusite, garnet and kyanite. Garnet is often rimmed by cordierite, while cordierite and andalusite are frequently retrograded to white mica and chlorite (Thompson, 1985). The migmatite is bordered by sillimanite gneiss, which is characterized by ellipsoidal knots of sillimanite aligned with the main foliation. Cordierite, when present, may be found rimming garnet or plagioclase (Thompson, 1985; 1986). Peripheral to the sillimanite schist is cordierite metagreywacke; a grey to brown biotite-rich rock with knots of cordierite, staurolite +/- andalusite. Porphyroblasts partly overgrow the main foliation and

LEGEND

PROTEROZOIC

- Diabase Dykes
- Goulburn Group

ARCHEAN

- Granite

Upper Plate

- Cordierite Wacke

Middle Plate

- Mylonitic Andalusite Schist
- Paragneiss
- Banded Iron Formation
- Sillimanite Gneiss

Lower Plate

- Migmatite Gneiss
- Tonalite Gneiss

STRUCTURES

- Proterozoic Faults
- Shear Zones
- F_3 Fold Axes
- S_0 Form Lines
- Migmatite Isograd
- Sillimanite Isograd

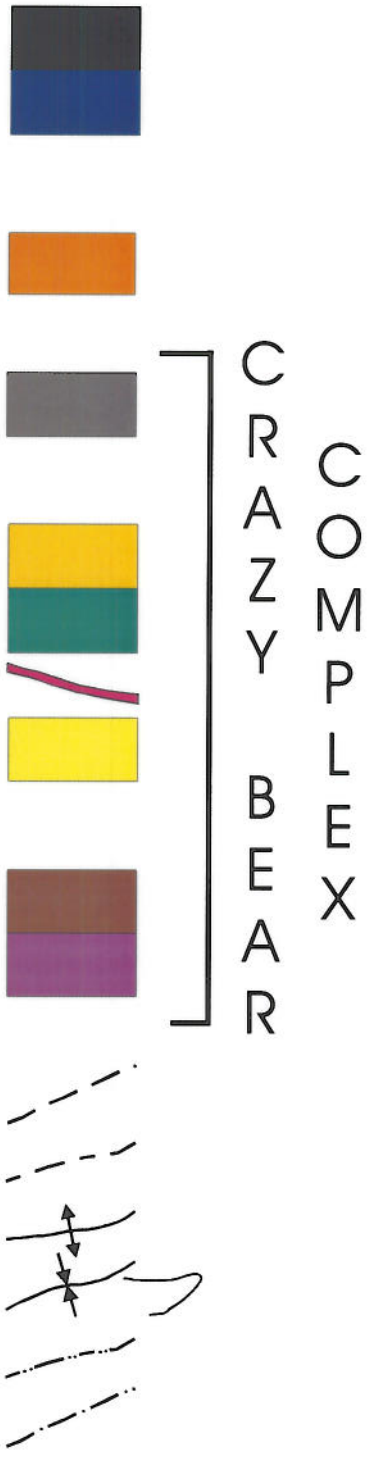

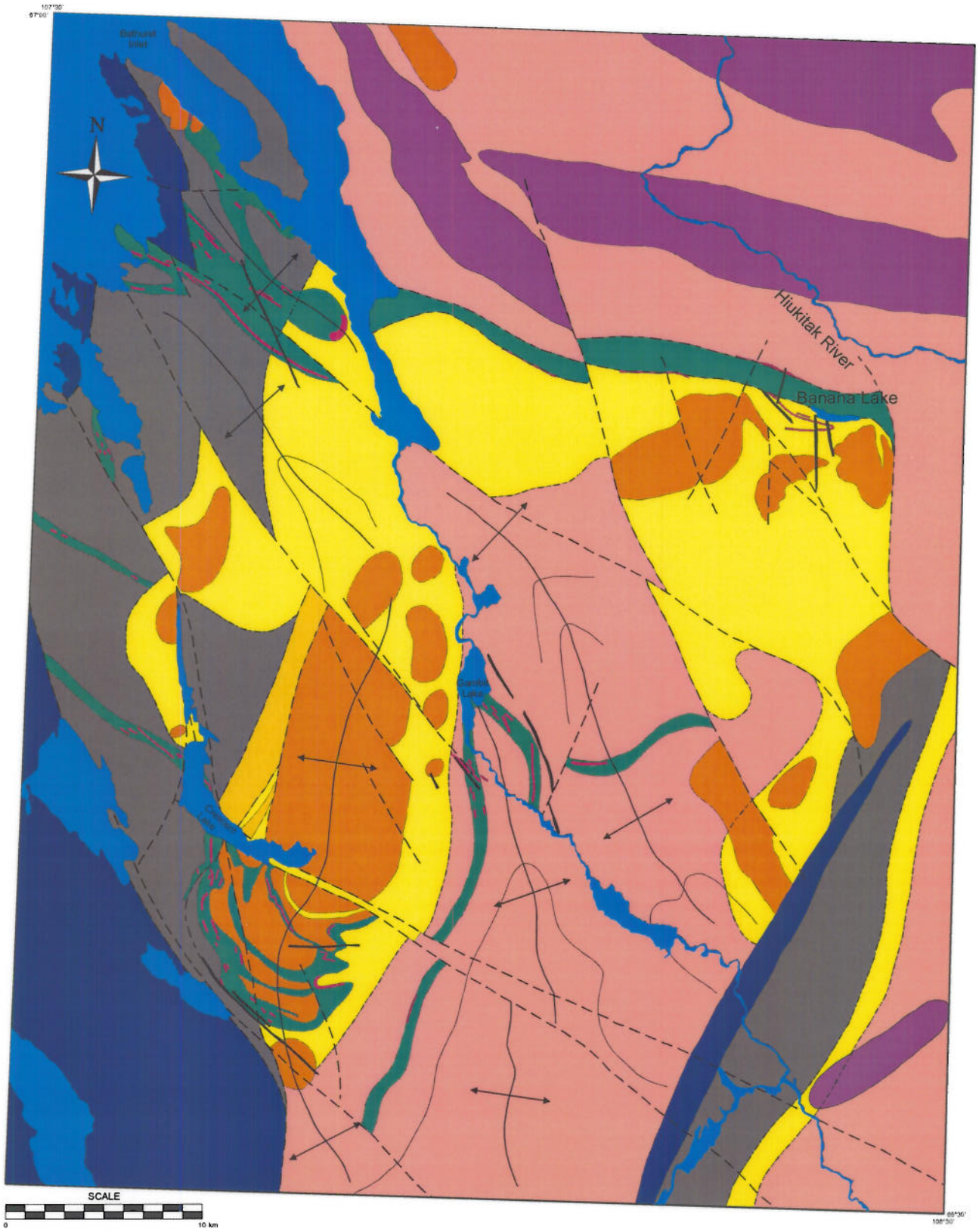

Figure 5: Geology of the Crazy Bear Metamorphic Complex (Duke, 2002).

often exhibit white-mica, chlorite or biotite retrogression. This unit commonly preserves primary sedimentary structures allowing top determinations (Thompson, 1985).

Banded iron formation occurs as mostly silicate and lesser oxide facies material within cordierite metasediments on the margins of the CBMC. Sulphide facies tend to form restricted podiform domains. Strike lengths of the BIF varies from a few hundred meters to several kilometers with widths of 1 to 5 m.

Medium grained syn-tectonic two-mica granites outcrop extensively in the sillimanite zone and near the migmatite and sillimanite isograds (Figure 4). An age of 2597 Ma was obtained from foliated granite on the northeast shore of Crescent Lake. Younger undeformed post-tectonic quartz monzogranite plutons and tourmaline pegmatite sheets also occur extensively throughout the Bathurst Inlet Terrane. Potassium-feldspar, plagioclase, quartz, muscovite and biotite make up the primary mineralogy with minor, locally significant amounts of tourmaline. Most of the pegmatitic sheets intrude subparallel to D_2 layering.

Basic dykes in the Bathurst Inlet Terrane can be subdivided into four groups (Figure 6): 1) relatively fresh, Franklin dykes (about 723 Ma); 2) basic dykes of the Mackenzie swarm (1.2 Ga); 3) older, metamorphosed dykes discordant to the regional grain; and 4) garnet amphibolite and metadiabasic bodies concordant with regional trends.

2.2.2 Metamorphism

The Bathurst Inlet region has undergone two major deformation events; a Neoarchean upper amphibolite to granulite facies (Rb-Sr age of 2.56 Ga; Thompson, 1985), and a

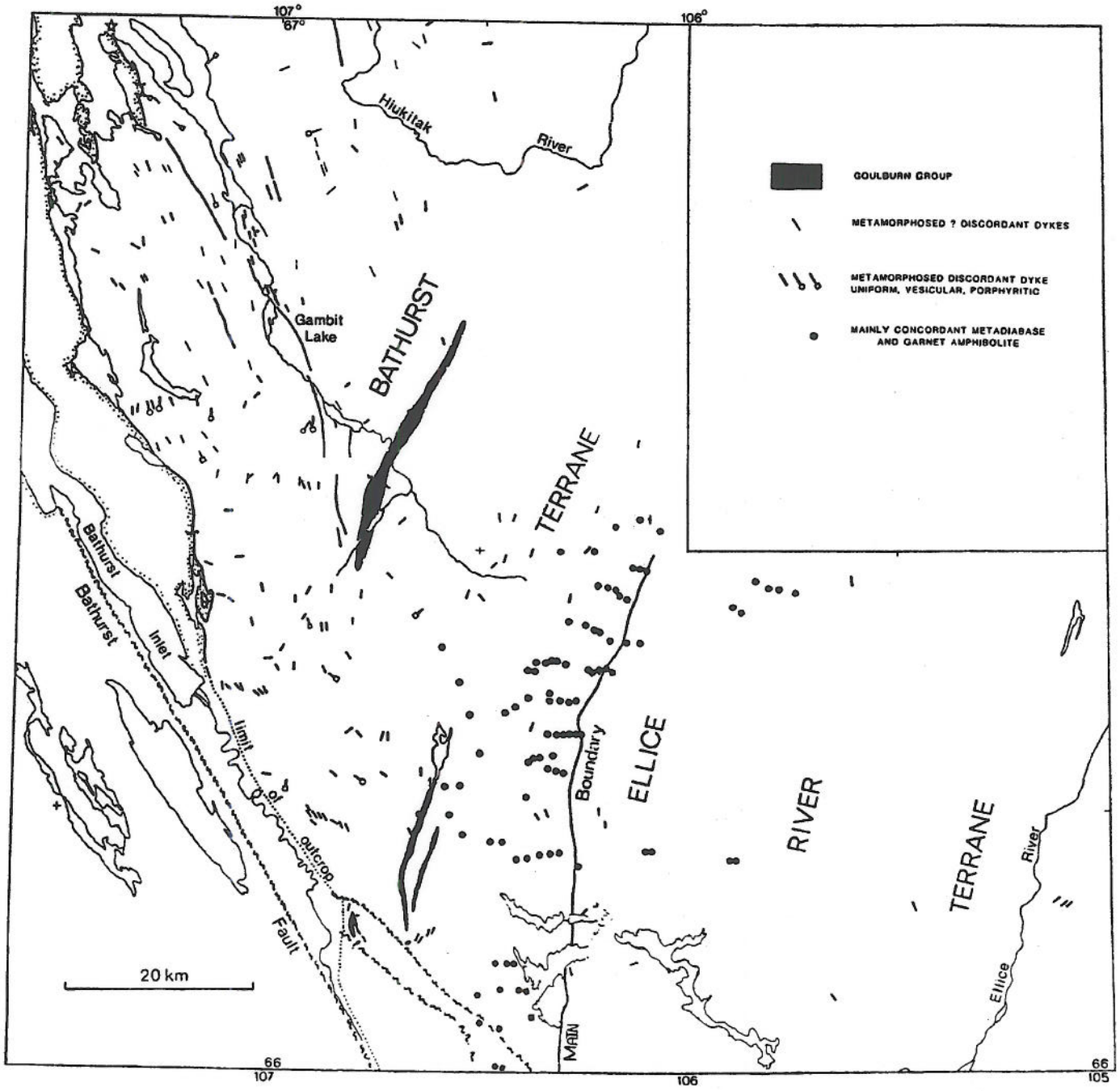

Figure 6 : Mafic dyke trends in the Bathurst Inlet region. Mackenzie dykes are not shown (Thomson *et al.*, 1985).

Proterozoic upper greenschist facies that overprints and retrogrades the main phase (K-Ar age between 1948 Ma-1765 Ma; van Breeman, 1987). Rifting prior to Proterozoic metamorphism resulted in the opening of the Kilohigok Basin, giving rise to the fault-bounded blocks of Goulburn Group sediments ("inliers") east of the basin.

The Neoarchean event produced low-plunging folds with northwest axes and northwest-trending foliations in the northern and western areas of the Bathurst Inlet Terrane (Thompson *et al.*, 1985). Peak temperatures of approximately 675 °C and pressures of 6-7 kilobars have been suggested by Thompson *et al.*, 1985. Foliations in the west of the CBMC are deflected around the core migmatites parallel to the borders of this late Archean metamorphic complex (Figure 7). The northern boundary of the CBMC is a belt of high strain dipping moderately to the north-northeast (Thompson *et al.*, 1985). Domains 2 and 3 (Figure 7) often exhibit northwest-trending stretching lineations, particularly in highly strained zones such as between Domains 2 and 3 and at the base of granites in the northeast of Domain 3. These high-strain zones correspond closely with sillimanite isograds and are interpreted by Thompson *et al.*, (1985; 1986) to be slide/shear zones subdividing the Archean crust into a lower mobile layer overlain by a less ductile roof. The northern strain zone trending ESE from Gordon Bay is thought to represent a D_2 ductile thrust zone separating allochthonous migmatites rooted in the north from underlying lower grade sillimanite schists. Ductility contrasts between the two layers may explain the ponding of granitic material within a mid-crustal discontinuity. Updoming of the CBMC in the Neoarchean rejuvenation these D_2 structures as D_3 mylonitic shears. This will be discussed in more detail in Chapter 5.

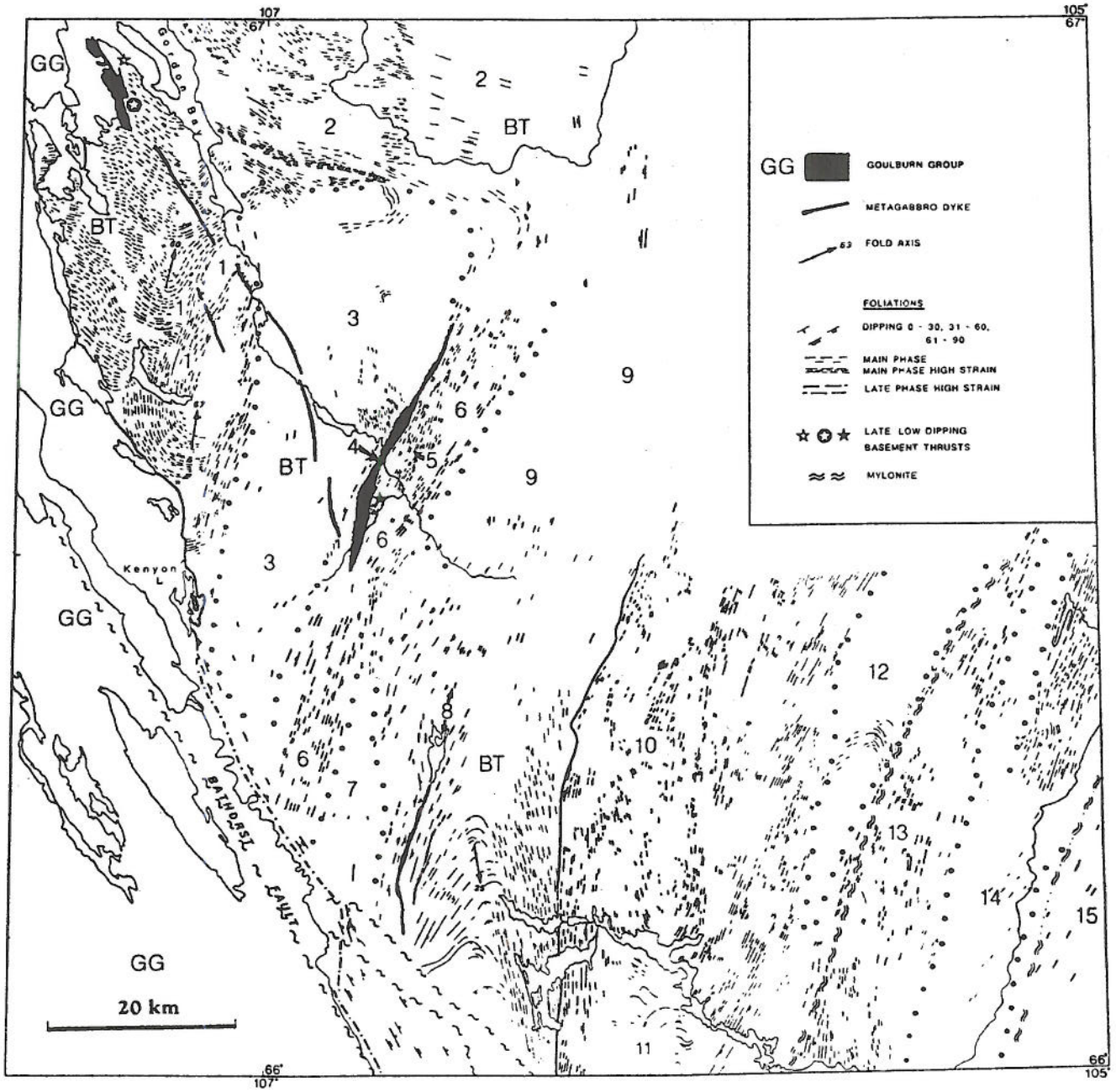

Figure 7: Structural trends in the Bathurst Inlet region. GG, Goulburn Group; BT, Bathurst Terrane. Numbers indicate terranes (Thompson *et al.*, 1985).

The Proterozoic metamorphic overprint is limited to the eastern margin of the Bathurst Inlet Terrane (Domains 5, 6 and 8; Figure 7; Thompson *et al.,* 1985). Upper greenschist conditions prevailed and caused extensive sericite and chlorite retrogression of cordierite, andalusite, mica and feldspar. Proterozoic deformation is also linked to east-west thrusting, and is associated with the straightening of main phase fabrics into a north-south orientation (Thompson *et al.,* 1985).

Chapter 3.0

Petrography of Banded Iron Formation on the Hen and Bear Creek Claims

3.1 Geological Setting of Banded Iron Formation

The Hen claims are underlain by cordierite schist/metagreywacke on the southwest margin of the CBMC. The property extends towards the west to the fault-bounded Archean/Proterozoic unconformity on the eastern edge of the Kilohigok Basin. There is an abrupt transition eastward into higher-grade sillimanite gneisses and migmatites.

The pelitic to psammitic metagreywackes that underlie the Hen claims frequently preserve planar and graded bedding (Plate 1). The main deformation is a north-northwest structural grain that dips 45°-75° west. Interlayered iron formation bands are conformable with the enveloping clastic sediment and act as ideal marker beds for delineating stratigraphy. The main iron formation unit on the Hen claims was traced for several kilometers south of Crescent Lake. North of Crescent Lake the strike changes from north to northwest continuing as the 'Char' BIF towards the Bathurst Fault. The change in strike defines a broad open F2/F3 fold hinge near the center of Crescent Lake. Outcrop-scale F2 isoclinal folds were also observed throughout the Hen claims (Plate 2).

Deformed granitic plutons, undeformed pegmatitic sheets and metabasic dykes are common, and underlie a significant portion of the Hen claims. The syntectonic granite pluton east of the Hen claims has been dated at 2597 Ma (van Breeman *et al.*, 1987). Very coarse-grained tourmaline-bearing pegmatitic sheets are typically a few meters wide and strike for several tens of meters in a

Plate 1: Graded bedding in turbiditic greywackes: Hen claims.

Plate 2: F2/F3 fold nose developed in silicate-facies iron formation: Hen claims.

north-northwest direction (Plate 3). Porphyritic and non-porphyritic basic dykes, probably of the Franklin swarm (723 Ma) are typically 1-20 m wide and trend north-northwest.

The Bear Creek claims are located on the sillimanite schist/migmatite boundary on the northern margin of the CBMC. A thin panel of highly mylonitized granite and gneiss separate these two units. Thompson *et al.,* (1985; 1986) has suggested that this zone of high strain (the Bear Creek Valley Deformation Zone) may be a thrust boundary superimposing migmatites rooted in the north over sillimanite schists to the south. Primary bedding has been virtually destroyed and is replaced by a steep east-southeast gneissosity. Within the Bear Creek Valley Deformation Zone iron formation is strongly disrupted, occurring as narrow east-southeast trending segments of limited strike extent, and as isolated fold noses. Iron formation of the 'Egg' BIF south of the deformation zone is more continuous and was traced for over 2 km along strike.

3.2 Petrography of Banded Iron Formation Units

3.2.1 Iron Formation on the Hen Claims

Iron formation on the Hen claims is represented by numerous thin and semicontinuous units of silicate, oxide and sulphide facies in that order of abundance. Banding is outlined by 1-2 cm layers of Fe-amphiboles, garnet, quartz, magnetite and more rarely, pyrite-pyrrhotite. Mineralogical variations have allowed a general subdivision of iron formation of the Hen and Bear Creek claims into three facies: silicate, silicate/oxide and silicate/sulphide. In the following text these will be referred to as silicate, oxide and sulphide facies respectively.

On the Hen claims the silicate facies BIF is characterized by mm to cm scale bands of grunerite-cummingtonite + calcic amphibole, quartz, and garnet. Quartz typically composes less than 20% of the Fe-silicate facies. It occurs as 0.1-1.0 mm strained crystals concentrated into moderately defined layers. Banding-parallel vein quartz shows coarser polygonal textures in which the quartz is unstrained. The grunerite-cummingtonite amphiboles frequently occur as coarse (0.5 mm-1.0 cm) radiating subidioblastic to idioblastic splays (Plate 4). In most cases, the finer-grained grunerite blades are aligned with the iron formation bands. Calcic amphibole occurs as thin sharp rims on white amphiboles (Plate 5) as well as individual idioblasts. A late generation of calcic hornblende occasionally replaces the two intergrown amphibole species on the selvages of layer-parallel quartz veinlets (Plate 6).

Garnet regularly composes 20-50% of the silicate facies iron formation, with morphologies ranging from 2-5 mm pristine idioblasts to intensely microbrecciated aggregates. Chlorite occurs as a patchy retrograde phase of garnet as well as sharply bounded veins within large brecciated porphyroblasts. In most cases garnet is wrapped by the main foliation and contains magnetite, ilmenite, quartz and grunerite inclusion trains that parallel the primary schistosity (Plate 7; Plate 8). Less commonly, inclusion trains are slightly discordinate, with garnet partly overgrowing the main foliation, indicating minor late kinematic rotation.

Clinopyroxene, apatite and monazite as well as sulphides and oxides are also present in minor amounts within the silicate facies BIF. Microbrecciated clinopyroxene xenoblasts ranging from 0.5-1.0 mm were observed in two sections. Apatite occurs as small idioblasts within quartz-amphibole rich domains while monazite forms fine-grained inclusions within amphiboles and biotite. Pyrite, pyrrhotite,

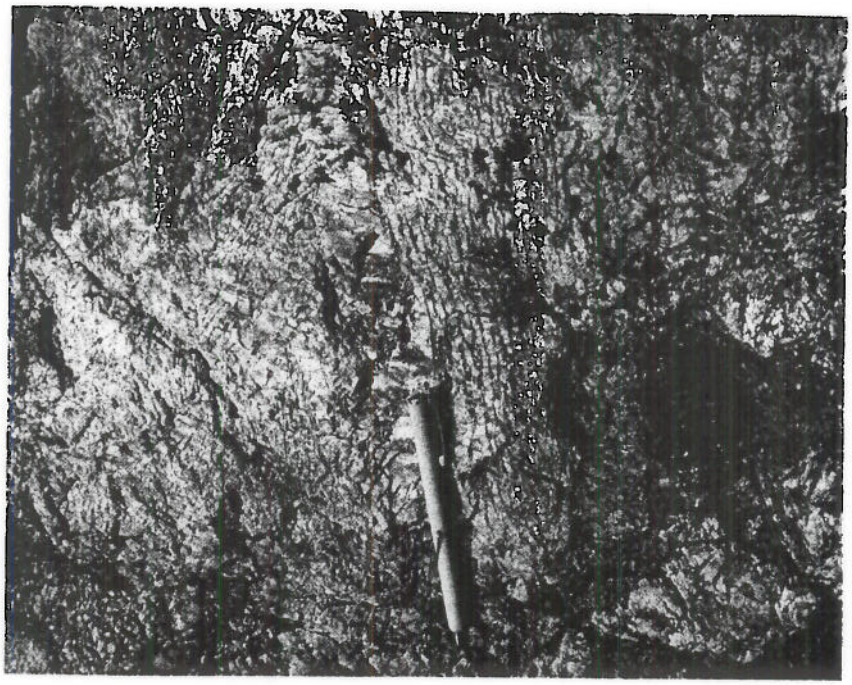

Plate 3: Tourmaline-bearing pegmatitic sheet with large potassium feldspars: Hen claims.

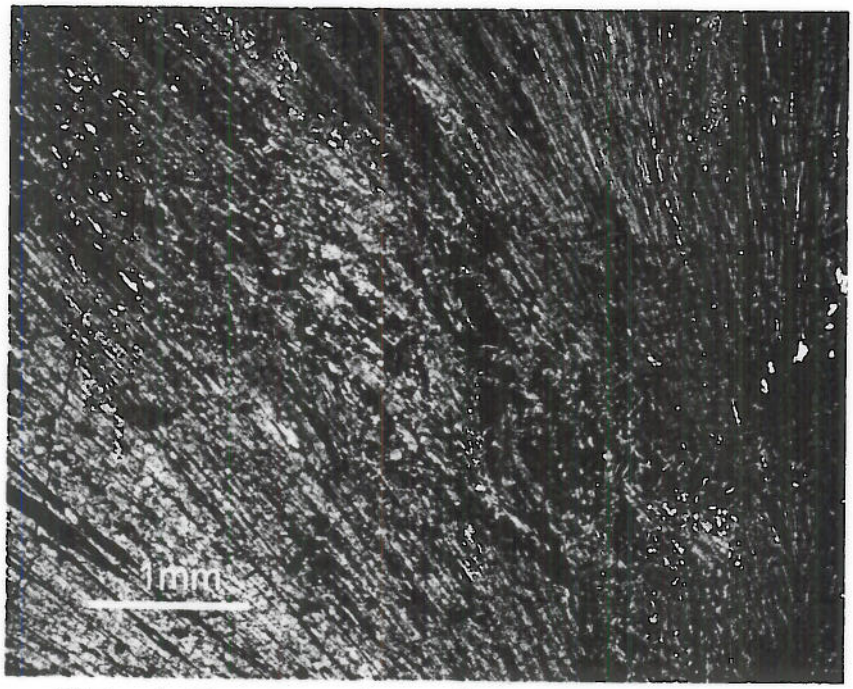

Plate 4: Coarse splays of idioblastic grunerite needles.

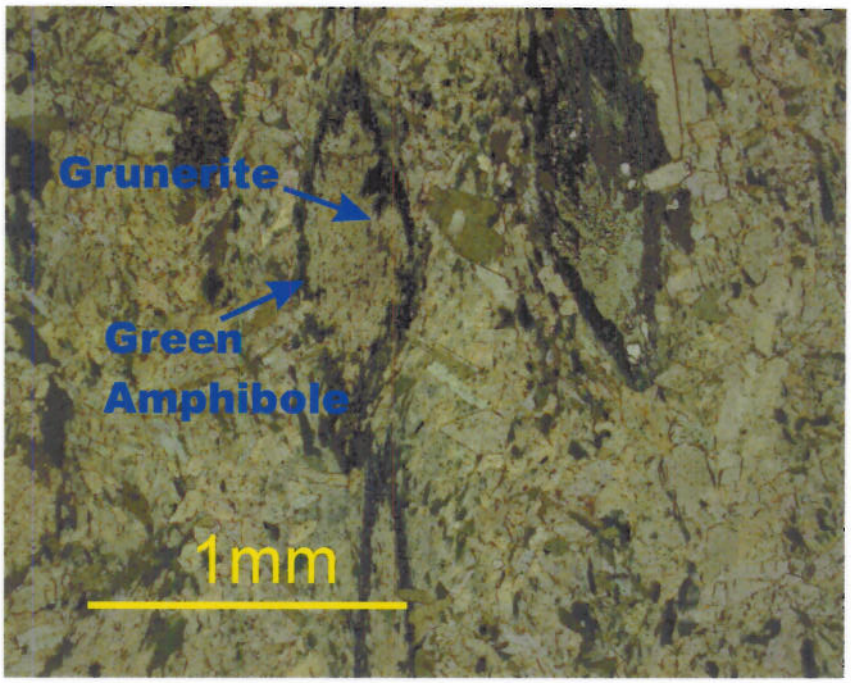

Plate 5: Green amphibole showing sharp contacts with grunerite along crystal boundaries and cleavage planes.

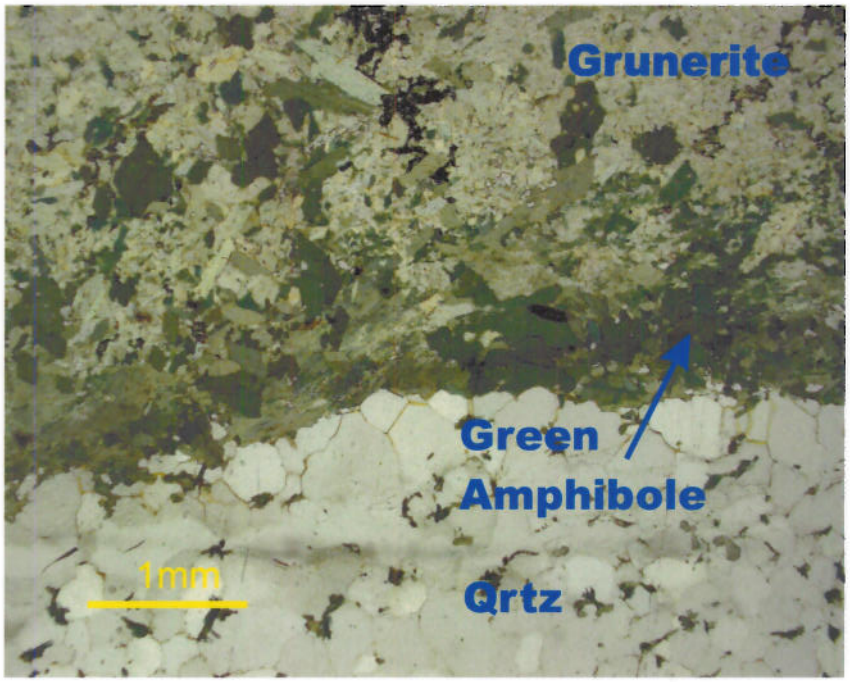

Plate 6: Green amphibole replacing grunerite along the margins of a quartz vein.

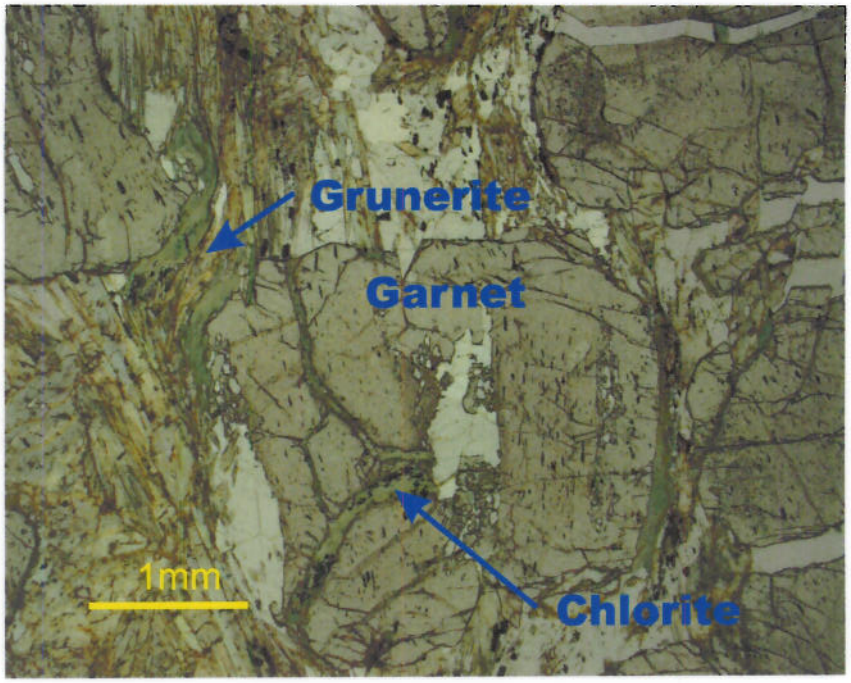

Plate 7: Crushed garnets with inclusion trains of quartz and magnetite. The garnet is rimmed by chlorite and grunerite and contains chlorite-filled microfractures.

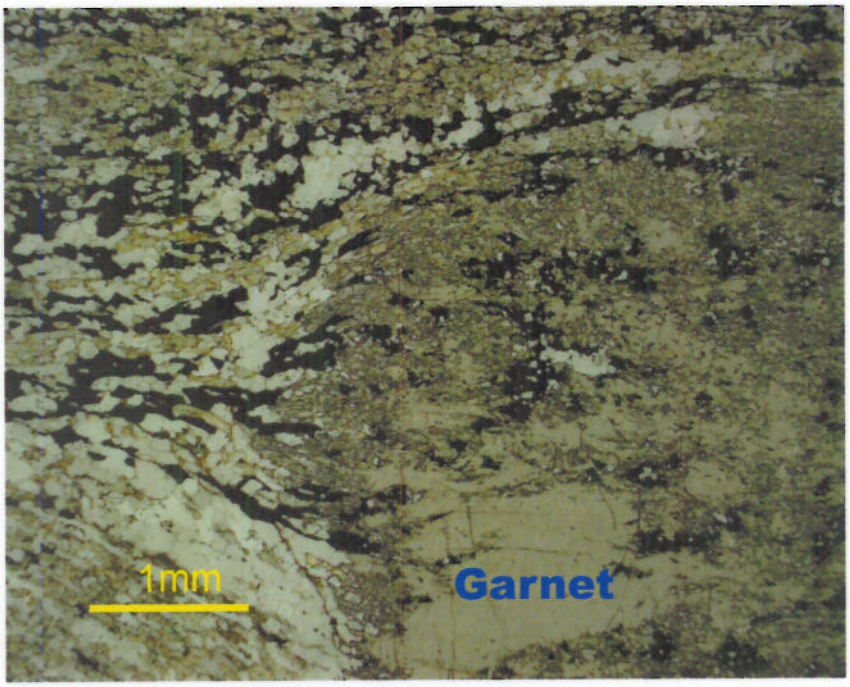

Plate 8: Garnet partly wrapped by quartz + grunerite and sulphide bands. Note that some of the sulphide bands continue into the garnet.

magnetite and ilmenite are found as small grain-boundary controlled blebs and as inclusions in garnet.

Oxide facies iron formation from the Hen claims is characterized by very well defined bands of magnetite + grunerite + calcic amphiboles interlayered with Fe-silicate + quartz rich bands. The fine-grained magnetite is grain boundary controlled, commonly exhibiting an unusual lacy to net texture (Plate 9; Plate 10). Calcic amphiboles, grunerite and quartz occur interior to the magnetite bands as small rounded xenoblasts. Grunerite also occurs in thin (2-5 mm) bands of very fine to medium grained subidioblastic blades partially replaced by calcic amphiboles. Well-defined quartz-rich bands host variable amounts of Fe-amphibole and exhibit unstrained granoblastic textures. Trace amounts of fine-grained chalcopyrite were also observed.

The sulphide facies iron formation contains a mineral assemblage similar to the silicate facies, but is host to a greater quantity of sulphides (>5%). Pyrite and pyrrhotite are the dominant sulphide species and occur as either thin well-defined bands or coarse (0.2-1.0 cm) polycrystalline masses. Both are invariably grain boundary controlled. Pyrite aggregates typically contain relict magnetite cores as well as rafts of relict pyrrhotite (Plate 11). Trace arsenopyrite occurs as coarse xenoblastic grains with loellingite and magnetite inclusions and as fine-grained disseminations (Plate 12). Trace chalcopyrite, secondary magnetite and gold form small rounded inclusions within pyrite and pyrhhotite as well as small isolated blebs. The chalcopyrite is typically concentrated at the rims of pyrite and pyrrhotite grains.

Prograde mineralogy of the Hen claims BIF is represented by garnet, grunerite, calcic amphiboles and more rarely, clinopyroxene. Prograde calcic amphiboles replace grunerite and its co-existing calcic amphibole as well as garnet on quartz-vein selvages. Retrograde mineralogy is

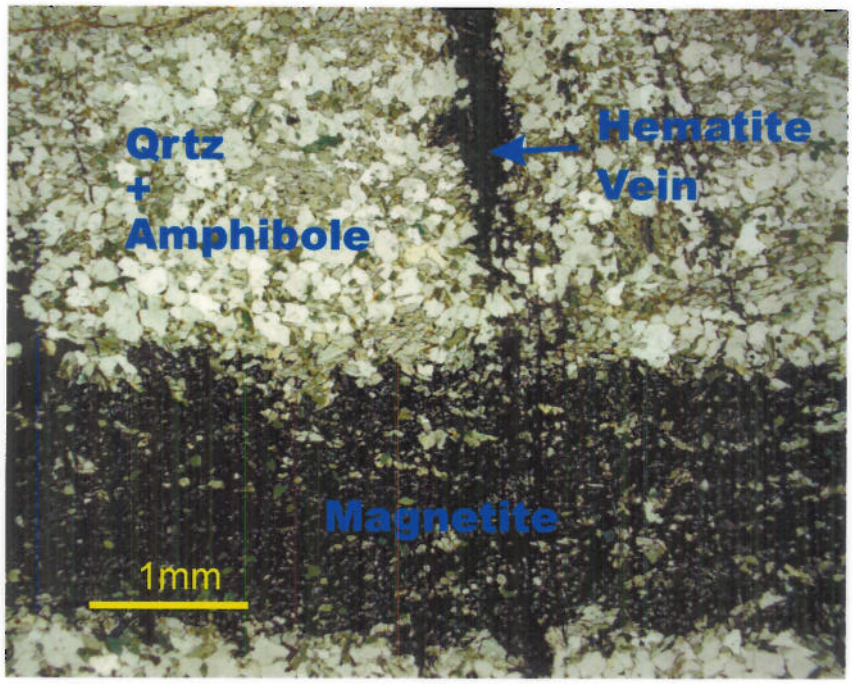

Plate 9: Bands of net textured magnetite and quartz + amphiboles. Note the crosscutting hematite vein.

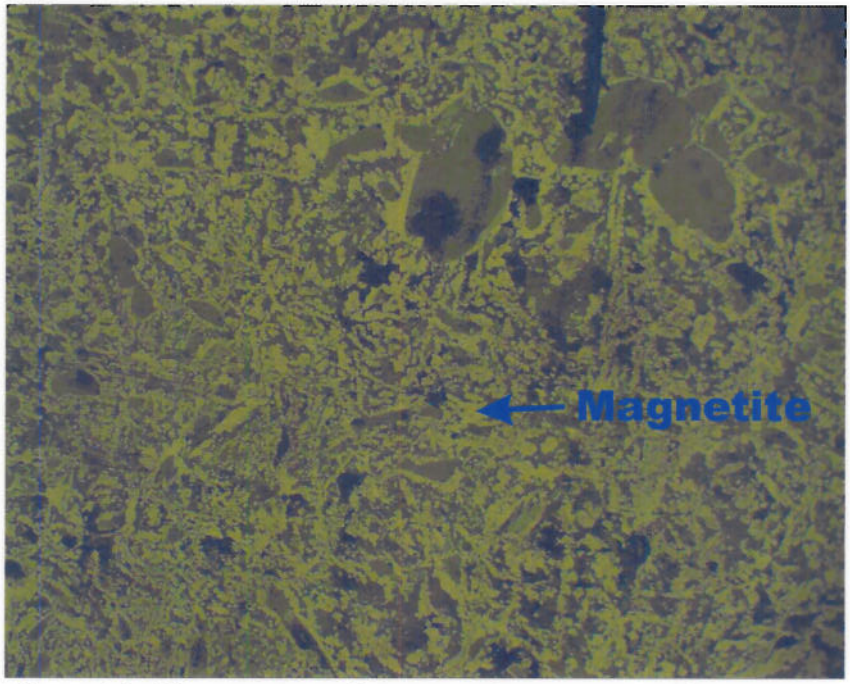

Plate 10: Net textured magnetite surrounding quartz and amphibole. Reflected light; 10X.

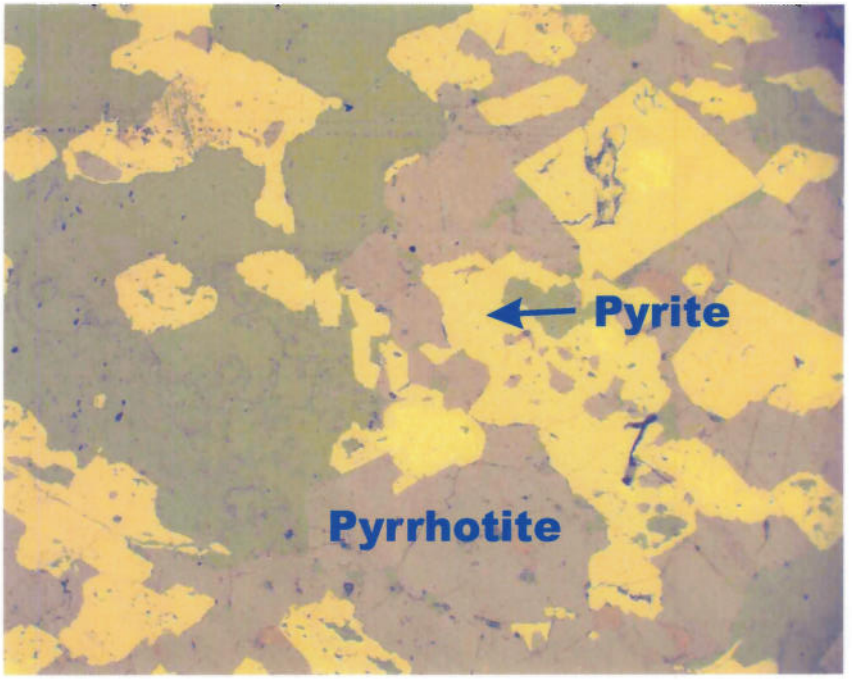

Plate 11: Subidioblastic to idioblastic pyrite with rafts of pyrrhotite. Reflected light; 10X.

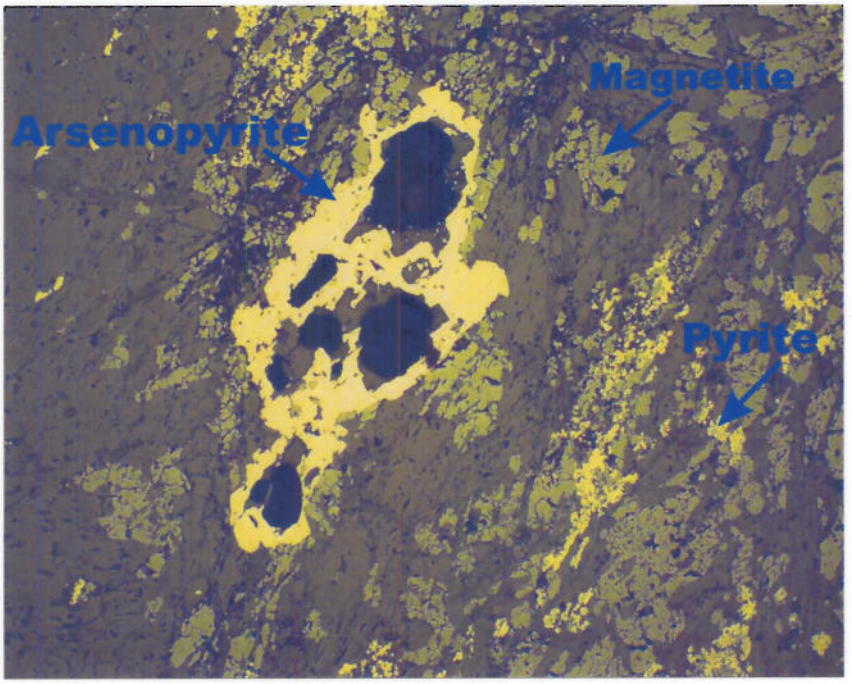

Plate 12: Coarse arsenopyrite enclosing silicates and surrounded by magnetite and pyrite. Reflected light; 4X.

characterized by significant chloritization (up to 40%), with variably intense chlorite replacement of garnet and Fe-amphiboles. Retrograde chlorite is also found as sharp-walled microveins within microbrecciated garnet porphyroblasts. Both prograde and retrograde assemblages are best observed in the silicate and sulphide facies BIFs.

3.2.2 Iron Formation on the Bear Creek Claims

In comparison to the Hen claims, the Bear Creek BIFs are characterized by less well defined banding and less retrogression. Silicate and sulphide facies dominate with rare occurrences of oxide facies. The iron formation from the Bear Creek claims is also richer in clinopyroxene and arsenopyrite.

Silicate facies iron formations of the Bear Creek Claims differ from the Hen claims in containing dominantly calcic amphiboles with only minor fine-grained relict grunerite. The green hornblende occurs as either coarse interlocking idioblasts or as patchy domains replacing clinopyroxene, grunerite and garnet. Clinopyroxene occurs as large chlorite-amphibole altered xenoblasts that are frequently highly fractured. Garnet ranges from large porphyroblasts with rounded irregular margins and calcic amphibole inclusions to microbrecciated fragments with interstitial green amphibole, chlorite and clinopyroxene. Patchy chlorite occurs in minor amounts as a replacement product of garnet, amphibole and clinopyroxene.

Pyrite and pyrrhotite are the most abundant sulphides present in the sulphide facies, with trace disseminated arsenopyrite, chalcopyrite, magnetite and gold. Pyrite frequently forms large polycrystalline masses with abundant relict pyrrhotite cores and late hematite rims (Plate 13). Both pyrrhotite and pyrite also occur as grain-boundary controlled xenoblastic blebs. Late oxidation of

pyrrhotite has resulted in liesegang rinds exhibiting several generations of magnetite and pyrite (Plate 14). A highly unusual replacement texture involving the pyrrhotization of biotite flakes was also noted (Plate 15).

3.3 Host Sediments

3.3.1 Host Sediments on The Hen Claims

The banded iron formations of the Hen claims are hosted within pelitic to psammitic metagreywackes that commonly preserve AE bouma sequences. Microbanding is defined by subtle variations in modal quartz and biotite. The main foliation as well as a locally developed spaced kink cleavage is defined by biotite, chlorite and muscovite. Porphyroblasts range in size from a few mm characteristic of staurolite and garnet, to several cm, demonstrated by andalusite. Most porphyroblasts have no obvious preferred orientation and overgrow the main foliation.

Quartz is the most abundant mineral, occurring as fine-grained granoblastic polygonal assemblages in the matrix and as inclusions within poikioblastic biotite, garnet, staurolite and amphibole. Fine-grained relict feldspars in the matrix are intensely altered to sericite. Trace disseminations of apatite, sulphides, oxides, tourmaline and carbonate occur in the matrix with quartz and feldspar.

The prograde metamorphic mineral assemblage consists of biotite, muscovite, staurolite, andalusite and more rarely, garnet and fibrolite. Retrogression of this assemblage is variably intense, dominated by white micas and to a lesser extent, chlorite. The ubiquitous aligned biotite laths in the metagreywackes occur as ragged 0.5-1.0 mm heavily chloritized grains with abundant monazite

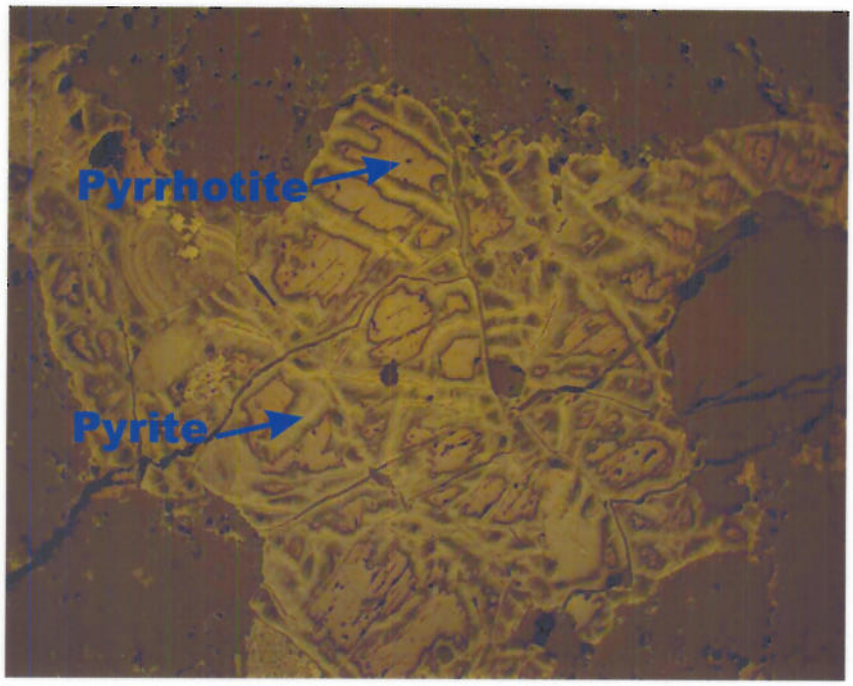

Plate 13: Large grain boundary controlled pyrite blebs with cores of pyrrhotite. Reflected light; 4X.

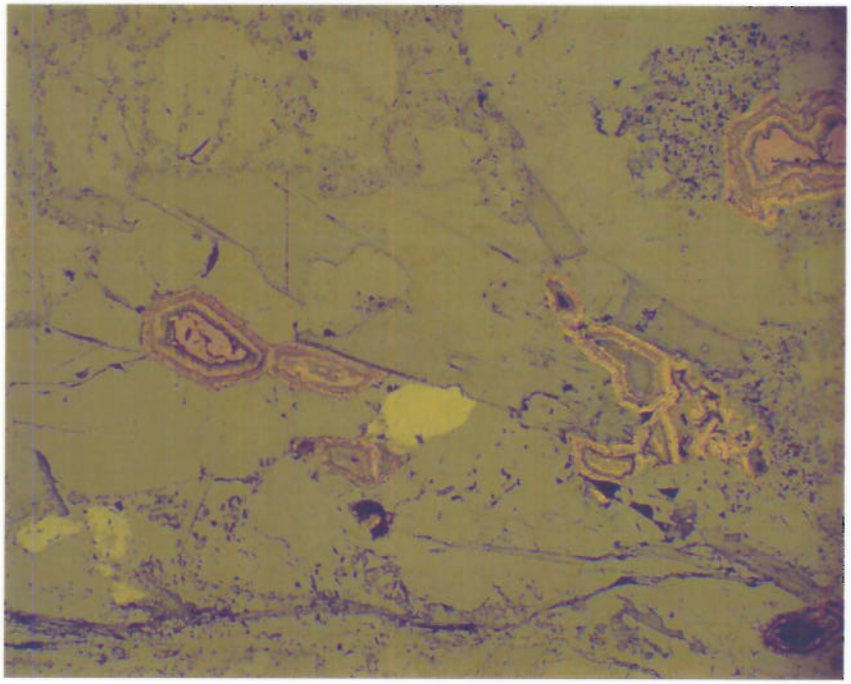

Plate 14: Pyrrhotite cores showing liesegang banding. Reflected light; 4X.

inclusions. Fresh blades of large subidioblastic retrograde muscovite are found as rims on andalusite and staurolite porphyroblasts (Plate 16) as well as fine-grained plates aligned with the primary foliation. Rare garnet occurs as 0.5 mm idioblasts interior to retrograded staurolite porphyroblasts and as small fractured crystals partly wrapped by the main foliation. Staurolite varies from 0.5 mm subidioblastic poikioblastic porphyroblasts with muscovite rims to intensely sericitized xenoblasts surrounding idioblastic garnet. Staurolite is also found as very fine rounded inclusions in the cores of andalusite porphyroblasts. Large andalusite porphyroblasts have been almost entirely altered, leaving behind small relict fragments. They exhibit cores of fine-grained quartz, biotite, tourmaline and staurolite (Plate 17) with rims of fibrolite, biotite and muscovite. The sheafy masses of fibrolite are found intergrown with muscovite and replacing biotite (Plate 18). Only one sample from the Hen claim suite (Sample RT-184) contained fibrolite. It was collected south of Crescent Lake, proximal to the sillimanite isograd.

3.3.2 Host Sediments on the Bear Creek Claims

In contrast to the Hen claims, the Bear Creek claims are noticeably higher grade, as illustrated by the abundance of fibrolite and lack of muscovite and staurolite. In general, the enveloping metasediments from Bear Creek also contain more abundant oxides and sulphides in the form of magnetite, pyrite and pyrrhotite, suggesting a more mixed iron formation + pelite assemblage. The prograde metamorphic mineral assemblage is represented by biotite, garnet, cordierite, andalusite and sillimanite. Garnet occurs as large amoeboid-shaped porphyroblasts exhibiting rims of cordierite altered to sericite (Plate 19). As in the Hen claims, there is ubiquitous oriented biotite which here

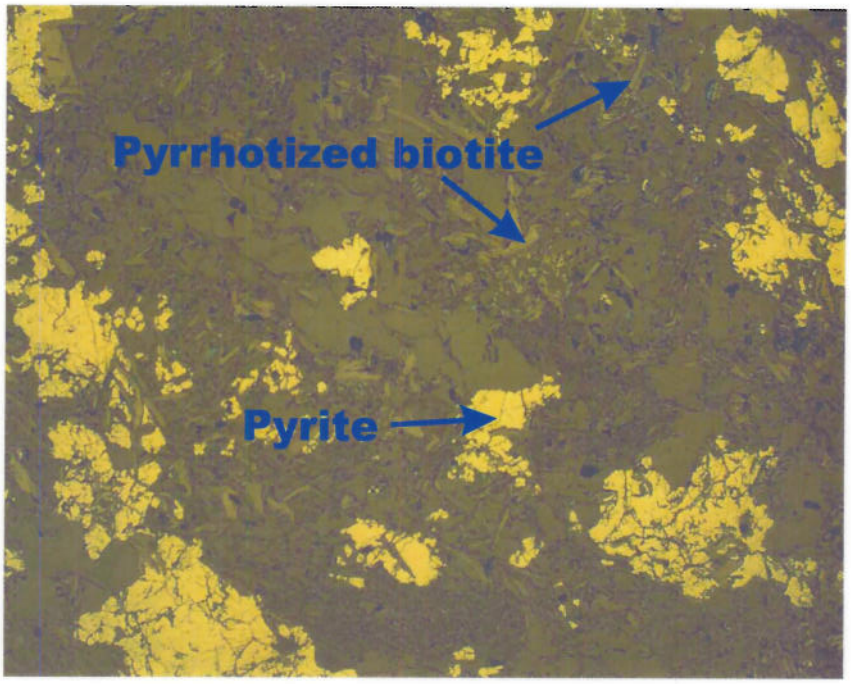

Plate 15: Coarse pyrite with fine pyrrhotized biotite flakes. Reflected light; 4X.

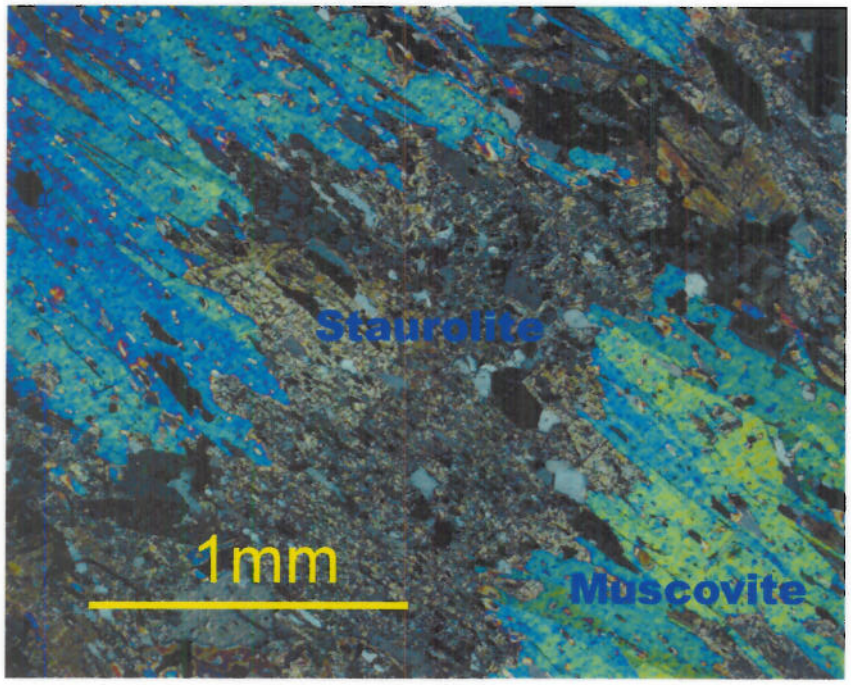

Plate 16: Staurolite porphyroblasts with coarse muscovite rims.

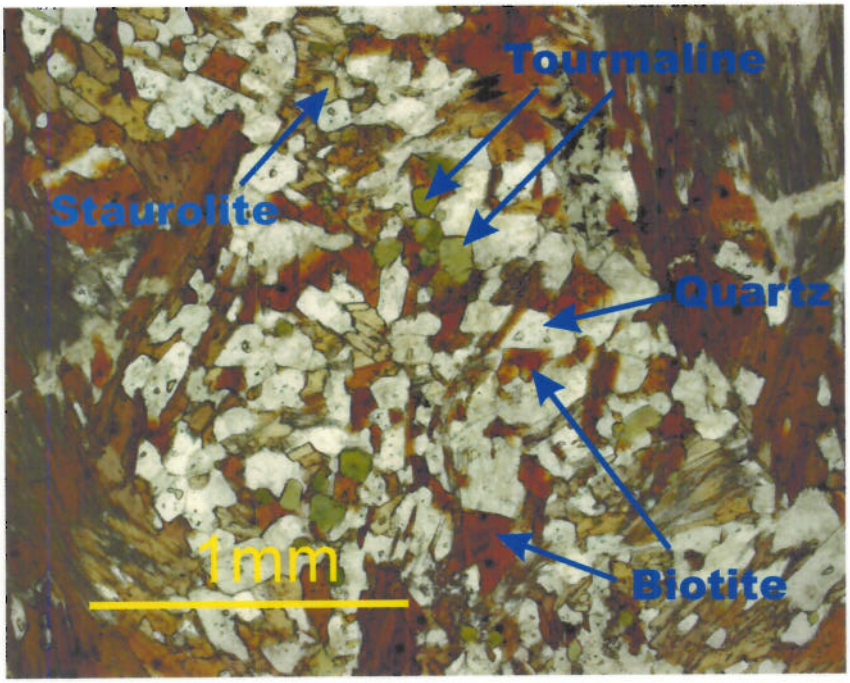

Plate 17: Biotite, quartz, staurolite and tourmaline in the core of an andalusite porphyroblast.

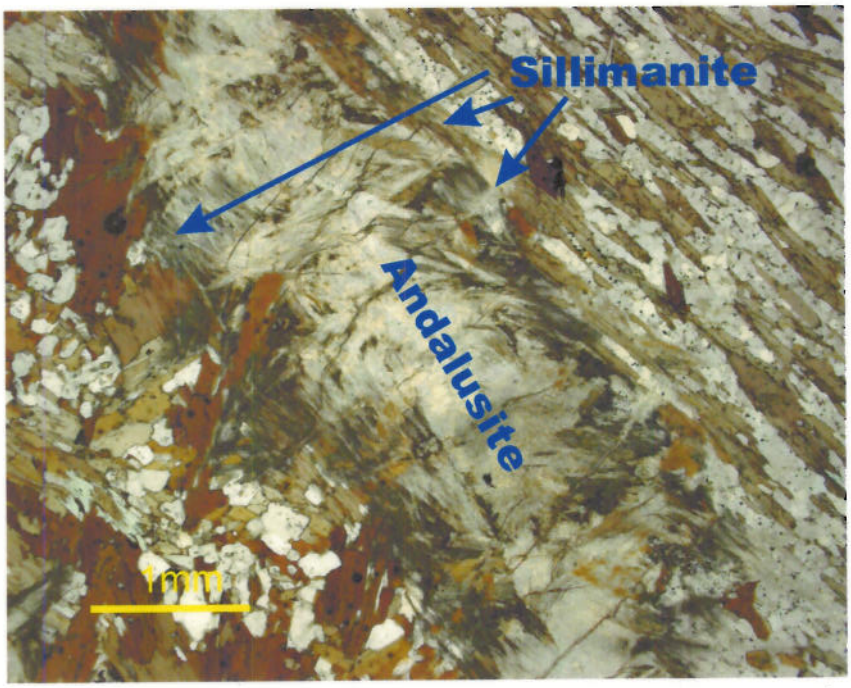

Plate 18: Sillimanite bundles replacing biotite on the margins of an andalusite porphyroblast.

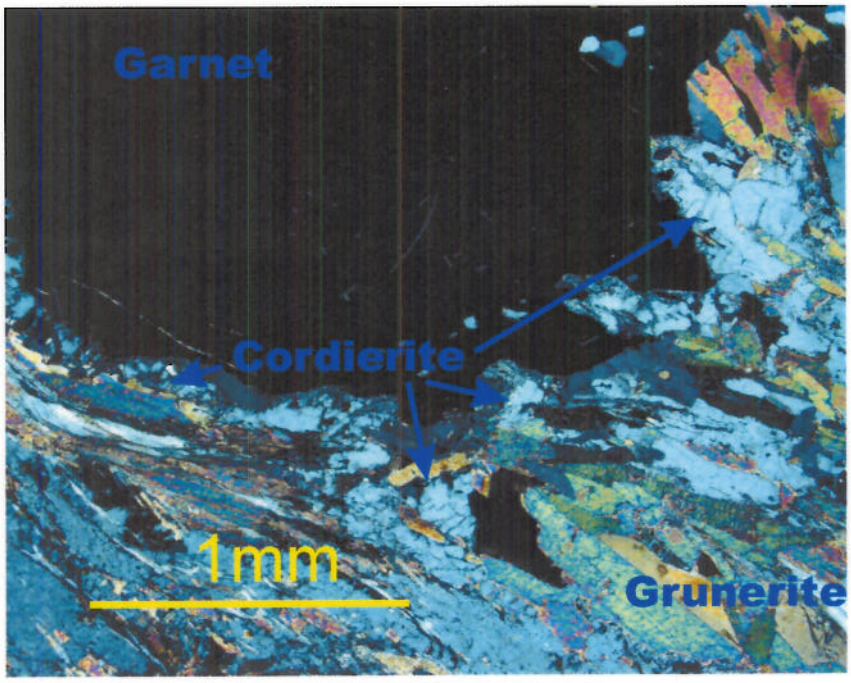

Plate 19: Cordierite rims on garnet.

shows only minor chlorite replacement. Frequently, the biotite exhibits thin rims of iron oxides and large patchy replacement by the associated oxides/sulphides. In sample TR1-15 pyrrhotite exhibits alternating liesegang bands of pyrite and magnetite. Andalusite is typically completely sericitized, but may also be found as 1-2 mm idioblasts with sericite rims. In most cases andalusite is difficult to distinguish from cordierite due to degree of retrogression. Large lensoidal bundles of fibrolite generally replace biotite exterior to cordierite rimmed garnet. Fibrolite also occurs as inclusions within quartz and feldspar. Generally, the fibrolite is aligned along a poorly developed S_3 cleavage. Patches of retrograde muscovite 1-2 mm in diameter are regularly encountered, representing sites of staurolite and andalusite porphyroblasts.

Retrogression of the Bear Creek schist/gneiss is dominated by sericitization. Abundant feldspars regularly show intense sericite alteration, as do former staurolite/andalusite porphyroblasts. Chlorite alteration is minimal, confined to minor overprinting of a few biotite laths and occurring with sericite bordering garnet porphyroblasts.

Chapter 4.0

Geochemistry

4.1 Bulk Rock Chemistry

Bulk rock analysis was carried out on nine samples representing Hen and Bear Creek BIFs and enveloping metasediments. Results are listed in Table 1 and Figures 8 and 9 (also see Appendix A). Total iron values for the iron formation (Figure 8) are consistently above 20 Wt%. Amphiboles and iron sulphides/oxides are the primary contributor to the high iron values within the BIF. Sample RT-131 contains 40-45% magnetite and iron amphibole, which accounts for its extremely high iron content. The CaO values range from 0.29 (Sample RT-131) to 9.10 Wt% (Sample TR2-11). Samples with high modal percents of calcic amphibole correlate well with elevated CaO values. The large CaO value in sample RT-147 is attributed to hornblende coexisting with clinopyroxene. Al_2O_3 values range from 1.43 (Sample RT-131) to 13.87 Wt % (Sample RT-188) corresponding directly with lower and higher abundances of garnet. Elevated MgO and MnO values roughly correlate with high modal percents of garnet and/or calcic amphibole. Slightly higher Na_2O and K_2O values in sample TR2-11 reflect the more abundant feldspars within the Bear Creek BIF. Noticeably elevated TiO_2 and P_2O_5 are attributed to ilmenite and monazite, which are common as inclusions within biotite, chlorite, amphibole and garnet.

Metasediments from the Hen and Bear Creek claims (Figure 9) have elevated iron values (up to 15%) and high Al_2O_3 values. Higher Al_2O_3 values are related to abundant micas and aluminosilicate minerals. The Al enrichment in the metasediments is most likely related to hydrothermal leaching of alkalies and SiO_2. Higher Na_2O and K_2O values in the metasediment are due to more abundant feldspars compared to the BIF.

Table 1: Bulk Chemistry of iron formation and enveloping metasediments: major oxide weight percents normalized to 100%.

SAMPLE	SiO_2	TiO_2	Al_2O_3	Fe_2O_3	MnO	MgO	CaO	K_2O	Na_2O	P_2O_5	L.O.I.	Total
Iron Formation												
TR2-11	43.26	1.45	10.80	25.54	1.47	4.80	9.10	0.42	0.17	0.04	2.95	100
RT-131	47.84	0.05	1.43	48.95	0.03	1.74	0.29	0.04	0.01	0.13	-0.51	100
RT-147	63.93	0.09	2.94	21.69	0.14	0.96	8.19	0.01	0.01	0.06	1.97	100
RT-171B	58.57	0.07	2.76	33.23	0.06	1.88	2.99	0.11	0.01	0.16	0.16	100
188	51.24	0.19	13.87	29.37	0.12	1.34	3.29	0.03	0.01	0.09	0.44	100
189	56.22	0.11	3.23	36.26	0.07	0.87	3.15	0.08	0.01	0.10	-0.11	100
191	67.52	0.04	2.35	26.65	0.05	1.03	1.16	0.07	0.01	0.18	0.93	100
Metasediment												
171A	56.12	0.68	19.33	11.21	0.09	4.12	0.25	3.65	0.53	0.12	3.90	100
TR2-3	42.79	1.03	32.99	9.67	0.09	4.93	0.58	2.45	0.77	0.05	4.66	100

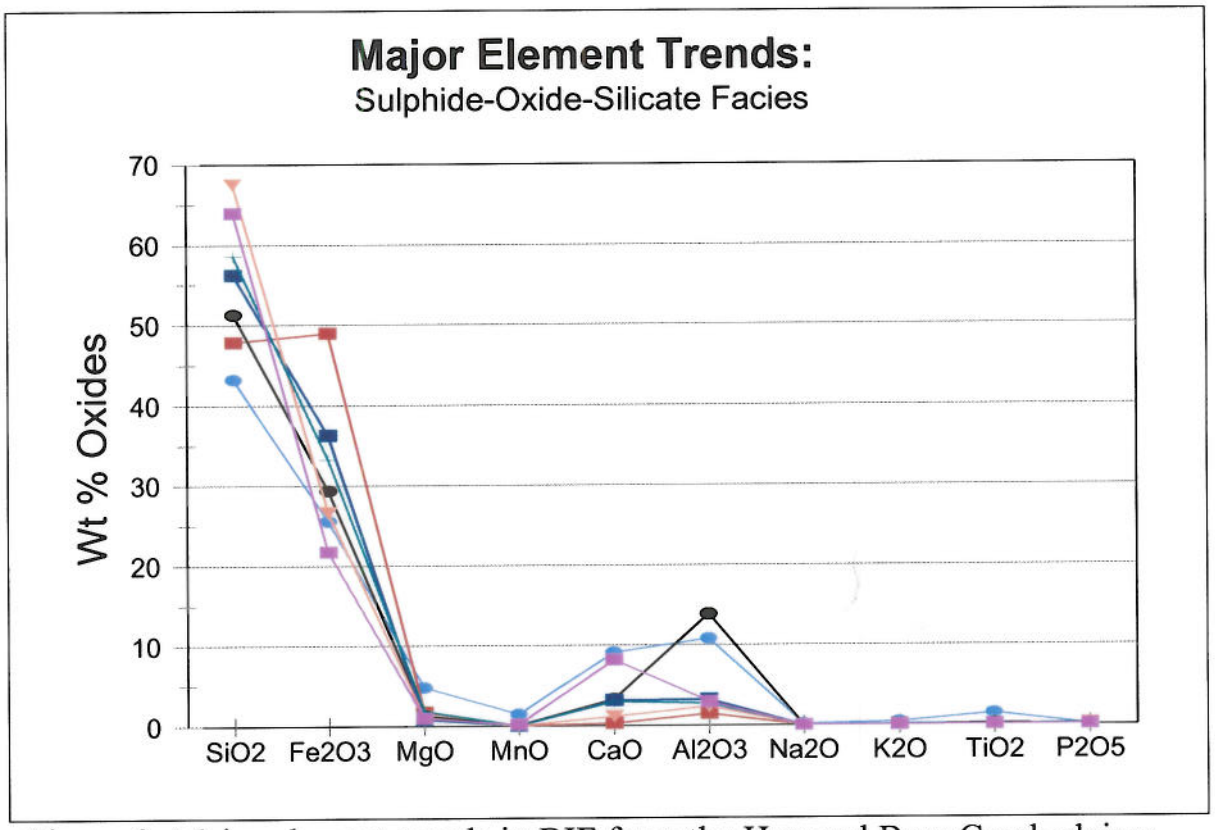

Figure 8: Major element trends in BIF from the Hen and Bear Creek claims.

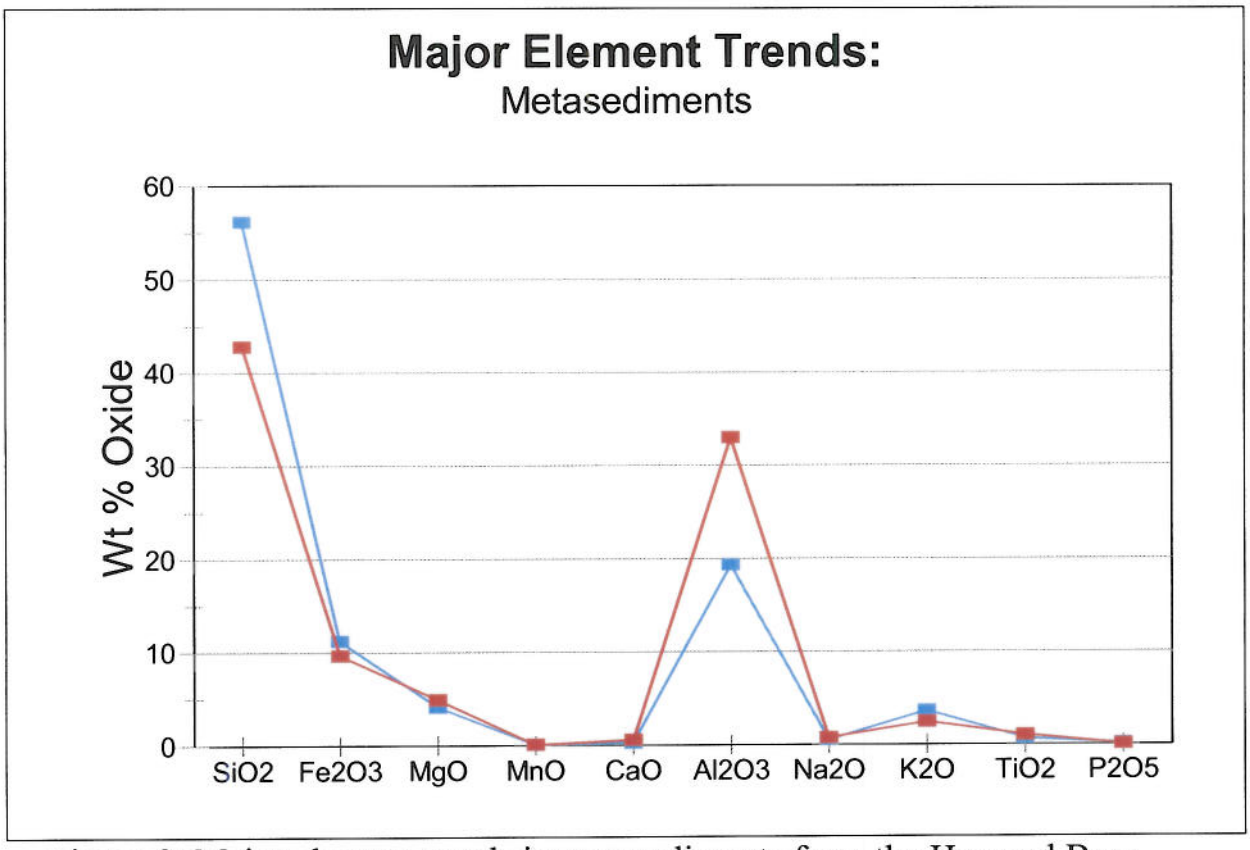

Figure 9: Major element trends in metasediments from the Hen and Bear Creek claims.

4.2 Mineral Chemistry

Mineral analyses were carried out on hornblende, garnet, biotite, muscovite and chlorite (Appendix B). An attempt was made to choose the most unaltered grains, and to analyze grains in several sections from widely spaced localities.

Figures 10 and 11 illustrate amphibole compositions from BIF on the Hen claims. Iron-rich amphiboles from the claims have two distinct chemistries. The calcium-poor species plots very close to end-member grunerite (Figure 10), while calcium-rich amphiboles plot as ferrohornblende and ferrotschermakite (Figure 11).

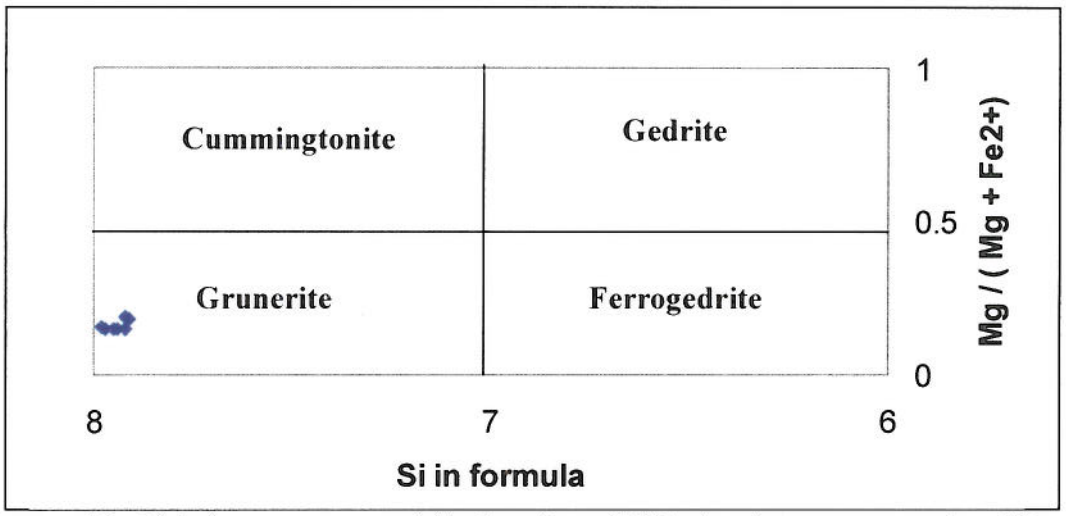

Figure 10: Calcium poor amphiboles from BIF plotting as grunerite: Hen claims.

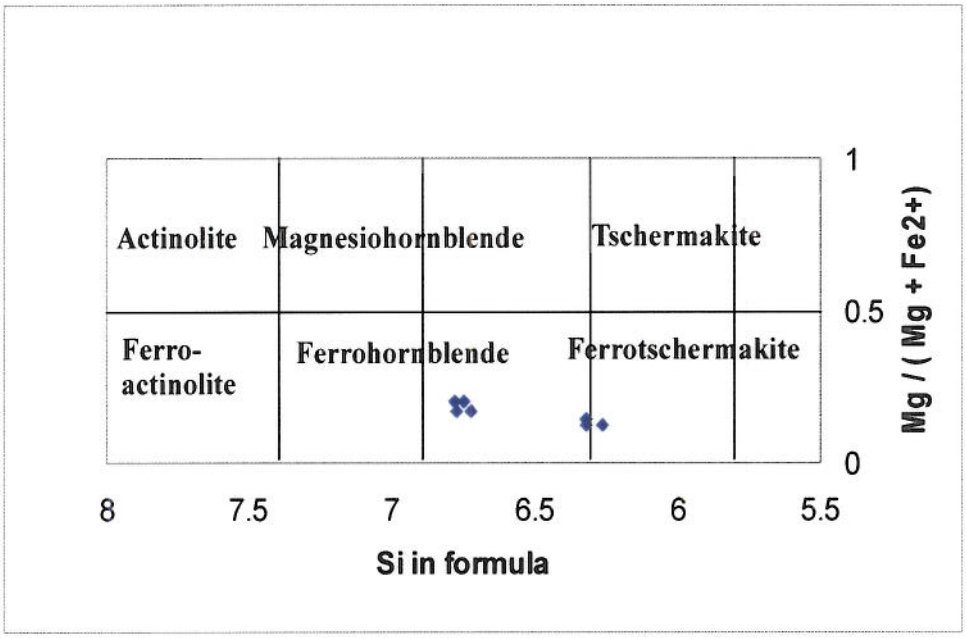

Figure 11: Calcium rich amphiboles from BIF plotting as ferrohornblende and ferrotschermakite: Hen claims.

Garnet compositions are shown in Figure 12. In general, a high iron almandine species of garnet characterizes the Hen claims. Four of the samples show slight enrichment in the grossular endmember (Domain 1; Figure 12). Elevated calcium in the garnet (Domain 2; Figure 12) is attributed to the same calcic metasomatism indicated by replacement of grunerite by calcium-rich amphiboles ± hedenbergite. Spessartine does not represent a significant component of the garnets, the highest Mn value being 0.46%.

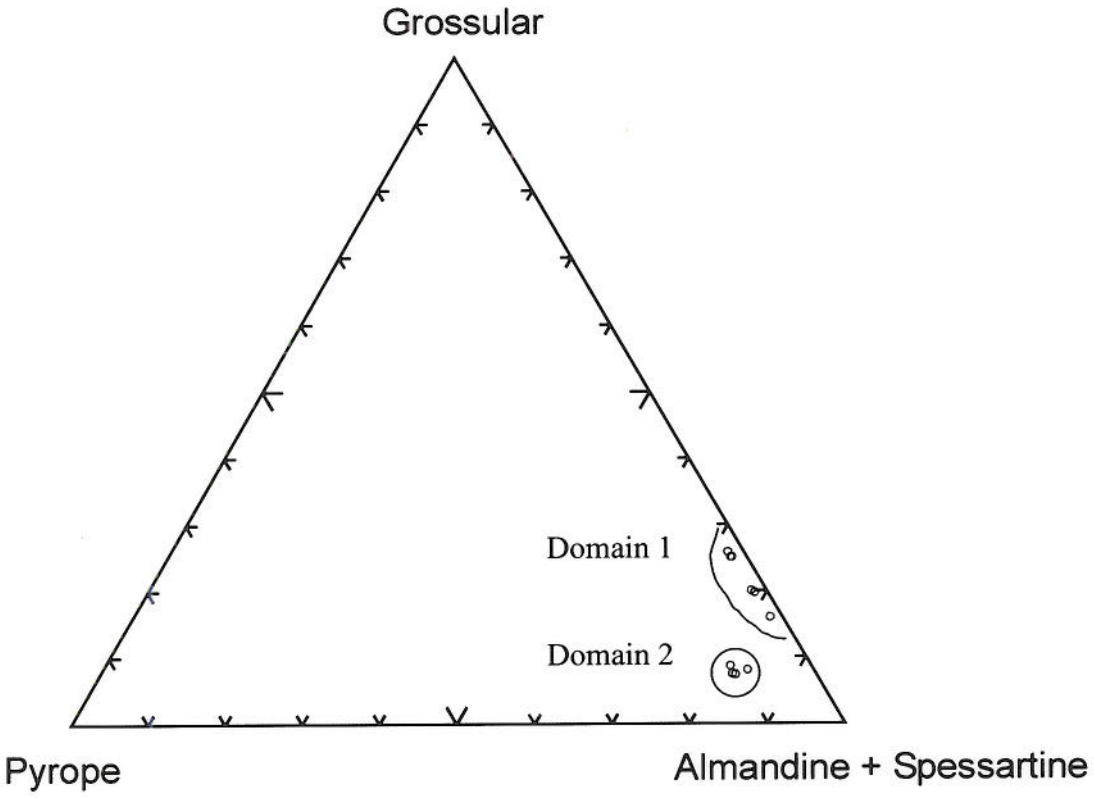

Figure 12: Composition of garnets from BIF plotting as high iron almandine series with minor calcium enrichment.

Muscovite compositions from the enveloping metasedimentary rocks are illustrated in Figures 13 and 14. Figure 13 reveals that muscovite from the Hen claims has a significant paragonitic component. Two distinct muscovite compositions are displayed in

Figure 14. Low Fe + Ti + Mn + Mg values are present in paragonitic muscovite that replaces staurolite and andalusite (Domain 1; Figure 14) while phengitic muscovite found in close association with biotite and chlorite tends to have elevated Fe values (Domain 2; Figure 14).

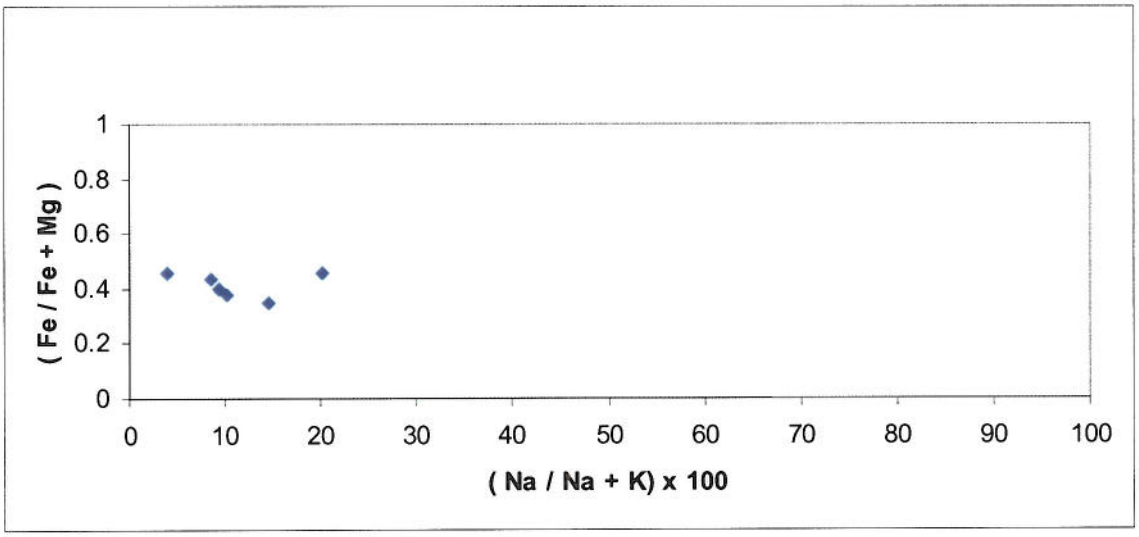

Figure 13: Composition of muscovite from metasediments showing a significant paragonitic component.

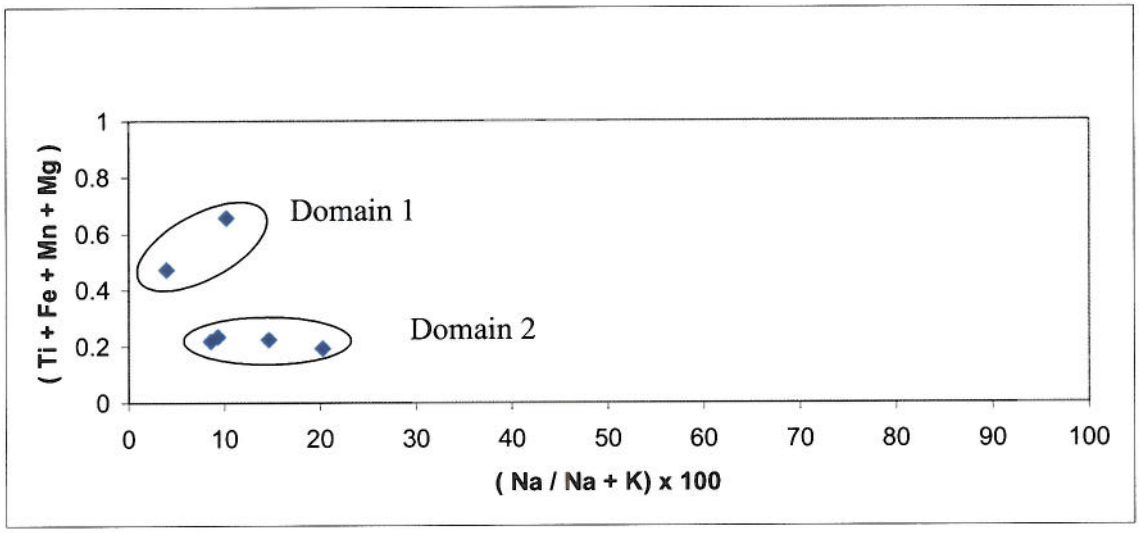

Figure 14: Composition of muscovite from metasediments. Domain 1 represents retrograde muscovite replacing staurolite and andalusite. Domain 2 are muscovite grains taken from biotite/chlorite rich domains.

The compositions of biotite and chlorite from the metasediments and BIF are illustrated in Figure 15 and 16 respectively. Biotite is typically chloritized, explaining why biotite and chlorite compositions are very similar. Retrograde chlorite tends to be slightly more magnesian compared to precursor biotite.

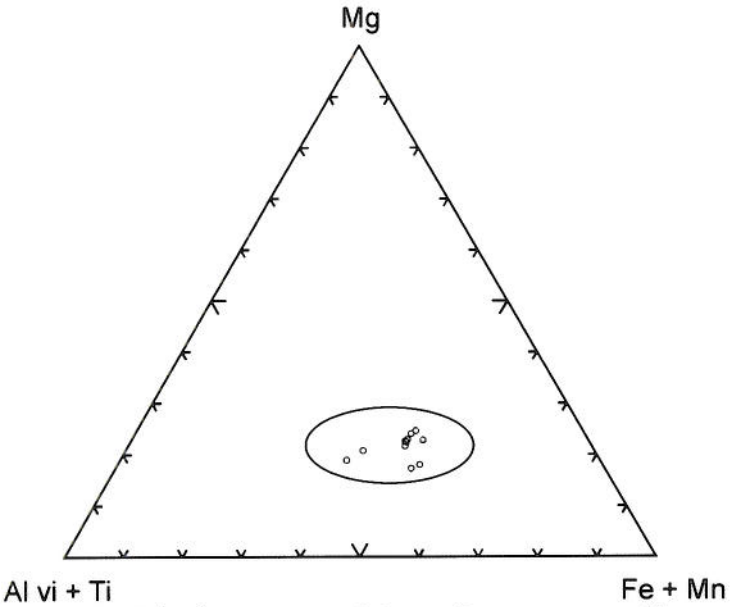

Figure 15: Biotite compositions from metasediments.

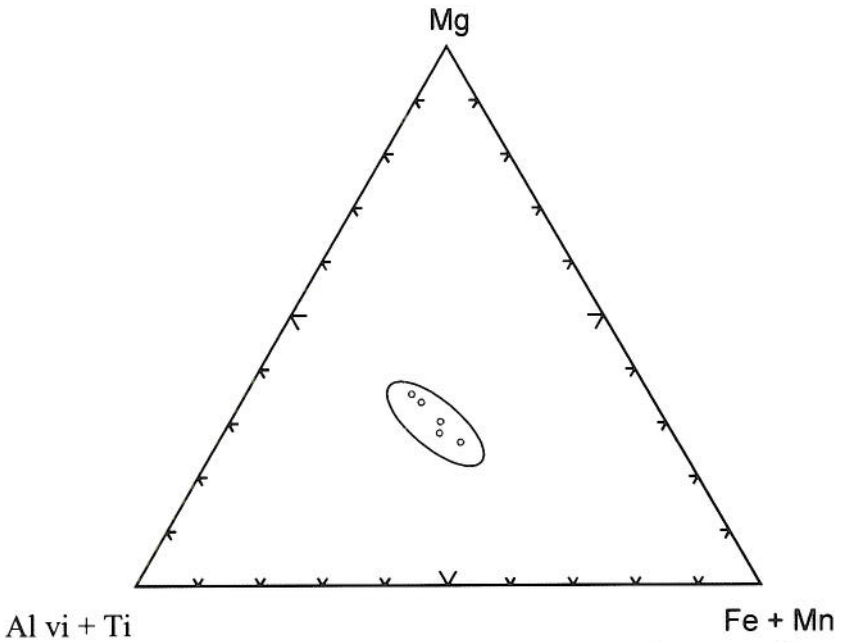

Figure 16: Chlorite compositions from BIF and metasediments.

4.3 Trace Element Chemistry

Forty-nine trace elements were analyzed from BIF collected on the Hen and Bear Creek claims (Appendix C). The most significant elements are shown below in Table 2.

Table 2: Trace element data from BIF on the Hen and Bear Creek claims.

Sample #	Au	As	Al	Ca	Fe	Mg	Na	S	Ti	Pb	Zn	Cu
	ppb	ppm	%	%	%	%	%	%	%	ppm	ppm	ppm
RT-131	52	175	1.22	1.71	23.2	1.09	0.02	0.351	0.09	14	24	20
RT-135	9	18.8	4.65	0.57	15.8	2.83	0.46	0.014	0.43	15	76	9
RT-138	12	400	1.62	0.91	26.7	0.76	0.02	0.239	0.16	11	43	23
RT-139	264	4.4	1.20	1.74	25.4	0.83	0.06	0.011	0.11	19	28	10
RT-142	179	0	1.08	1.19	27.9	1.18	0.04	0.186	0.08	39	22	18
RT-147	123	13.5	2.96	6.42	12.9	1.06	0.08	2.241	0.07	8	59	571
RT-148	6	2.3	4.27	0.87	4.7	1.66	2.79	0.781	0.45	24	111	106
RT-150	322	303	0.57	0.63	29.5	1.29	0.03	0.682	0.04	32	30	20
RT-151	60	7030	4.71	2.44	18.9	2.50	0.12	1.797	0.20	4	114	206
RT-152	563	195	1.36	1.26	20.4	1.43	0.04	4.276	0.15	21	99	262
RT-153	1020	13.2	0.90	1.04	30.4	0.67	0.07	1.257	0.06	17	26	95
RT-154	677	3390	1.54	2.05	23.1	1.25	0.13	6.634	0.06	27	40	373
RT-155	6700	23.6	2.19	4.02	22.9	1.32	0.27	3.898	0.12	14	36	66
RT-156A	91	8.1	1.60	4.83	16.8	1.06	0.2	0.123	0.08	16	37	16
RT-156B	162	29.3	1.04	4.71	13.1	2.40	0.01	4.807	0.04	6	12	88
RT-157	162	295	0.71	0.39	26.7	1.70	0.02	0.992	0.04	23	18	23
RT-159	89	3	1.76	4.40	26.7	0.91	0.11	1.134	0.06	13	17	136
RT-160	85	8.8	3.82	1.76	18.8	1.73	0.02	3.502	0.28	3	28	1008
RT-163	26	5.7	1.55	1.94	29.2	1.25	0.19	0.443	0.11	32	35	23
RT-164	29	7.3	3.79	0.94	20	1.72	0.05	12.544	0.22	58	37	172
RT-171B	495	907	0.99	1.26	24.4	0.98	0.09	6.806	0.06	33	30	140
RT-179	16	5.8	1.08	0.69	28.5	0.57	0.02	0.382	0.08	36	16	50
RT-186	332	7.2	3.07	3.58	21.2	1.67	0.1	1.654	0.20	16	60	83
RT-187A	269	35.5	2.82	2.88	17.3	0.92	0.05	3.491	0.11	12	39	184
RT-187B	664	58.9	2.57	3.81	20.8	0.76	0.04	1.631	0.11	27	44	133
RT-188	102	16.8	2.80	1.60	20.6	0.82	0.06	6.661	0.25	4	47	336
RT-189	87	38.5	0.84	2.15	28.7	0.39	0.09	0.818	0.06	45	24	74
RT-191	553	191	0.60	0.71	25.4	0.77	0.07	1.429	0.03	39	17	55
ND-203	61	10.3	1.16	7.04	14.5	0.50	0.03	5.888	0.04	29	68	471
ND-205	126	12.4	1.19	3.33	26.3	0.85	0.04	2.715	0.04	15	47	220
ND-206	939	7.8	1.08	2.49	18.5	0.87	0.15	2.884	0.07	27	40	116
ND-207	11	3.9	3.32	1.41	18.9	1.61	0.04	5.029	0.19	25	50	376
ND-210	31	24	1.85	3.15	23.6	1.00	0.14	7.440	0.10	33	52	789
ND-213	51	13.4	3.14	4.23	16.4	1.66	0.18	2.218	0.21	6	57	255
ND-214	125	5.8	4.19	2.09	18.2	1.39	0.01	0.485	0.19	17	50	141
ND-215	161	2.9	1.95	2.23	15.4	1.27	0.12	1.202	0.12	19	52	131
ND-217	428	2.6	2.15	3.08	22.9	1.45	0.08	0.097	0.06	24	59	34
ND-218	70	0	0.49	1.20	28.6	0.47	0.05	0.191	0.03	34	14	17
ND-219	60	3.5	0.56	1.11	28.4	0.76	0.04	0.209	0.04	15	16	23

Sample #	Au	As	Al	Ca	Fe	Mg	Na	S	Ti	Pb	Zn	Cu
	ppb	ppm	%	%	%	%	%	%	%	ppm	ppm	ppm
ND-221	3	12.3	1.42	15.70	5.18	9.59	0.02	0.188	0.06	0	4	166
ND-222	17	284	4.47	10.42	12.9	2.97	0.07	0.039	0.10	0	0	17
ND-223	774	90	2.34	0.76	6.65	1.87	0.09	2.245	0.12	48	33	354
ND-225	28	392	3.94	1.72	15.3	1.75	0.04	0.061	0.27	15	57	14
ND-226a	5	-0.5	2.94	1.17	15.4	2.14	0.02	0.127	0.20	15	76	26
ND-226B	5	22.7	3.79	0.43	16.7	2.09	0.03	2.800	0.25	30	32	52
ND-233	22	5.1	10.86	0.36	4.16	2.54	2.52	0.320	0.57	11	73	40
ND-238	1500	17.1	0.53	0.42	28.1	1.01	0.04	2.574	0.04	31	16	68
ND-240	15	12.6	4.51	0.22	17.2	2.43	0.02	1.029	0.27	16	50	76
ND-241	229	59.8	0.50	5.76	25.4	3.69	0.02	0	0.04	30	45	14
ND-242	208	351	0.31	11.68	4.81	6.56	0.03	0.073	0.03	227	42	7
ND-243	6	50.6	0.52	0.91	27.3	1.17	0.06	0.243	0.04	9	14	22
ND-246	49	162	0.55	5.89	3.22	2.95	0.02	0.049	0.08	903	26	6
PM-182C	692	160	1.80	3.99	16.6	0.48	0.08	5.542	0.04	19	42	501
PM-162	0	3	0.96	0.20	1.95	0.77	0.07	0.501	0.05	0	21	48
PM-182	1790	98.4	1.58	6.52	15.7	0.46	0.02	5.655	0.03	22	53	381
PM-176	2	96.7	6.89	5.70	10.7	3.98	0.94	2.264	1.34	10	165	195
PM-179	0	3.2	5.56	2.52	8.62	4.73	1.42	0.290	1.63	5	90	48
TR1-9	76	2420	2.98	1.15	1.76	0.44	2.44	0.131	0.11	38	37	35
TR1-11	59	377	2.27	2.39	23.5	1.28	0.09	0.123	0.18	34	37	42
BEAR8	3820	56600	1.83	0.32	18.3	0.98	0.05	13.345	0.08	35	27	641
TR2-3	36	7.1	7.15	0.32	7.38	2.46	0.97	2.532	0.42	16	119	187
TR2-5	61	5.7	1.15	1.56	8.22	1.17	0.05	4.375	0.07	17	39	481
TR2-7A	0	3.5	1.79	0.03	19.8	0.61	0.02	14.124	0.17	44	339	285
TR2-8	109	4.2	3.01	6.80	15.6	2.03	0.25	4.687	0.34	24	232	142
TR2-9	25	0	3.09	0.03	5.61	0.43	0.4	6.978	0.36	55	40	50
TR2-11	23	0	3.17	7.66	16.4	2.25	0.19	3.049	0.16	27	135	101

Figure 17 illustrates a general association of arsenic with gold. When gold is present in anomalous amounts, arsenic is generally elevated. Arsenic is also roughly associated with high sulphur values (pyrite and pyrrhotite). Figure 18 demonstrates the relationship between gold and total iron + sulphur. High gold values correspond to high iron + sulphur, although elevated iron and sulphur does not necessarily indicate high gold. Figure 19 displays the association of gold with copper. High gold values often indicate traces of chalcopyrite, however, the reverse is not always true.

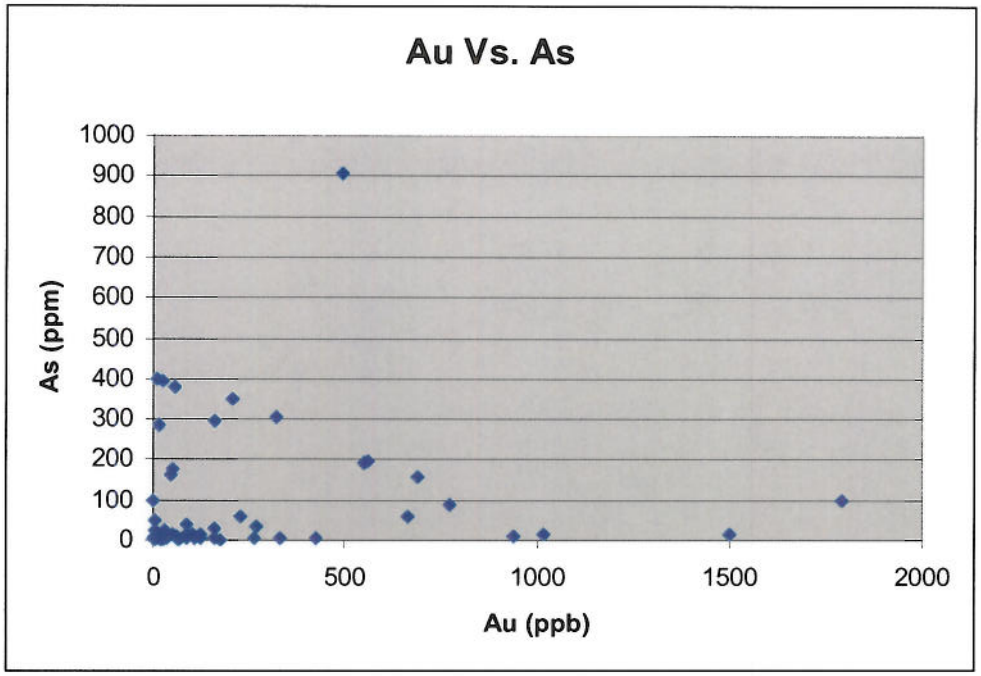

Figure 17: Gold Vs. arsenic from BIF on the Hen and Bear Creek claims. Elevated gold values are often associated with high arsenic.

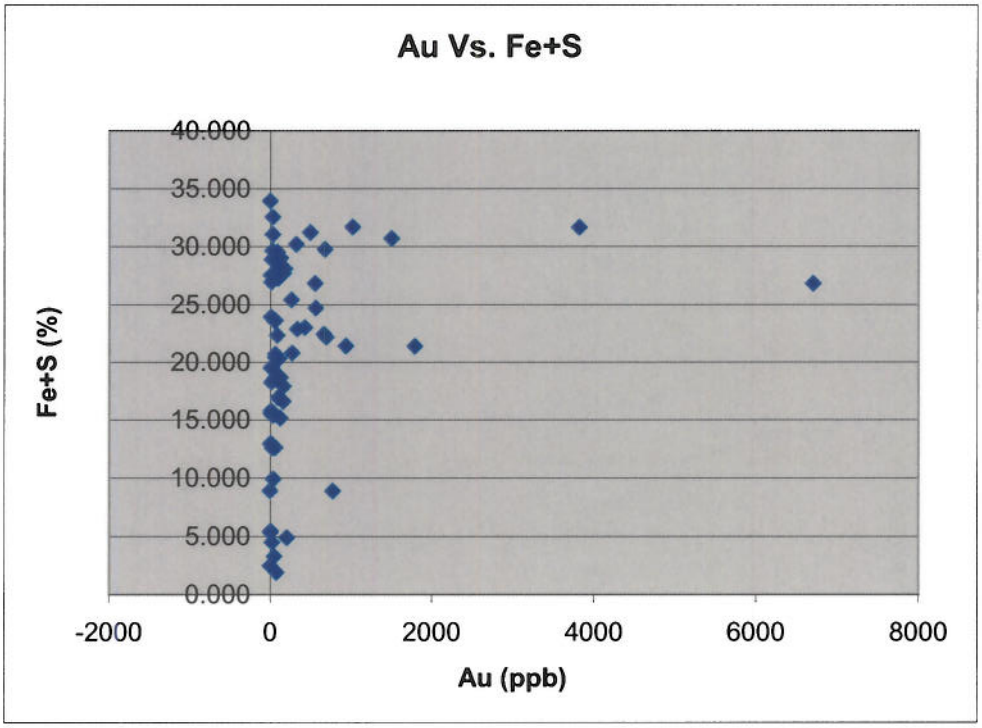

Figure 18: Gold Vs. Total Fe + S from BIF on the Hen and Bear Creek claims. High gold values are linked to high Fe + S.

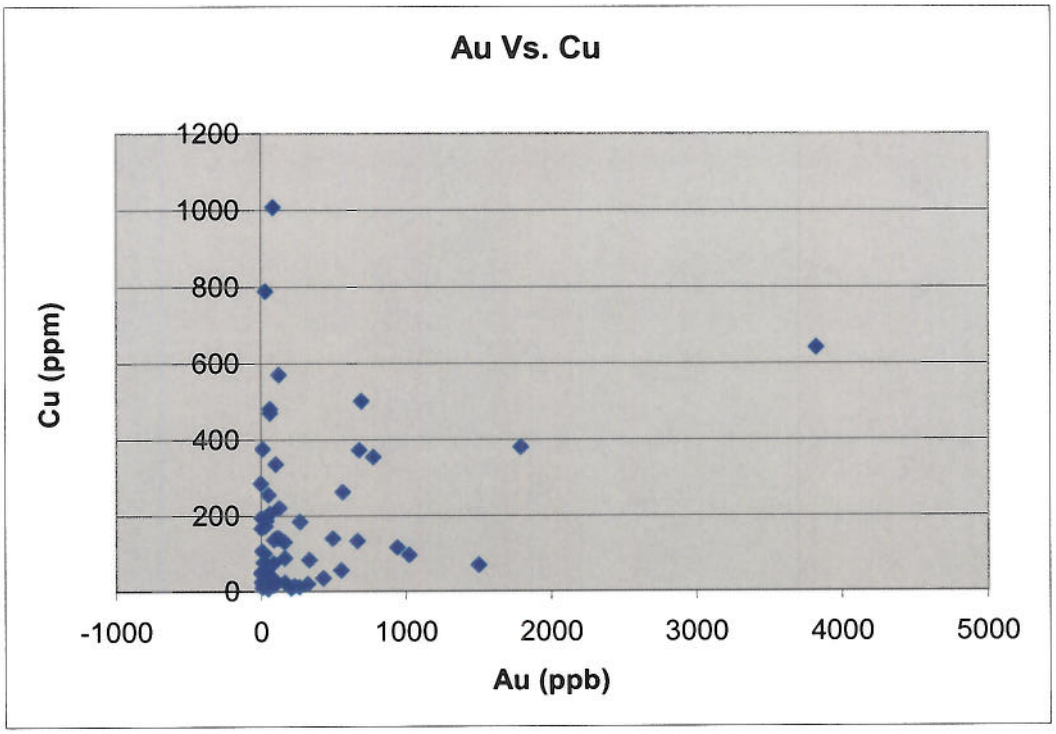

Figure 19: Gold Vs. copper from BIF on the Hen and Bear Creek claims. Elevated gold is generally associated with high copper.

Sample locations and gold values in g Au/t for the Hen and Bear Creek claims are illustrated in Figures 20 and 21. The highest gold values from the Hen claims were obtained east of Unsafe Lake (Samples RT-154: 0.677g Au/t and RT-155: 6.7g Au/t; Figure 20), consistent with Echo Bay Mines exploration results (Fraser *et al.*, 1985). Sample RT-171B was collected from an outcrop-scale isoclinal fold on the Hen claims, and also shows significant gold mineralization (0.495 g Au/t; Figure 20). The highest gold value from the Bear Creek claims was obtained from an arsenopyrite rich sample (BEAR8: 3.82g Au/t; Figure 21) on the western edge of the Egg BIF.

Gold is preferentially hosted within silicate and sulphide facies BIF from both the Hen and Bear Creek claims. There is a relatively strong correlation between degree of sulphidization and gold content, although several low-sulphide silicate/oxide-rich samples contained anomalous gold (e.g. RT-139 and ND-217; Table 2). The sulpide

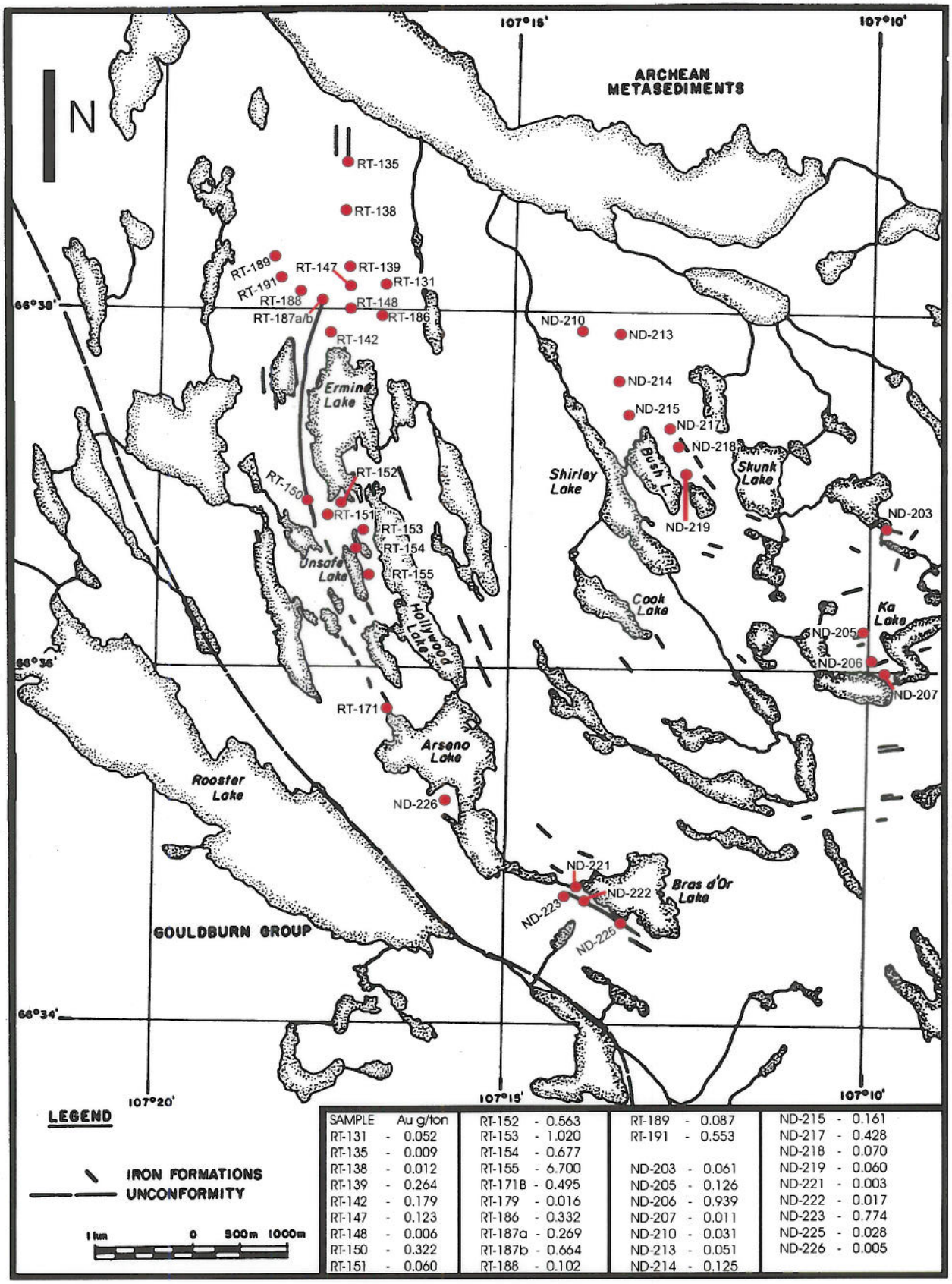

SAMPLE	Au g/ton
RT-131	0.052
RT-135	0.009
RT-138	0.012
RT-139	0.264
RT-142	0.179
RT-147	0.123
RT-148	0.006
RT-150	0.322
RT-151	0.060
RT-152	0.563
RT-153	1.020
RT-154	0.677
RT-155	6.700
RT-171B	0.495
RT-179	0.016
RT-186	0.332
RT-187a	0.269
RT-187b	0.664
RT-188	0.102
RT-189	0.087
RT-191	0.553
ND-203	0.061
ND-205	0.126
ND-206	0.939
ND-207	0.011
ND-210	0.031
ND-213	0.051
ND-214	0.125
ND-215	0.161
ND-217	0.428
ND-218	0.070
ND-219	0.060
ND-221	0.003
ND-222	0.017
ND-223	0.774
ND-225	0.028
ND-226	0.005

Figure 20: Sample locations and gold values for the Hen claims. Unplotted samples are located north of the Hen claims proper. (Modified from Fraser *et al.,* 1985).

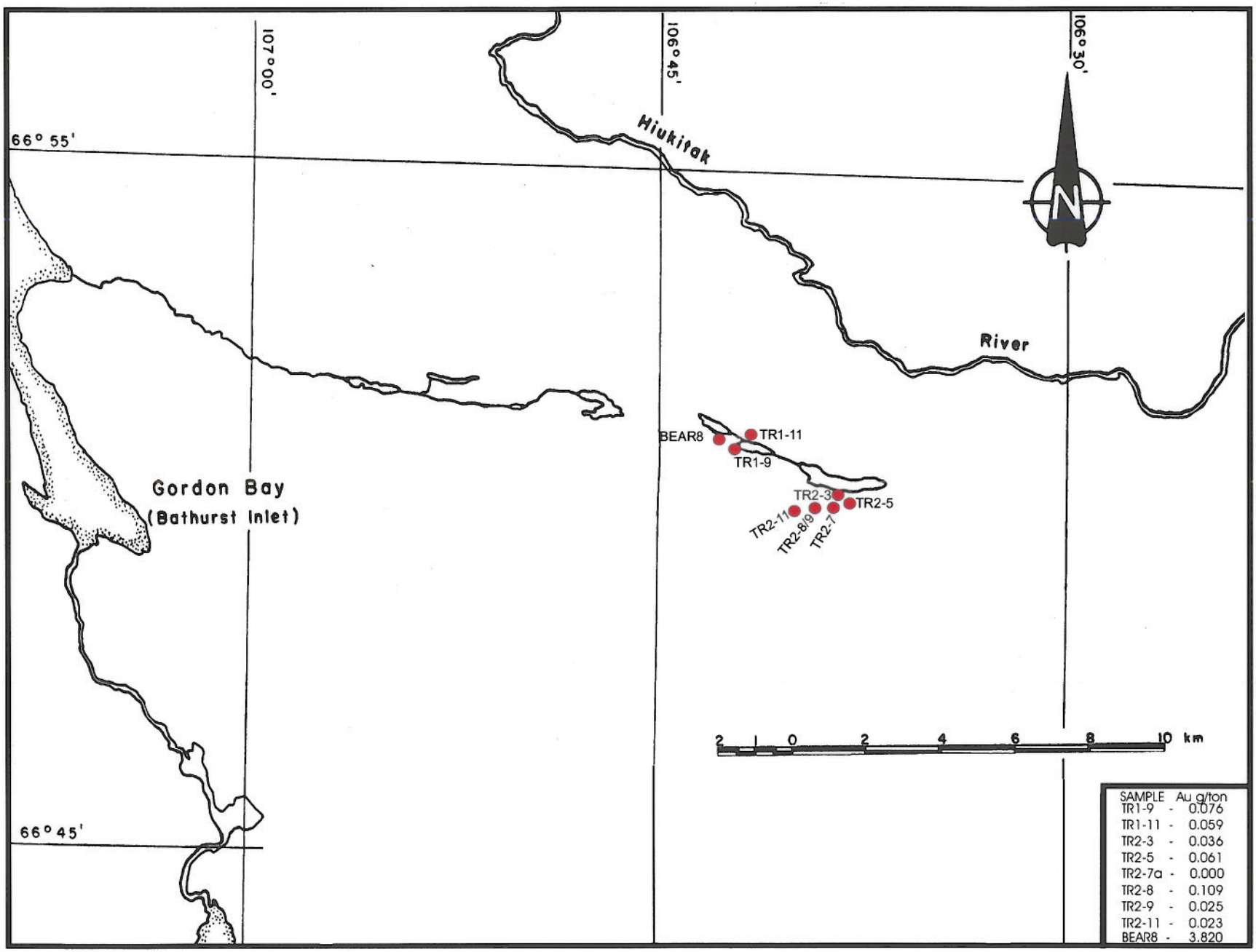

Figure 21: Sample locations and gold values for the Egg claims. (Modified from Fraser *et al.*, 1986).

association is best observed in samples with abundant pyrrhotite (e.g. RT-155), whereas samples with only pyrite tend to yield much lower gold values (e.g. RT-164 and TR2-9). In addition, there is a moderately strong correlation between gold and degree of metasomatic alteration + quartz veining. Samples that contain abundant quartz veinlets and/or prograde calcic amphiboles tend to assay higher than those with only retrograde chlorite/sericite.

Chapter 5

Discussion and Conclusions

5.1 Metamorphic Model for the CBMC

The regional D_2 metamorphic grade expressed within the metagreywackes exterior to the Crazy Bear Metamorphic Complex is cordierite facies. A prograde D_3 thermal overprint of this regional facies has produced the mineral assemblage biotite + garnet + staurolite + andalusite + fibrolite. The aluminosilicates are rarely fresh, commonly exhibiting strong chlorite-sericite alteration. Inclusions of staurolite in andalusite and idioblastic garnet within staurolite suggest that andalusite and some of the garnet formed at the expense of staurolite during thermal progradation. Woodland (1963) proposes the following reactions:

3 staurolite + 2 quartz $\leftrightarrow$ almandine + andalusite + 3 water (1)

staurolite + muscovite + quartz $\leftrightarrow$ andalusite + biotite + water (2)

On the Bear Creek claims cordierite is found as rims on garnet. This coronitic texture is indicative of rapid uplift and depressurization accompanied by increasing temperatures during the unroofing of the migmatite complex. Hollister (1977) proposes the following reaction:

5 quartz + 2 garnet + 4 sillimanite $\leftrightarrow$ 3 cordierite (3)

Also on the Bear Creek claims, well-developed sheafy fibrolite mats and knots form at the expense of biotite, defining a poorly developed S_3 foliation. This fibrolite occurs distal to cordierite-rimmed garnet porphyroblasts, providing further evidence that cordierite formed at the expense of both fibrolite and garnet. On the Hen claims fibrolite occurs on the boundaries of andalusite porphyroblasts intergrown with coarse muscovite. The conversion of andalusite and muscovite to sillimanite was promoted by an increase in temperature accompanying the progradation of the sillimanite defluidization front. This resulted in sillimanite becoming the stable phase over andalusite. The texture and habit of fibrolite on the Hen and Bear Creek claims is very similar to fibrolite observed at Hemlo in northern Ontario. Fibrolitic sillimanite at Hemlo is interpreted to have crystallized during a post peak metamorphic fluid event (Kuhns *et al.*, 1994; Powell *et al.*, 1999). The interpretation that temperatures were maintained and pressures were somewhat lower during late-stage fibrolite growth at Hemlo is consistent with the proposed unroofing history of the CBMC. The liberation of water at the dehydration front via reactions (1) and (2) most likely provided the necessary fluids to stabilize sillimanite. Figure 22 proposes a possible pressure/temperature path for the Bathurst Terrane. The prograde reactions of staurolite to andalusite, staurolite to garnet and andalusite to sillimanite are illustrated.

Late to post-kinematic granitoid plutons and pegmatitic sheets are common to metamorphic terranes undergoing extensional unroofing (Kusky, 1993). Such granitoids are derived from decompression melting of metamorphic infrastructures attending rapid uplift. The post S_2 quartz monzonites and pegmatitic sheets discussed earlier are interpreted to have formed in this way.

Belts of high strain separate a more brittle upper plate from a more ductile lower plate at the margins of the CBMC. Thompson et al., (1985; 1986) propose that these brittle-ductile regions represent original D_2 thrusts. During the 2002 field season, particular attention was paid to the Bear

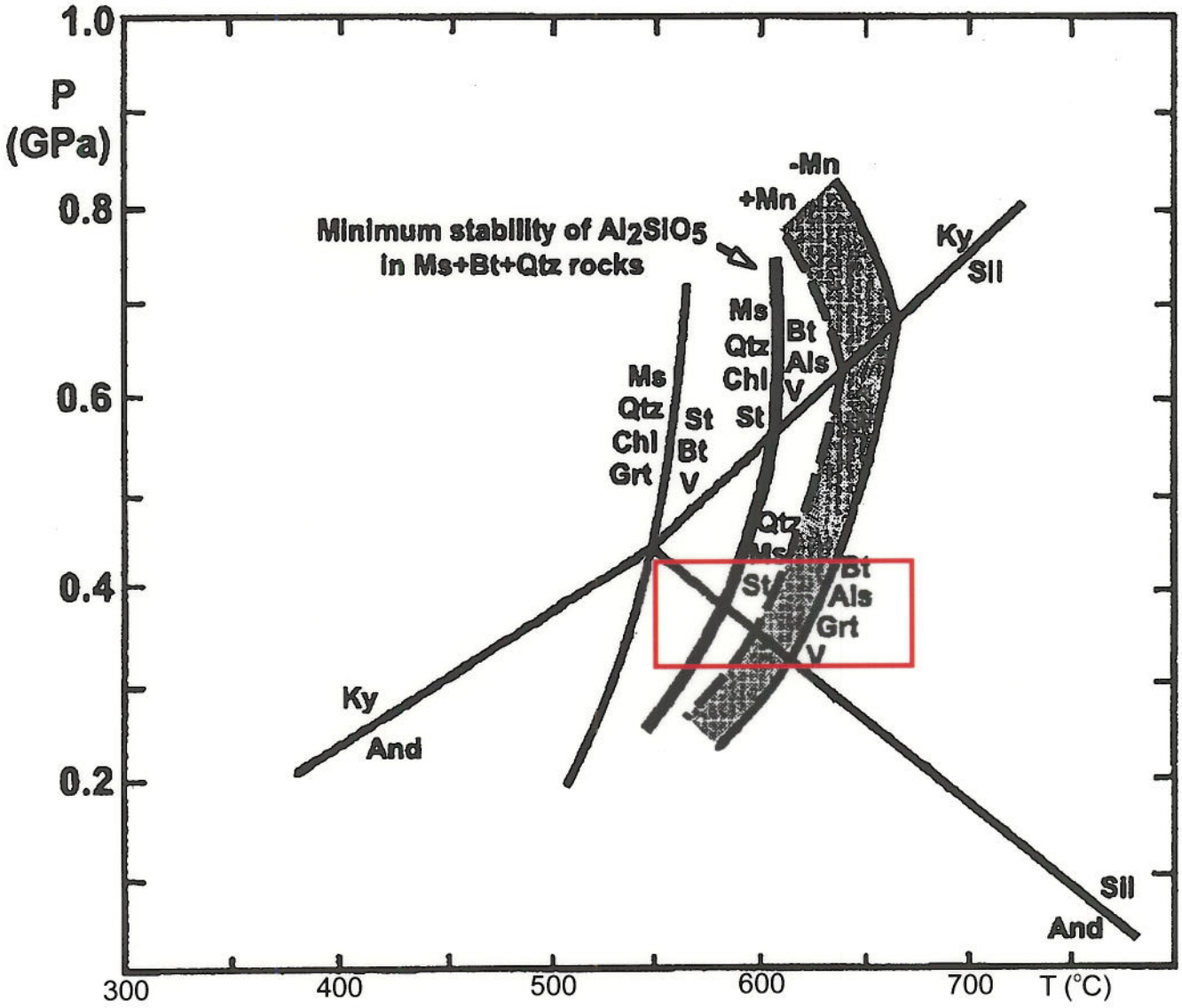

Figure 22: Petrogenetic grid for metapelites with proposed prograde pressure/temperature conditions for the CBMC indicated by the red rectangle. Ms muscovite; Qtz quartz; Grt garnet; Ky kyanite; And andalusite; Sil sillimanite; St staurolite; Bt biotite; Als aluminosilicate;V vapor. +Mn and -Mn indicate Mn-rich and Mn-poor garnet respectively. (Modified from Powell *et al*, 1999).

Creek Valley Deformation zone on the northern margin of the CBMC. Mapping revealed that D_2 was mylonitically deformed. This suggests that these D_2 thrusts were reactivated as D_3 mylonitic shearing to accommodate the exhumation of the CBMC.

A simplified crustal section of Crazy Bear Metamorphic Complex is presented in Figure 23. This section depicts crustal thickening and the formation of lower crustal migmatites, mid crustal sillimanite gneisses and upper crustal cordierite metagreywackes. Partial melting of the sediments during this stage produced 2-mica granitoids coincident with D_2 deformation. Unroofing and decompression melting gave rise to syn-D_3 quartz monzonites, which migrated and ponded within the sillimanite gneiss carapace along the high strain mylonite boundary. Tourmaline-bearing pegmatitic sheets derived from these granitoids punctured through the mylonitic carapace into peripheral knotted schists/greywackes.

5.2 Metamorphism and Gold Mineralization of the BIF

The precursor lithology of BIF from the Hen and Bear Creek claims is primarily well-banded silicate facies iron formation. Prograde thermal metamorphism in the Neoarchean recrystallized the primary iron silicates to grunerite, calcic amphibole, garnet and clinopyroxene. Grunerite commonly exhibits sharp narrow boundaries against calcic amphibole. This texture is not indicative of replacement but rather represents an immiscibility gap between the two amphiboles with the calcic phase crystallizing post-grunerite (Ford and Duke, 1993). This assemblage is overprinted by sulphides and calcic amphibole related to quartz veining resulting from the structural ponding of metamorphic fluids. Chlorite

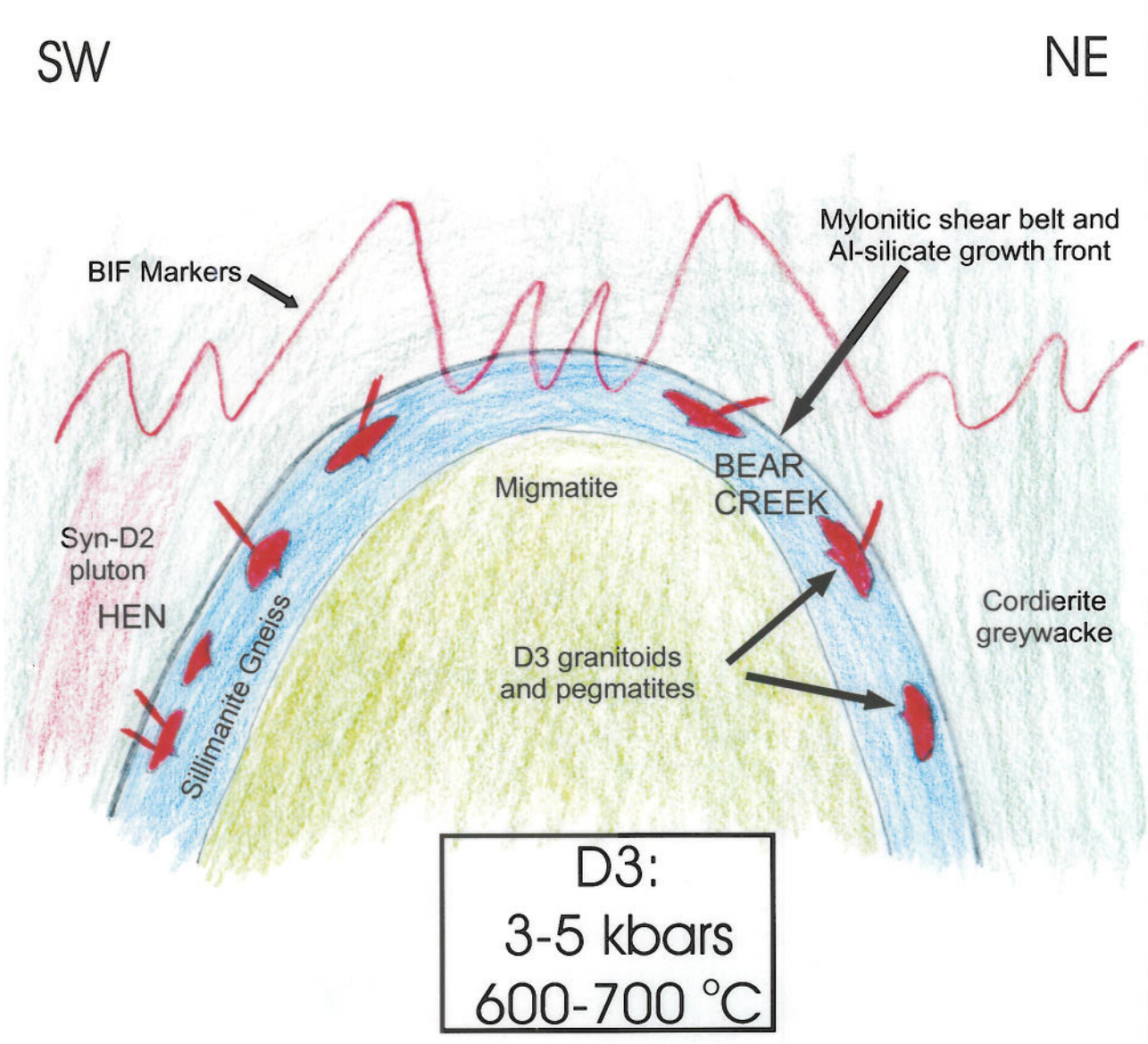

Figure 23: Crustal cartoon of the Crazy Bear Metamorphic Complex.

retrogression of biotite, garnet and amphibole occurred during waning thermal conditions at the terminal stages of updoming of the CBMC.

The introduction of gold into the iron formation is related to hydrothermal defluidization accompanying the partial melting of the greywackes in the core of the CBMC. Fluid generated at the outer limit of aluminosilicate growth migrated upward and outward from the central migmatites, leaching gold from the sediments and transporting it to the prograde/retrograde mylonite front where is was precipitated within the chemically reactive BIF units. It is possible that the iron-rich sequences were originally enriched in gold and sulphur over background turbidites and the gold was simply remobilized into local structural sites by migrating hydrothermal fluids. Gold on the Hen and Bear Creek claims is closely associated with pyrrhotite ± chalcopyrite and to a lesser extent, pyrite and arsenopyrite. Samples that show greater degrees of calcium metasomatism consistently contain more gold. This indicates that the fluids carrying gold were also the cause of calcium metasomatization and the precipitation of sulphides. Remnant pyrrhotite cores within large pyritic domains suggest that the main sulphidization event (pyrrhotite + gold) was postdated by late pyrite flooding. The evidence of pyrrhotite replacing biotite flakes and pyrrhotite laminae penetrating garnet porphyroblasts indicate that mineralization was late in the thermal history of the CBMC. There is no obvious association between degree of retrogression and gold content within the BIF units.

The ponding of gold-bearing fluids is controlled by structural discontinuities such as folds within the BIF. This accounts for higher gold and calcium values in hinge zones (Ford and Duke, 1993). No major fold closures were observed on the Hen claims, however one location (RT-171a/b) did contain several outcrop-scale isoclinal folds. Assay results yielded an anomalous value of 0.5g Au/ton suggesting that folding had a structural influence on the concentration of gold. The Egg BIF defines a

tight isoclinal fold closure at its eastern termination, however, only limited sampling was performed in the area during the 2002 field season.

5.3 Conclusions

The following conclusions are drawn based on the results of this study:

1) The following sequence of events is proposed for the evolution of the CBMC: a) Contraction and crustal thickening caused migmitization in the core of a metamorphic infrastructure, generating syn-D_2 2-mica granitic melts; b) late thermal doming resulted in aluminosilicates overgrowing D_2- fabrics and decompressive melts of quartz monzonite and pegmatites; c) the front of aluminosilicate growth was a site for mylonitic shearing against cordierite facies metagreywackes.
2) The fluids derived from the dehydration of the pelites and psammites transported significant amounts of Au, S, Cu, As, and Ca. As these fluids migrated into the chemically reactive iron formation units the fluid/rock reactivity caused the precipitation of pyrrhotite, chalcopyrite, arsenopyrite, calcium amphiboles ± pyroxene and gold. Textural evidence has shown that this probably occurred near the peak of thermal metamorphism. Gold was not significantly affected by chlorite/sericite retrogression but may have been leached in domains of late pyrite-flooding.

References

Ames, D.L. 1986, A study of the Nest Property's gold bearing iron formation Bathurst Inlet, N.W.T: B.Sc. thesis, University of Western Ontario.

Buhlmann, E. 1984, Report on the G&T-Fox-Char claim group (Warner Property) Bathurst Inlet Area, Mackenzie Mining District Northwest Territories, NTS 76J/11: Silver Hart Mines Ltd.

Bullis, H.R., Hureau, R.A., and Penner, B.D. 1994, Distribution of gold and sulphides at Lupin, Northwest Territories: Bulletin of the Society of Economic Geologists, v. 89, p. 1217-1227.

Bethune, K.M., Villeneuve, M.E., and Bleeker, W. 1998, Laser $^{40}Ar/^{39}Ar$ thermochronology of Archean rocks in Yellowknife Domain, southwestern Slave Province: insights into the cooling history of an Archean granite-greenstone terrane: Canadian Journal of Earth Sciences, v. 36, p. 1189-1206.

Campbell, F.H.A and Cecile, M.P. 1975, Report on the geology of the Kilohigok Basin, Goulburn Group, Bathurst Inlet, Northwest Territories: *in* Report of Activities Part A., Geological Survey of Canada, Paper 75-1A, p. 297-306.

Campbell, F.H.A and Cecile, M.P. 1976, Geology of the Kilohigok Basin, Goulburn Group, Bathurst Inlet, Northwest Territories: *in* Report of Activities Part A., Geological Survey of Canada, Paper 76-1A, p. 369-377.

Campbell, F.H.A. and Cecile, M.P. 1981, Evolution of the early Proterozoic Kilohigok Basin, Bathurst Inlet-Victoria Island, Northwest Territories: *in* Proterozoic Basins of Canada, ed. F.H.A. Campbell, Geological Survey of Canada, Paper 81-10, p. 103-131.

Campbell, F.H.A. 1978, Geology of the Helikian rocks of the Bathurst Inlet area, Coronation Gulf, Northwest Territories: *in* Current Research Part A., Geological Survey of Canada, Paper 78-1A, p. 97-106.

Cathro, R.J. 1980, Cot gold prospect Bathurst Inlet, N.W.T: Archer, Cathro, & Associates Ltd., Consulting Geological Engineers.

Davis, W.J., and Bleeker, W. 1999, Timing of plutonism, deformation, and metamorphism in the Yellowknife Domain, Slave Province, Canada: Canadian Journal of Earth Sciences, v. 36, p. 1169-1187.

Ford, R.C. 1988, Comparative geology of gold-bearing Archean iron formation, Slave structural province, Northwest Territories: M.Sc thesis, University of Western Ontario.

Ford, R.C., Duke, N.A. 1993, Concentration of gold during retrograde metamorphism of Archean banded iron formations, Slave Province, Canada: Canadian Journal of Earth Sciences, v. 30, p. 1566-1581.

Fraser, J.A. 1964, Geological notes on northeastern District of Mackenzie, Northwest Territories: Geological Survey of Canada, Paper 63-40, 20 p.

Fraser, J.A. 1968, Geology across Thelon Front, District of Mackenzie: *in* Report of activities, Part A., May to October, 1967, Geological Survey of Canada, Paper 68-1.

Fraser, J.A. 1972, Artillery Lake map-area, District of Mackenzie: Geological Survey of Canada, Paper 71-38, 17 p.

Fraser. S., Muller, F., Muller, D. 1985, 1985 Geological and Geophysical Report Hen Claims – NTS area 76J/11 Bathurst Inlet, Volume I and II: Prepared by Echo Bay Mines Ltd.

Fraser, S., Erdmer, E. 1986, 1986 exploration Egg, Egg 3 Claim group NTS 76J/15 & 16: Prepared by Echo Bay Mines Ltd.

Freeman, M.E. 1994, Echo Bay Mines Ltd. exploration for gold – 1994 Hunt 1, Hunt 2, Hen 1, Hen 6 and Bear 2 mineral claims Bathurst Inlet region District of Mackenzie, NWT: Prepared by Apex Geoscience Ltd.

Fyon, J.A., Crocket, J.H., and Schwarcz, H.P. 1983, The Carshaw and Malga iron- formation-hosted gold deposits of the Timmins area: *in* The Geology of Gold in Ontario, ed. A.C. Colvine, Ontario Geological Survey Miscellaneous Paper, 110, p. 98-110.

Henderson, J.B., Thompson, P.H. 1981, The Healey Lake map area and the enigmatic Thelon Front, District of Mackenzie: *in* Current Research, Part A., Geological Survey of Canada, Paper 81-1A, p. 175-180.

Henderson, J.B., Thompson, P.H., James, D.T. 1982, The Healey Lake map area and the Thelon Front problem, District of Mackenzie: *in* Current Research, Part A., Geological Survey of Canada, Paper 82-1A, p. 191-195.

Henderson, J.B., Macfie, R.I. 1985, The northern Artillery Lake map area: A transect across the Thelon Front, District of Mackenzie: *in* Current Research, Part A., Geological Survey of Canada, Paper 85-1A, p. 441-448.

Henderson, J.B., McGrath, P.H., James, D.T., and Macfie, R.I. 1987, An integrated geological, gravity and magnetic study of the Artillery Lake area and the Thelon Tectonic Zone, District of Mackenzie: *in* Current Research, Part A., Geological Survey of Canada, Paper 87-1A, p. 803-814.

Hollister, L.S. 1977, The reaction forming cordierite from garnet, the Khtada Lake metamorphic complex, British Columbia: Canadian Mineralogist, v. 15, p. 217-229.

James, D.T. 1985, Geology of the Moraine Lake area and the Thelon Front, District of Mackenzie: *in* Current Research, Part A., Geological Survey of Canada, Paper 85-1A, p. 449-454.

James, D.T., and Mortensen, J.K. 1992, An Archean metamorphic core complex in the southern Slave Province: basement-cover structural relationships between the Sleepy Dragon Complex and the Yellowknife Supergroup: Canadian Journal of Earth Sciences, v. 29, p. 2133-2145.

Kuhns, R.J., Sawkins, F.J., and Ito, E. 1994, Magmatism, metamorphism and deformation at Hemlo, Ontario, and the timing of Au-Mo mineralization in the Golden Giant Mine: Economic Geology, v. 89, p. 720-756.

Kusky, T.M. Collapse of Archean orogens and the generation of late-to postkinematic granitoids: Geology, v. 21, p. 925-928.

Lhotka, P.G. and Nesbitt, B.E., 1989, Geology of unmineralized and gold-bearing iron formation, Contwoyto Lake-Point Lake region, Northwest Territories, Canada:
Canadian Journal of Earth Sciences, v. 26, p. 46-64.

Macdonald, A.J. 1983, The iron formation-gold association evidence from Geraldton area: *in* The Geology of Gold in Ontario, ed. A.C. Colvine, Ontario Geological Survey Miscellaneous Paper, 110, p. 75-83.

Mason, J.K., and McConell, C.D. 1983, Gold mineralization in the Beardmore-Geraldton area: *in* The Geology of Gold in Ontario, ed. A.C. Colvine, Ontario Geological Survey Miscellaneous Paper, 110, p. 84-97.

Muller, F. 1985, Exploration – 1985, Bear 1-10, Egg, Egg 2-3 mineral claims, Bathurst Inlet area, Mackenzie Mining District, N.W.T., NTS 76J/14, 15 & 16; Assessment Report, #082558: prepared by Echo Bay Mines Ltd.

Powell, W.G., Pattison, D.R.M., and Johnston, P. 1999, Metamorphic history of the Hemlo gold deposit from Al2SiO5 mineral assemblages, with implications for the timing of mineralization: Canadian Journal of Earth Sciences, v. 36, p. 33-46.

Smith, F.M. 1986, Report on the Warner property, Mackenzie Mining District, Bathurst Inlet area, Northwest Territories, NTS 76J/11; Assessment Report, #062214: prepared by Vanstates Resources Ltd.

Thompson, P.H. 1978, Archean regional metamorphism in the Slave structural province – A new perspective on some old rocks: *in* Metamorphism in the Canadian Shield, Geological Survey of Canada, Paper 78-10, p. 85-102.

Thompson, P.L., and Ashton, K.1984, Preliminary Report on the geology of the Tinney Hills-Overby Lake (west half) map area, District of Mackenzie: A look at the Thelon Tectonic Zone Northeast of the Bathurst Fault: *in* Current Research, Part A., Geological Survey of Canada, Paper 84-1A, p. 415-423.

Thompson, P.H., Culshaw, N., Thompson, D.L. and Buchanan, B.R.1985, Geology across the western boundary of the Thelon Tectonic Zone in the Tinney Hills-Overby Lake (west half) map area, District of Mackenzie: *in* Current Research, Part A., Geological Survey of Canada, Paper 85-1A, p. 555-572.

Thompson, P.H., Culshaw, N., Buchanan, J.R., and Manojilovic, P.1986, Geology of the Slave Province and the Thelon Tectonic Zone in the Tinney Hills-Overby Lake (west half map area, District of Mackenzie: *in* Current Research, Part A, Geological Survey of Canada, Paper 86-A, p. 275-289.

Tirrul, R. 1985, Nappes in the Kilohigok basin, and their relation to the Thelon Tectonic Zone, District of Mackenzie: *in* Current Research, Part A., Geological Survey of Canada, Paper 85-1A, p. 407-420.

van Breemen, O., Thompson, P.H., Hunt, P.A., and Culshaw, N. 1987, U-Pb and monazite geochronology from the northern Thelon Tectonic Zone, District of Mackenzie: *in* Radiogenic Age and Isotopic Studies: Report 1, Geological Survey of Canada, paper 87-2, p. 81-93.

Woodland, B.G. 1963, A petrographic study of thermally metamorphosed pelitic rocks in the Burke area, Northeastern Vermont: American Journal of Science, v. 261, p. 354-375.

Wright, G.M. 1957, Geological notes on eastern district of Mackenzie Northwest Territories: Geological Survey of Canada, Paper 56-10, 23 p.

Appendix A: Bulk Rock Data

SAMPLE	SiO_2	TiO_2	Al_2O_3	Fe_2O_3	MnO	MgO	CaO	K_2O	Na_2O	P_2O_5	L.O.I.	Total
HEN CLAIM												
RT-131	46.79	0.05	1.40	47.88	0.03	1.70	0.28	0.04	0.01	0.13	-0.50	97.81
RT-147	62.98	0.09	2.90	21.37	0.14	0.95	8.07	0.01	0.01	0.06	1.94	98.52
RT-171A	55.41	0.67	19.08	11.07	0.09	4.07	0.25	3.60	0.52	0.12	3.85	98.73
RT-171B	58.00	0.07	2.73	32.90	0.06	1.86	2.96	0.11	0.01	0.16	0.16	99.02
RT-188	50.87	0.19	13.77	29.16	0.12	1.33	3.27	0.03	0.01	0.09	0.44	99.28
RT-189	55.65	0.11	3.20	35.89	0.07	0.86	3.12	0.08	0.01	0.10	-0.11	98.98
RT-191	66.85	0.04	2.33	26.39	0.05	1.02	1.15	0.07	0.01	0.18	0.92	99.01
BEAR CREEK												
TR2-3	42.26	1.02	32.58	9.55	0.09	4.87	0.57	2.42	0.76	0.05	4.60	98.77
TR2-5	73.59	0.12	3.53	12.32	0.04	1.73	2.14	0.32	0.01	0.16	5.04	99.00
TR2-11	42.48	1.42	10.61	25.08	1.44	4.71	8.94	0.41	0.17	0.04	2.90	98.20

Appendix B: Mineral Chemistry Data

AMPHIBOLE

	SiO_2	TiO_2	A_2O_3	C_2O_3	FeO	MgO	MnO	CaO	K_2O	Na_2O	F	Cl	Sum	-0 = F+Cl	Sum
1	40.45	0.47	11.92	0.05	30.46	2.25	0.07	10.75	0.75	0.77	0.63	0.01	98.58	0.27	98.31
2	43.80	0.61	9.70	0.07	29.86	2.97	0.06	11.22	0.51	0.66	0.55	0.00	100.01	0.23	99.78
3	43.33	0.60	9.21	0.08	29.49	2.92	0.10	10.90	0.55	0.58	0.64	0.00	98.40	0.27	98.13
4	50.60	0.06	0.57	0.02	43.01	4.36	0.17	0.89	0.00	0.10	0.74	0.00	100.52	0.31	100.21
5	50.24	0.03	0.50	0.00	43.34	4.35	0.15	0.90	0.00	0.07	0.73	0.00	100.31	0.31	100.00
6	50.04	0.05	0.47	0.07	42.62	4.37	0.12	0.79	0.00	0.06	0.72	0.00	99.31	0.30	99.01
7	49.69	0.04	0.81	0.05	41.32	5.05	0.12	1.05	0.02	0.13	0.74	0.00	99.02	0.31	98.71
8	49.78	0.07	0.54	0.08	43.44	4.28	0.21	0.77	0.00	0.07	0.75	0.00	99.99	0.32	99.67
9	48.86	0.06	0.56	0.03	42.35	4.23	0.10	0.72	0.00	0.07	0.78	0.00	97.76	0.33	97.43
10	41.03	0.26	15.82	0.05	27.18	1.87	0.03	11.69	0.32	0.71	0.53	0.00	99.49	0.22	99.27
11	40.30	0.22	15.12	0.01	26.28	1.92	0.07	11.25	0.32	0.80	0.55	0.00	96.84	0.23	96.61
12	50.23	0.07	0.66	0.00	41.77	5.34	0.20	0.79	0.00	0.08	0.72	0.00	99.86	0.30	99.56
13	44.40	0.44	10.31	0.12	28.00	3.54	0.13	11.03	0.25	0.72	0.59	0.00	99.53	0.25	99.28
14	43.74	0.41	10.79	0.14	27.13	3.43	0.11	11.19	0.25	0.78	0.57	0.00	98.54	0.24	98.30

1 ****SAMPLE 189 OVER ON GRUN,
2 REL DARK DOMAIN
3 REL DARK DOMAIN
4 CENTRAL TO HBLE, C-1
5 CENTRAL TO HBLE, C-1
6 CENTRAL TO HBLE, C-1
7 INT W ALMANDINE, C-1
8 ****SAMPLE 152 IN C W HBLE C-2
9 152 IN C W HBLE C-2
10 SMALL DOMAIN WITHIN ALM-GRUN
11 SMALL DOMAIN WITHIN ALM-GRUN
12 W C ALM INCL HBLE, C-2
13 RHOMB IN GRUN
14 RHOMB IN GRUN

GARNET

	SiO_2	TiO_2	A_2O_3	C_2O_3	FeO	MgO	MnO	CaO	Sum
1	37.40	0.16	21.67	0.08	31.66	0.53	0.38	8.64	100.52
2	36.73	0.22	21.85	0.00	32.10	0.49	0.22	8.69	100.30
3	36.25	0.19	21.96	0.16	31.59	0.52	0.17	8.91	99.75
4	35.74	0.09	22.37	0.00	33.77	0.50	0.40	6.87	99.74
5	36.22	0.13	22.40	0.02	34.25	0.42	0.45	6.82	100.71
6	36.40	0.12	22.58	0.02	34.79	0.39	0.63	5.38	100.31
7	36.22	0.05	23.03	0.08	32.36	2.53	2.48	2.91	99.66
8	36.94	0.00	22.71	0.09	31.90	2.02	3.36	2.66	99.68
9	37.05	0.03	22.71	0.04	32.94	2.53	2.58	2.48	100.36
10	36.69	0.05	23.29	0.00	32.59	2.58	2.28	2.49	99.97

1 ****SAMPLE 189 INT W GRUN, C-1
2 INCL RHOMBS OF GRUN
3 INCL ILM AND QTZ C-1
4 ****SAMPLE 152 COARSE MASS INCL ASP, GRUN, C-1
5 INCL GRUN
6 COARSE MASS C-3
7 ****SAMPLE 171A SMALL GRAIN, RELICT?
8 ZONED GRAIN CENTRAL, C-2
9 AT MARGIN
10 ADJ GRAIN

MUSCOVITE

	SiO_2	TiO_2	A_2O_3	C_2O_3	FeO	MgO	MnO	BaO	CaO	K_2O	Na_2O	F	Cl	Sum	-0 = F+Cl	Sum
1	45.99	0.04	37.16	0.04	0.83	0.70	0.00	0.17	0.00	9.47	0.64	0.11	0.00	95.15	0.05	95.10
2	47.21	0.06	37.70	0.03	0.85	0.62	0.00	0.23	0.00	9.88	0.61	0.17	0.00	97.36	0.07	97.29
3	46.31	0.00	34.60	0.00	2.22	2.06	0.00	0.31	0.00	8.80	0.66	0.13	0.00	95.09	0.05	95.04
4	46.00	0.20	37.81	0.06	0.71	0.48	0.00	0.08	0.00	9.34	1.56	0.05	0.00	96.29	0.02	96.27
5	47.02	0.03	33.74	0.00	1.92	1.27	0.02	0.01	0.00	10.69	0.29	0.13	0.00	95.12	0.05	95.07
6	46.57	0.37	36.38	0.08	0.59	0.62	0.00	0.11	0.00	9.57	1.08	0.07	0.00	95.44	0.03	95.41

1 ****SAMPLE 184, INT W SILL REPL ANDAL, C-1
2 ANOTHER REPL, BIOTITE W SILL
3 W CHL REPL BIO, C-2
4 ****SAMPLE 161, ADJ PLATE,
5 W ALT BIO TO CHL
6 INCL CHL

BIOTITE

	SiO_2	TiO_2	A_2O_3	C_2O_3	FeO	MgO	MnO	BaO	CaO	K_2O	Na_2O	F	Cl	Sum	-0 = F+Cl	Sum
1	33.82	2.21	20.13	0.04	19.21	9.30	0.18	0.29	0.00	8.89	0.21	0.60	0.00	94.88	0.25	94.63
2	34.14	2.03	20.29	0.08	18.20	9.76	0.25	0.14	0.00	8.95	0.23	0.64	0.05	94.76	0.28	94.48
3	35.83	1.99	20.72	0.07	18.51	9.61	0.25	0.21	0.00	9.08	0.26	0.70	0.00	97.23	0.29	96.94
4	33.67	1.65	20.02	0.14	18.45	10.98	0.19	0.23	0.00	8.09	0.25	0.63	0.11	94.41	0.29	94.12
5	31.64	1.44	19.64	0.21	19.42	11.94	0.19	0.08	0.02	6.15	0.22	0.59	0.20	91.74	0.29	91.45
6	34.94	2.02	19.81	0.09	17.91	9.74	0.20	0.24	0.00	9.11	0.31	0.57	0.03	94.97	0.25	94.72
7	44.97	0.40	29.57	0.11	7.52	4.09	0.01	0.00	0.00	7.21	0.27	0.29	0.02	94.46	0.13	94.33
8	44.91	0.64	26.02	0.06	7.14	4.29	0.05	0.00	0.00	8.35	0.17	0.26	0.00	91.89	0.11	91.78
9	31.16	1.86	19.62	0.02	24.25	7.21	0.14	0.11	0.00	7.12	0.73	0.61	0.23	93.06	0.31	92.75
10	31.00	1.40	19.41	0.02	25.54	7.81	0.23	0.07	0.00	6.44	0.11	0.67	0.02	92.72	0.29	92.43
11	30.64	1.27	19.11	0.10	22.45	10.89	0.11	0.03	0.00	4.32	0.13	0.58	0.04	89.67	0.25	89.42

1 ****SAMPLE 184, INT W TOURM C-1
2 ADJ GRAIN ALTERED
3 REPL BY CHL
4 SAMLL PLATE WITHIN STAUR, C-2
5 ADJ LATH IN STAUR
6 ADJ LATH IN STAUR
7 ****SAMPLE 161, ZONED GRAIN DARK CENTRAL
8 DARK ZONE IN BIO
9 LATH W ALM, C-2
10 ANOTHER PLATE
11 INT W MUSC

CHLORITE

	SiO_2	TiO_2	A_2O_3	C_2O_3	FeO	MgO	MnO	CaO	K_2O	Na_2O	F	Cl	Sum	-0 = F+C	Sum
1	25.40	0.04	21.73	0.03	23.38	15.65	0.41	0.00	0.00	0.08	0.52	0.00	87.24	0.22	87.02
2	25.55	0.00	21.99	0.00	21.43	16.17	0.25	0.00	0.19	0.19	0.47	0.04	86.24	0.20	86.04
3	25.88	0.04	20.49	0.05	27.03	13.67	0.09	0.00	0.00	0.04	0.52	0.00	87.81	0.22	87.59
4	26.17	0.67	19.87	0.08	26.42	12.14	0.19	0.01	0.34	0.14	0.54	0.03	86.57	0.23	86.34
5	25.20	0.02	19.12	0.00	29.94	11.52	0.27	0.00	0.00	0.07	0.57	0.00	86.71	0.24	86.47

1 ****SAMPLE 184, REPL BIOTITE, C-1
2 WITH MUSC REPL BIO, C-2
3 ****SAMPLE 161-191? ENCL MONAZITE, AP, C-1
4 OUTER ZONE ON POSS STIP
5 INCL RELICT ALM, C-2

TOURMALINE

	SiO_2	TiO_2	A_2O_3	C_2O_3	FeO	MgO	MnO	BaO	CaO	K_2O	Na_2O	F	Cl	Sum	-0 = F+Cl	Sum
1	34.66	0.51	34.52	0.02	5.18	6.66	0.00	0.00	0.56	0.00	1.96	0.22	0.00	84.29	0.09	84.20
2	35.07	0.45	35.52	0.08	5.40	6.46	0.00	0.00	0.60	0.00	2.00	0.21	0.00	85.79	0.09	85.70
3	35.11	0.50	35.54	0.00	5.26	6.63	0.05	0.00	0.56	0.00	1.95	0.31	0.00	85.91	0.13	85.78

1 ****SAMPLE 184, INCL IN ANDAL, C-1
2 INCL IN ANDAL, C-1
3 ADJ GRAIN INT W BIOTITE, C-1

STAUROLITE

	SiO_2	TiO_2	A_2O_3	FeO	MnO	MgO	CaO	Sum
1	26.61	0.56	55.4	12.99	0.37	1.36	0	97.3
2	26.25	0.69	55.96	11.87	0.57	1.18	0	96.5

1 ****SAMPLE 184, MINUTE WITHIN ANDAL, C-1, STAUR
2 C W BIOTITE, C-2

Appendix C: Trace Element Data

Sample ID	Au	Ag*	Al*	As	Ba	Be*	Bi*	Br	Ca*	Cd*	Co	Cr	Cs	Cu*	Fe
	ppb	ppm	%	ppm	ppm	ppm	ppm	ppm	%	ppm	ppm	ppm	ppm	ppm	%
RT-131	52	-0.3	1.22	175	-50	-1	7	2.2	1.71	-0.3	4	34	77	20	23.2
RT-135	9	0.4	4.65	18.8	320	2	-2	-0.5	0.57	-0.3	18	156	4	9	15.8
RT-138	12	0.5	1.62	400	-50	-1	-2	-0.5	0.91	-0.3	20	212	3	23	26.7
RT-139	264	0.9	1.20	4.4	120	-1	-2	-0.5	1.74	1.1	6	42	3	10	25.4
RT-142	179	0.4	1.08	-0.5	160	-1	-2	-0.5	1.19	-0.3	5	29	10	18	27.9
RT-147	123	1.5	2.96	13.5	160	2	4	-0.5	6.42	-0.3	8	35	1	571	12.9
RT-148	6	0.9	4.27	2.3	600	2	-2	-0.5	0.87	-0.3	36	232	18	106	4.7
RT-150	322	0.5	0.57	303	-50	1	-2	5.7	0.63	-0.3	3	24	4	20	29.5
RT-151	60	0.7	4.71	7030	-50	2	-2	-0.5	2.44	3.1	48	102	-1	206	18.9
RT-152	563	1.1	1.36	195	-50	-1	-2	-0.5	1.26	-0.3	3	53	-1	262	20.4
RT-153	1020	0.9	0.90	13.2	-50	-1	-2	-0.5	1.04	-0.3	5	26	-1	95	30.4
RT-154	677	2.7	1.54	3390	-51	-1	-2	-0.5	2.05	2.6	12	18	4	373	23.1
RT-155	6700	1.7	2.19	23.6	-50	-1	-2	-0.5	4.02	-0.3	3	51	-1	66	22.9
RT-156A	91	0.3	1.60	8.1	-50	3	-2	-0.5	4.83	0.4	4	37	-1	16	16.8
RT-156B	162	0.7	1.04	29.3	-50	1	-2	3.2	4.71	-0.3	24	20	1	88	13.1
RT-157	162	0.4	0.71	295	120	-1	-2	2	0.39	-0.3	3	21	9	23	26.7
RT-159	89	0.6	1.76	3	-50	3	-2	2.3	4.40	-0.3	4	20	2	136	26.7
RT-160	85	1.0	3.82	8.8	-50	-1	-2	-0.5	1.76	-0.3	22	112	5	1008	18.8
RT-163	26	0.4	1.55	5.7	300	2	-2	-0.5	1.94	1.0	9	39	71	23	29.2
RT-164	29	1.0	3.79	7.3	-50	-1	2	-0.5	0.94	-0.3	50	90	1	172	20
RT-171B	495	1.2	0.99	907	-50	-1	3	-0.5	1.26	-0.3	4	27	3	140	24.4
RT-179	16	0.4	1.08	5.8	-50	-1	-2	-0.5	0.69	-0.3	4	29	-1	50	28.5
RT-186	332	0.4	3.07	7.2	110	1	-2	-0.5	3.58	-0.3	11	84	-1	83	21.2
RT-187A	269	0.8	2.82	35.5	-50	-1	-2	1.6	2.88	0.6	9	39	1	184	17.3
RT-187B	664	0.8	2.57	58.9	-50	-1	4	-0.5	3.81	-0.3	7	33	-1	133	20.8
RT-188	102	1.3	2.80	16.8	-50	-1	2	-0.5	1.60	0.5	9	46	1	336	20.6
RT-189	87	0.4	0.84	38.5	110	1	3	1.6	2.15	-0.3	5	45	-1	74	28.7
RT-191	553	0.7	0.60	191	-50	-1	-2	-0.5	0.71	0.5	3	22	3	55	25.4
ND-203	61	1.6	1.16	10.3	-50	-1	2	1.2	7.04	-0.3	16	25	-1	471	14.5
ND-205	126	1.1	1.19	12.4	-50	-1	-2	-0.5	3.33	-0.3	10	29	-1	220	26.3
ND-206	939	0.9	1.08	7.8	-50	3	3	-0.5	2.49	-0.3	5	27	2	116	18.5
ND-207	11	1.1	3.32	3.9	-50	-1	-2	-0.5	1.41	-0.3	15	68	2	376	18.9
ND-210	31	1.6	1.85	24	-50	2	-2	-0.5	3.15	-0.3	21	30	-1	789	23.6
ND-213	51	0.6	3.14	13.4	-50	-1	-2	-0.5	4.23	-0.3	14	93	-1	255	16.4
ND-214	125	0.5	4.19	5.8	100	-1	-2	-0.5	2.09	-0.3	7	75	-1	141	18.2
ND-215	161	0.6	1.95	2.9	100	2	-2	-0.5	2.23	-0.3	4	48	4	131	15.4
ND-217	428	0.4	2.15	2.6	-50	-1	-2	-0.5	3.08	0.6	5	32	9	34	22.9
ND-218	70	0.4	0.49	-0.5	-50	-1	-2	1.6	1.20	-0.3	3	17	-1	17	28.6
ND-219	60	-0.3	0.56	3.5	120	-1	-2	-0.5	1.11	-0.3	4	30	2	23	28.4
ND-221	3	-0.3	1.42	12.3	130	-1	6	11.8	15.70	-0.3	5	28	-1	166	5.18
ND-222	17	-0.3	4.47	284	-50	2	-2	3.8	10.42	-0.3	22	33	-1	17	12.9
ND-223	774	1.3	2.34	90	-50	1	4	1.9	0.76	-0.3	10	44	-1	354	6.65
ND-225	28	-0.3	3.94	392	62	-1	-2	-0.5	1.72	-0.3	16	115	1	14	15.3
ND-226a	5	-0.3	2.94	-0.5	-50	2	-2	-0.5	1.17	-0.3	9	62	2	26	15.4
ND-226B	5	0.6	3.79	22.7	-50	-1	2	-0.5	0.43	-0.3	8	85	9	52	16.7
ND-233	22	0.6	10.86	5.1	380	2	-2	-0.5	0.36	-0.3	16	239	8	40	4.16
ND-238	1500	0.6	0.53	17.1	-50	-1	-2	-0.5	0.42	-0.3	5	24	3	68	28.1
ND-240	15	-0.3	4.51	12.6	-50	2	-2	1.2	0.22	-0.3	12	88	23	76	17.2
ND-241	229	-0.3	0.50	59.8	-50	4	-2	7.9	5.76	-0.3	9	21	-1	14	25.4
ND-242	208	-0.3	0.31	351	-50	3	6	6.9	11.68	-0.3	22	41	-1	7	4.81
ND-243	6	-0.3	0.52	50.6	-50	-1	-2	-0.5	0.91	1.2	3	23	7	22	27.3
ND-246	49	-0.3	0.55	162	-50	2	5	3.2	5.89	-0.3	8	50	-1	6	3.22
PM-182C	692	-0.3	1.80	160	-50	2	-2	-0.5	3.99	0.7	32	25	1	501	16.6
PM-162	-2	-0.3	0.96	3	-50	-1	-2	3.8	0.20	-0.3	2	21	-1	48	1.95
PM-182	1790	0.3	1.58	98.4	-50	2	3	-0.5	6.52	-0.3	24	30	-1	381	15.7
PM-176	2	0.8	6.89	96.7	230	2	-2	-0.5	5.70	2.9	46	67	-1	195	10.7
PM-179	-2	-0.3	5.56	3.2	540	2	-2	4	2.52	-0.3	40	98	11	48	8.62
TR1-9	76	-0.3	2.98	2420	-60	-1	-2	-0.5	1.15	1.5	6	34	2	35	1.76
TR1-11	59	0.3	2.27	377	-50	-1	-2	-0.5	2.39	-0.3	12	61	-1	42	23.5
BEAR8	3820	2.2	1.83	56600	240	2	-2	-0.5	0.32	148.3	153	20	1	641	18.3
TR2-3	36	0.9	7.15	7.1	1300	2	13	-0.5	0.32	-0.3	40	280	4	187	7.38
TR2-5	61	1.6	1.15	5.7	-50	3	-2	3.5	1.56	-0.3	55	23	-1	481	8.22
TR2-7A	-2	1.9	1.79	3.5	-50	-1	-2	-0.5	0.03	-0.3	130	38	-1	285	19.8
TR2-8	109	0.8	3.01	4.2	-50	-1	-2	-0.5	6.80	1.3	30	29	-1	142	15.6
TR2-9	25	2.2	3.09	-0.5	1600	-1	-2	-0.5	0.03	-0.3	51	49	2	50	5.61
TR2-11	23	0.9	3.17	-0.5	-50	-1	-2	-0.5	7.66	0.7	11	13	-1	101	16.4

Sample ID	Hf	Hg	Ir	K*	Mg*	Mn*	Mo	Na	Ni*	P*	Pb*	Rb	S*	Sb	Sc
	ppm	ppm	ppb	%	%	ppm	ppm	%	ppm	%	ppm	ppm	%	ppm	ppm
RT-131	-1	-1	-5	0.17	1.09	356	-1	0.02	15	0.057	14	51	0.351	1.2	4.2
RT-135	3	-1	-5	0.32	2.83	771	3	0.46	86	0.037	15	-15	0.014	-0.1	16
RT-138	4	-1	-5	-0.01	0.76	1439	-1	0.02	90	0.006	11	23	0.239	-0.1	43.9
RT-139	-1	-1	-5	0.04	0.83	538	-1	0.06	29	0.068	19	-15	0.011	0.5	4.7
RT-142	-1	-1	-5	0.07	1.18	687	-1	0.04	28	0.057	39	-15	0.186	-0.1	3.6
RT-147	-1	-1	-5	0.12	1.06	1529	10	0.08	24	0.101	8	-15	2.241	0.1	3.7
RT-148	14	-1	-5	1.41	1.66	270	4	2.79	86	0.016	24	79	0.781	0.2	14.3
RT-150	-1	-1	-5	0.02	1.29	632	-1	0.03	16	0.078	32	-15	0.682	-0.1	2.3
RT-151	3	-1	-5	0.93	2.50	1199	2	0.12	80	0.190	4	-15	1.797	0.7	9.7
RT-152	-1	-1	-5	0.01	1.43	1018	-1	0.04	18	0.032	21	-15	4.276	-0.1	5.7
RT-153	-1	-1	-5	0.04	0.67	326	-1	0.07	30	0.044	17	-15	1.257	-0.1	2.7
RT-154	-1	-1	-5	0.12	1.25	255	-1	0.13	28	0.039	27	-15	6.634	-0.2	2.6
RT-155	1	-1	-5	0.11	1.32	381	-1	0.27	15	0.060	14	-15	3.898	0.1	5.2
RT-156A	-1	-1	-5	0.08	1.06	744	3	0.2	15	0.028	16	-15	0.123	-0.1	3.7
RT-156B	-1	-1	-5	0.02	2.40	974	2	0.01	36	0.077	6	-15	4.807	0.2	2.4
RT-157	-1	-1	-5	0.04	1.70	571	-1	0.02	30	0.029	23	-15	0.992	-0.1	2.3
RT-159	-1	-1	-5	0.06	0.91	616	-1	0.11	22	0.108	13	-15	1.134	-0.1	3.1
RT-160	2	-1	-5	0.13	1.73	1278	-1	0.02	48	0.036	3	48	3.502	0.2	11.4
RT-163	-1	-1	-5	0.36	1.25	558	-1	0.19	27	0.030	32	68	0.443	1.2	6.3
RT-164	1	-1	-5	0.61	1.72	457	-1	0.05	77	0.155	58	47	12.544	0.9	8.9
RT-171B	-1	-1	-5	0.08	0.98	360	-1	0.09	15	0.066	33	-15	6.806	-0.1	3.3
RT-179	-1	-1	-5	-0.01	0.57	415	-1	0.02	23	0.039	36	30	0.382	0.2	3.3
RT-186	1	-1	-5	0.02	1.67	1251	-1	0.1	40	0.057	16	-15	1.654	-0.1	8.7
RT-187A	-1	-1	-5	0.02	0.92	729	-1	0.05	27	0.207	12	-15	3.491	0.3	4.4
RT-187B	-1	-1	-5	-0.01	0.76	954	-1	0.04	23	0.190	27	-15	1.631	-0.1	4.3
RT-188	-1	-1	-5	0.04	0.82	834	3	0.06	33	0.037	4	-15	6.661	0.3	5
RT-189	-1	-1	-5	0.05	0.39	471	-1	0.09	23	0.031	45	-15	0.818	-0.1	2.8
RT-191	-1	-1	-5	0.04	0.77	352	-1	0.07	16	0.052	39	-15	1.429	-0.1	1.7
ND-203	-1	-1	-5	0.01	0.50	522	-1	0.03	36	0.048	29	-15	5.888	-0.1	1.6
ND-205	-1	-1	-5	0.02	0.85	477	-1	0.04	26	0.030	15	-15	2.715	-0.1	2.7
ND-206	-1	-1	-5	0.14	0.87	261	2	0.15	14	0.063	27	-15	2.884	0.2	3.2
ND-207	1	-1	-5	0.08	1.61	1079	-1	0.04	46	0.062	25	-15	5.029	-0.1	7.7
ND-210	-1	-1	-5	0.05	1.00	427	1	0.14	44	0.085	33	-15	7.440	0.2	5
ND-213	2	-1	-5	0.08	1.66	1046	-1	0.18	41	0.042	6	-15	2.218	-0.1	8.3
ND-214	1	-1	-5	0.02	1.39	1098	2	0.01	28	0.022	17	-15	0.485	-0.1	7.1
ND-215	-1	-1	-5	0.11	1.27	483	-1	0.12	18	0.019	19	-15	1.202	-0.1	4.6
ND-217	-1	-1	-5	0.09	1.45	934	-1	0.08	23	0.025	24	29	0.097	0.2	5.6
ND-218	-1	-1	-5	0.10	0.47	178	-1	0.05	13	0.034	34	23	0.191	-0.1	1.5
ND-219	-1	-1	-5	0.04	0.76	267	-1	0.04	16	0.044	15	-15	0.209	0.3	2.2
ND-221	1	-1	-5	0.34	9.59	2354	6	0.02	13	0.016	-3	20	0.188	0.4	9.3
ND-222	-1	-1	-5	0.27	2.97	1380	7	0.07	47	0.125	-3	-15	0.039	2	6.2
ND-223	1	-1	-5	0.17	1.87	232	2	0.09	26	0.055	48	-15	2.245	1	4.2
ND-225	2	-1	-5	0.14	1.75	786	-1	0.04	59	0.049	15	-15	0.061	-0.1	10.9
ND-226a	1	-1	-5	0.05	2.14	660	-1	0.02	33	0.021	15	-15	0.127	0.2	7.9
ND-226B	2	-1	-5	0.18	2.09	446	2	0.03	38	0.047	30	-15	2.800	0.3	9.1
ND-233	11	-1	-5	1.65	2.54	515	5	2.52	66	0.051	11	45	0.320	0.3	13.9
ND-238	-1	-1	-5	0.07	1.01	277	-1	0.04	13	0.095	31	-15	2.574	-0.1	2.3
ND-240	2	-1	-5	0.67	2.43	682	-1	0.02	55	0.050	16	51	1.029	0.8	11.9
ND-241	-1	-1	-5	-0.01	3.69	1822	-1	0.02	19	0.084	30	-15	-0.001	2	2.2
ND-242	-1	-1	-5	0.03	6.56	2859	5	0.03	35	0.116	227	-15	0.073	35.8	3.4
ND-243	-1	-1	-5	0.05	1.17	350	-1	0.06	15	0.031	9	-15	0.243	-0.1	2
ND-246	-1	-1	-5	0.02	2.95	985	2	0.02	13	0.539	903	-15	0.049	7.3	4.3
PM-182C	-1	-1	-5	0.20	0.48	218	1	0.08	52	0.053	19	-15	5.542	-0.1	1.6
PM-162	-1	-1	-5	0.18	0.77	153	1	0.07	7	0.051	-3	15	0.501	0.2	2.3
PM-182	-1	-1	-5	-0.01	0.46	437	1	0.02	32	0.052	22	-15	5.655	0.3	1.2
PM-176	3	-1	-5	0.84	3.98	1719	4	0.94	35	0.053	10	-15	2.264	-0.1	33.7
PM-179	4	-1	-5	2.24	4.73	1207	-1	1.42	55	0.123	5	119	0.290	-0.1	18.1
TR1-9	1	-1	-5	0.71	0.44	151	2	2.44	12	0.049	38	-15	0.131	-0.3	5.1
TR1-11	1	-1	-5	0.07	1.28	455	-1	0.09	32	0.053	34	-15	0.123	-0.1	7.5
BEAR8	-1	-1	-5	0.32	0.98	57	-1	0.05	96	0.093	35	-15	13.345	0.5	3
TR2-3	4	-1	-5	1.63	2.46	622	-1	0.97	136	0.024	16	47	2.532	-0.1	27.7
TR2-5	-1	-1	-5	0.22	1.17	188	5	0.05	130	0.057	17	-15	4.375	0.2	2.5
TR2-7A	2	-1	-5	0.29	0.61	243	2	0.02	163	0.022	44	-15	14.124	-0.1	8.6
TR2-8	5	-1	-5	0.21	2.03	8614	4	0.25	42	0.037	24	39	4.687	0.2	15.9
TR2-9	4	-1	-5	2.07	0.43	107	14	0.4	73	0.003	55	59	6.978	-0.1	4.2
TR2-11	5	-1	-5	0.06	2.25	16735	3	0.19	19	0.013	27	-15	3.049	-0.1	10.9

Sample ID	Se	Sn	Sr*	Ta	Th	Ti*	U	V*	W	Y*	Zn*	La	Ce	Nd	Sm
	ppm	%	ppm	ppm	ppm	%	ppm	ppm	ppm	ppm	ppm	ppm	ppm	ppm	ppm
RT-131	-3	-0.02	66	-0.5	1.7	0.09	-0.5	25	-1	10	24	3.7	9	-5	0.8
RT-135	-3	-0.01	98	1	6.6	0.43	2.5	127	5	14	76	29.2	55	22	3.9
RT-138	-3	-0.02	2	-0.5	7.7	0.16	1.9	106	-1	4	43	35.3	67	25	5.9
RT-139	-3	-0.01	28	-0.5	1.9	0.11	-0.5	33	2	10	28	5.1	14	-5	1
RT-142	-3	-0.01	36	-0.5	1.5	0.08	-0.5	19	2	11	22	7.5	15	-5	1.1
RT-147	-3	-0.01	96	-0.5	1.1	0.07	-0.5	35	34	25	59	14.6	28	11	2.3
RT-148	-3	-0.01	298	-0.5	27.3	0.45	11.9	102	-1	10	111	80.8	149	51	8.1
RT-150	-3	-0.01	28	-0.5	1	0.04	0.9	9	-1	7	30	3.4	7	-5	0.6
RT-151	-3	-0.03	20	3	4.3	0.20	-0.5	95	-1	12	114	12.1	25	10	2.1
RT-152	-3	-0.01	14	0.6	2.5	0.15	1.2	32	-1	12	99	9.3	20	8	1.3
RT-153	-3	-0.01	39	0.7	1.1	0.06	-0.5	12	-1	7	26	4.7	11	-5	0.7
RT-154	-3	-0.01	40	-0.5	1.6	0.06	-0.5	16	-1	8	40	4.4	11	-5	0.9
RT-155	-3	-0.02	316	-0.5	1.8	0.12	-0.5	31	13	11	36	7	15	-5	1.3
RT-156A	-3	-0.01	150	-0.5	1.2	0.08	-0.5	24	-1	7	37	2.9	7	-5	0.6
RT-156B	-3	-0.01	32	-0.5	0.7	0.04	-0.5	18	6	10	12	7.6	16	-5	1.6
RT-157	-3	-0.01	42	-0.5	0.7	0.04	-0.5	10	4	5	18	4.4	9	-5	0.8
RT-159	-3	-0.01	94	-0.5	-0.2	0.06	-0.5	23	850	10	17	3.5	10	-5	0.7
RT-160	-3	-0.01	6	-0.5	5.2	0.28	1.8	60	-1	12	28	14.5	30	12	2.4
RT-163	-3	-0.01	181	-0.5	2	0.11	0.8	31	-1	11	35	6.1	14	8	1.1
RT-164	-3	-0.01	28	-0.5	3.4	0.22	-0.5	66	4	12	37	15.3	33	-5	2.1
RT-171B	-3	-0.02	85	-0.5	1.6	0.06	-0.5	14	-1	9	30	5.8	13	-5	1
RT-179	-3	-0.01	5	-0.5	1.3	0.08	-0.5	17	-1	10	16	6.4	11	-5	0.9
RT-186	-3	-0.01	36	-0.5	3.7	0.20	1.7	65	-1	11	60	13.1	24	10	1.9
RT-187A	-3	-0.01	10	-0.5	1.5	0.11	0.6	58	-1	9	39	11.4	18	8	1.4
RT-187B	-3	-0.01	8	-0.5	1.1	0.11	0.9	68	-1	6	44	6.9	12	8	1.1
RT-188	3	-0.01	9	0.6	3	0.25	-0.5	51	-1	11	47	10.2	20	8	1.5
RT-189	-3	-0.01	17	-0.5	0.7	0.06	-0.5	15	-1	8	24	4.8	8	-5	0.9
RT-191	-3	-0.01	25	-0.5	0.5	0.03	-0.5	7	-1	7	17	2.7	6	10	0.6
ND-203	-3	-0.01	237	-0.5	0.3	0.04	-0.5	15	3	7	68	2.2	4	-5	0.5
ND-205	-3	-0.01	99	-0.5	0.8	0.04	-0.5	13	-1	7	47	2	5	-5	0.6
ND-206	-3	-0.01	149	-0.5	0.5	0.07	-0.5	22	2	10	40	3.9	10	-5	1
ND-207	3	-0.01	4	-0.5	3.1	0.19	0.9	50	-1	9	50	13.9	27	11	2.3
ND-210	-3	-0.01	23	-0.5	1.8	0.10	1	37	-1	11	52	23.2	37	11	2.1
ND-213	3	-0.01	42	0.6	3.5	0.21	1.5	60	5	10	57	8.3	16	9	1.9
ND-214	-3	-0.01	9	-0.5	2.7	0.19	0.7	49	3	14	50	12	23	8	1.8
ND-215	-3	-0.01	41	-0.5	1.4	0.12	-0.5	38	-1	7	52	4.6	11	-5	1.1
ND-217	-3	-0.01	10	-0.5	0.9	0.06	0.7	48	-1	6	59	1.5	4	-5	0.5
ND-218	-3	-0.01	119	-0.5	0.5	0.03	-0.5	6	-1	6	14	2.6	7	-5	0.5
ND-219	-3	-0.01	79	-0.5	1	0.04	-0.5	10	-1	8	16	3.8	11	6	0.8
ND-221	-3	-0.01	8	-0.5	1.7	0.06	1	17	1	37	4	9.3	27	15	5
ND-222	-3	-0.01	450	-0.5	2.7	0.10	2.7	27	3100	24	-1	4.1	7	-5	1.6
ND-223	-3	-0.01	15	-0.5	2.3	0.12	1.3	30	2	13	33	10.1	22	8	1.8
ND-225	-3	-0.01	14	-0.5	4.9	0.27	2	68	-1	20	57	26.5	51	17	3.7
ND-226a	-3	-0.01	13	-0.5	3.9	0.20	0.9	55	-1	12	76	10.6	25	10	2.1
ND-226B	-3	-0.01	37	-0.5	4.3	0.25	1.4	62	6	9	32	17.6	32	11	2.4
ND-233	-3	-0.02	171	-0.5	18.6	0.57	6.7	112	-1	33	73	37.1	76	23	4.6
ND-238	-3	-0.01	69	-0.5	0.8	0.04	0.7	8	-1	6	16	5	12	-5	0.9
ND-240	-3	-0.01	13	-0.5	4.3	0.27	1.4	95	-1	25	50	52.6	87	36	6.1
ND-241	-3	-0.01	47	-0.5	0.7	0.04	5.2	10	6	14	45	4	10	8	1.9
ND-242	-3	-0.01	29	-0.5	0.8	0.03	1.8	136	9	22	42	5.4	13	11	4.1
ND-243	-3	-0.01	86	-0.5	-0.2	0.04	0.9	10	-1	6	14	3.7	9	-5	0.7
ND-246	-3	-0.01	29	-0.5	1.9	0.08	8.8	107	6	22	26	35.8	43	15	4.6
PM-182C	-3	-0.01	175	-0.5	-0.2	0.04	1	15	6	8	42	3.1	9	-5	0.6
PM-162	-3	-0.01	12	-0.5	-0.2	0.05	-0.5	24	-1	3	21	0.9	-3	-5	0.3
PM-182	-3	-0.01	156	-0.5	0.7	0.03	-0.5	14	97	8	53	4	10	-5	0.7
PM-176	-3	-0.01	397	-0.5	1.5	1.34	-0.5	292	-1	29	165	13.4	36	17	5.2
PM-179	-3	-0.01	253	1.9	3.6	1.63	-0.5	178	-1	21	90	38	79	28	6.9
TR1-9	-3	-0.01	310	-0.8	0.8	0.11	-0.5	23	-1	6	37	7.8	19	-5	1.4
TR1-11	-3	-0.01	87	-0.5	3.7	0.18	-0.5	43	-1	13	37	11.8	27	17	2.3
BEAR8	-3	-0.01	6	-0.5	0.9	0.08	-0.5	44	20	5	27	8	14	-5	1.5
TR2-3	-3	-0.01	106	1.1	7.7	0.42	2	225	5	4	119	20.1	46	22	4.4
TR2-5	-3	-0.01	32	0.9	1.7	0.07	2.1	22	2	8	39	3.5	10	-5	0.7
TR2-7A	8	-0.01	6	-0.5	2.3	0.17	-0.5	48	-1	11	339	8.8	22	10	2.4
TR2-8	-3	-0.01	52	-0.5	1.3	0.34	-0.5	71	-1	34	232	9.3	22	13	3.7
TR2-9	-3	-0.01	7	-0.5	3.7	0.36	2	52	5	11	40	15.9	36	13	3
TR2-11	-3	-0.01	25	0.5	1.9	0.16	-0.5	32	-1	48	135	12.4	29	12	4.2

Sample ID	Eu	Tb	Yb	Lu	UTM		NTS	Co-ordinate
	ppm	ppm	ppm	ppm	Easting	Northing	50k	System
RT-131	-0.2	-0.5	1	0.17	398945	7392351	76J/11	NAD27
RT-135	1.1	-0.5	1.6	0.24	398664	7393673	76J/11	NAD27
RT-138	1.9	1.2	2.6	0.4	398638	7393087	76J/11	NAD27
RT-139	0.4	-0.5	0.9	0.16	398554	7392602	76J/11	NAD27
RT-142	0.3	-0.5	1	0.17	398362	7391449	76J/11	NAD27
RT-147	0.4	-0.5	2	0.29	398568	7392544	76J/11	NAD27
RT-148	2.2	0.9	2.5	0.38	398645	7392052	76J/11	NAD27
RT-150	-0.2	-0.5	0.8	0.13	398201	7390173	76J/11	NAD27
RT-151	0.5	-0.5	1	0.15	398537	7390062	76J/11	NAD27
RT-152	0.5	-0.5	1.1	0.19	398623	7390113	76J/11	NAD27
RT-153	0.2	-0.5	0.6	0.11	398769	7389819	76J/11	NAD27
RT-154	-0.2	-0.5	0.6	0.1	398730	7389688	76J/11	NAD27
RT-155	0.8	-0.5	1.1	0.16	398848	7389498	76J/11	NAD27
RT-156A	0.3	-0.5	0.8	0.13	397204	7398042	76J/11	NAD27
RT-156B	1.1	-0.5	1.3	0.2	397204	7398042	76J/11	NAD27
RT-157	0.3	-0.5	0.8	0.1	397119	7398017	76J/11	NAD27
RT-159	-0.2	-0.5	1.6	0.24	396833	7397938	76J/11	NAD27
RT-160	0.5	-0.5	1.2	0.2	396727	7397923	76J/11	NAD27
RT-163	0.5	-0.5	1.6	0.25	395259	7399231	76J/11	NAD27
RT-164	0.5	-0.5	1.5	0.23	394949	7399195	76J/11	NAD27
RT-171B	0.5	-0.5	0.9	0.16	399022	7388005	76J/11	NAD27
RT-179	-0.2	-0.5	0.9	0.13	402206	7418710	76J/11	NAD27
RT-186	0.5	-0.5	1.3	0.21	399034	7392097	76J/11	NAD27
RT-187A	0.5	-0.5	0.9	0.14	398429	7392391	76J/11	NAD27
RT-187B	0.4	-0.5	0.9	0.14	398429	7392391	76J/11	NAD27
RT-188	0.4	-0.5	0.9	0.16	398183	7392447	76J/11	NAD27
RT-189	0.4	-0.5	0.8	0.13	397936	7392614	76J/11	NAD27
RT-191	-0.2	-0.5	0.5	0.08	397946	7392480	76J/11	NAD27
ND-203	0.2	-0.5	0.7	0.13	404247	7389907	76J/11	NAD83
ND-205	0.3	-0.5	1	0.15	403881	7388744	76J/11	NAD83
ND-206	0.3	-0.5	1.1	0.15	403926	7388548	76J/11	NAD83
ND-207	0.5	0.5	1.1	0.18	404061	7388545	76J/11	NAD83
ND-210	-0.2	-0.5	1	0.16	401125	7392048	76J/11	NAD83
ND-213	0.5	-0.5	1.2	0.19	401237	7392102	76J/11	NAD83
ND-214	0.5	-0.5	1.7	0.29	401393	7391579	76J/11	NAD83
ND-215	0.3	-0.5	0.7	0.12	401419	7391382	76J/11	NAD83
ND-217	0.3	-0.5	1.1	0.16	401789	7391038	76J/11	NAD83
ND-218	0.2	-0.5	0.6	0.09	401899	7390942	76J/11	NAD83
ND-219	0.3	-0.5	1	0.14	402058	7390599	76J/11	NAD83
ND-221	2.1	1	4.2	0.65	400946	7386257	76J/11	NAD83
ND-222	1.2	1.7	3.6	0.55	400911	7386199	76J/11	NAD83
ND-223	0.4	-0.5	1	0.15	400893	7386083	76J/11	NAD83
ND-225	1.4	0.6	1.8	0.32	401366	7385807	76J/11	NAD83
ND-226a	0.5	-0.5	1.2	0.2	399610	7387234	76J/11	NAD83
ND-226B	0.7	-0.5	1.3	0.21	399610	7387234	76J/11	NAD83
ND-233	1.4	-0.5	1.9	0.3	400080	7395038	76J/11	NAD83
ND-238	0.3	-0.5	0.9	0.16	398851	7396058	76J/11	NAD83
ND-240	1.5	0.7	2.6	0.41	398447	7396853	76J/11	NAD83
ND-241	1.2	-0.5	1.2	0.2	398529	7397101	76J/11	NAD83
ND-242	2	0.8	1.5	0.22	398468	7397149	76J/11	NAD83
ND-243	0.3	-0.5	0.7	0.14	398418	7397203	76J/11	NAD83
ND-246	2.3	0.7	1.3	0.18	398488	7397147	76J/11	NAD83
PM-182C	0.3	-0.5	0.6	0.11	411103	7397445	76J/11	NAD27
PM-162	-0.2	-0.5	0.4	0.06	400633	7399459	76J/11	NAD27
PM-182	0.4	-0.5	0.8	0.14	411103	7397445	76J/11	NAD27
PM-176	1.5	-0.5	2.8	0.42	398871	7401790	76J/11	NAD27
PM-179	2.3	0.8	1.8	0.26	409831	7398257	76J/11	NAD27
TR1-9	1	-0.5	0.9	0.15	425073	7415483	76J/15	NAD83
TR1-11	0.7	-0.5	1.4	0.21	425290	7415636	76J/15	NAD83
BEAR8	0.3	-0.5	0.5	0.08	425090	7415431	76J/15	NAD83
TR2-3	1.1	-0.5	2	0.3	427969	7414052	76J/15	NAD83
TR2-5	0.4	-0.5	0.6	0.1	428169	7413985	76J/15	NAD83
TR2-7A	1.1	-0.5	1.8	0.27	427959	7413922	76J/15	NAD83
TR2-8	1.6	-0.5	4.5	0.7	427687	7413867	76J/15	NAD83
TR2-9	1.5	-0.5	2.9	0.46	427647	7413888	76J/15	NAD83
TR2-11	1.2	0.9	5.8	0.88	426996	7413843	76J/15	NAD83